

**KINETIC STUDY OF CHEMICAL LOOPING COMBUSTION USING IRON AS
AN OXYGEN CARRIER**

by

Amir Naji

Submitted in partial fulfilment of the requirements
for the degree of Master of Applied Science

at

Dalhousie University
Halifax, Nova Scotia
November 2011

© Copyright by Amir Naji, 2011

DALHOUSIE UNIVERSITY

PROCESS ENGINEERING AND APPLIED SCIENCE

The undersigned hereby certify that they have read and recommend to the Faculty of Graduate Studies for acceptance a thesis entitled “KINETIC STUDY OF CHEMICAL LOOPING COMBUSTION USING IRON AS AN OXYGEN CARRIER” by Amir Naji in partial fulfilment of the requirements for the degree of Master of Applied Science.

Dated: 15 November, 2011

Supervisor: _____

Readers: _____

DALHOUSIE UNIVERSITY

DATE: 15 November, 2011

AUTHOR: Amir Naji

TITLE: KINETIC STUDY OF CHEMICAL LOOPING COMBUSTION USING
IRON AS AN OXYGEN CARRIER

DEPARTMENT OR SCHOOL: Process Engineering And Applied Science

DEGREE: MAsC CONVOCATION: May YEAR: 2012

Permission is herewith granted to Dalhousie University to circulate and to have copied for non-commercial purposes, at its discretion, the above title upon the request of individuals or institutions. I understand that my thesis will be electronically available to the public.

The author reserves other publication rights, and neither the thesis nor extensive extracts from it may be printed or otherwise reproduced without the author's written permission.

The author attests that permission has been obtained for the use of any copyrighted material appearing in the thesis (other than the brief excerpts requiring only proper acknowledgement in scholarly writing), and that all such use is clearly acknowledged.

Signature of Author

TABLE OF CONTENTS

LIST OF TABLES	vii
LIST OF FIGURES	viii
ABSTRACT	X
LIST OF ABBREVIATIONS AND SYMBOLS USED	xi
ACKNOWLEDGEMENTS	xiii
CHAPTER 1: INTRODUCTION	1
1.1 BACKGROUND	1
1.2 OBJECTIVES	3
CHAPTER 2: LITERATURE REVIEW	4
2.1 CHEMICAL LOOPING COMBUSTION (CLC).....	4
2.1.1 OXYGEN CARRIERS.....	7
2.2 KINETIC STUDIES	13
2.2.1 KINETIC EQUATIONS	14
2.3 KINETIC STUDY METHODS	16
2.3.1 TEMPERATURE PROGRAM REDUCTION (TPR)	16
2.3.1.1 TPR EXPERIMENTAL CONDITIONS	21
2.3.2 THERMO GRAVIMETRIC ANALYSIS (TGA).....	21
CHAPTER 3: EXPERIMENTAL PROCEDURE.....	24
3.1 EXPERIMENTAL APPARATUS (TPR)	24
3.1.1 SUPPLY SECTION	24
3.1.2 REACTION SECTION	25
3.1.3 SAMPLING SECTION.....	27
3.1.4 PREPARATION STEPS	27
3.2 EXPERIMENTAL APPARATUS (TGA)	29
CHAPTER 4: RESULTS AND DISCUSSION.....	30

4.1 IRON OXIDE CHARACTERIZATION.....	30
4.2 TEMPERATURE PROGRAMED REDUCTION RESULTS.....	34
4.2.1 EXPERIMENTAL ERROR IN TPR EXPERIMENT	39
4.3 THERMO GRAVIMETRIC ANALYSIS RESULTS	41
4.4 REACTION MECHANISM.....	46
CHAPTER 5: CONCLUSIONS.....	49
REFERENCES.....	50
APPENDIX A1: SCANNING ELECTRON MICROSCOPE (SEM) ANALYSIS	55
APPENDIX A2:X-RAY DIFFRACTION ANALYSIS (XRD).....	58
APPENDIX A2.1: XRD SPECTRUM (TGA TEST 2 PRODUCT)	58
APPENDIX A2.2: XRD ANALYSIS SHOWING THE PRESENCE OF FEO IN TGA TEST 2 SAMPLE.....	59
APPENDIX A2.3: XRD ANALYSIS SHOWING THE PRESENCE OF Fe_3O_4 IN TGA TEST 2 SAMPLE	60
APPENDIX A2.4: XRD SPECTRUM (RAW MATERIAL)	61
APPENDIX A2.5: XRD ANALYSIS SHOWING THE PRESENCE OF Fe_2O_3 IN RAW MATERIAL	62
APPENDIX A2.6: XRD SPECTRUM (TGA TEST 1 PRODUCT)	63
APPENDIX A2.7: XRD ANALYSIS SHOWING THE PRESENCE OF Fe_3O_4 IN TGA TEST 1 PRODUCT	64
APPENDIX B1: GAS CHROMATOGRAPH FILES OF TPR (B=5)	65
APPENDIX B2: GAS CHROMATOGRAPH FILES OF TPR (B=10)	89
APPENDIX B3: GAS CHROMATOGRAPH FILES OF TPR (B=15)	104
APPENDIX B4: TGA GRAPHS.....	112
APPENDIX B4.1: TGA GRAPH OF OXIDATION OF IRON OXIDE OBTAINED FROM TPR TEST 2 WITH AIR, B=15	112
APPENDIX B4.2: TGA GRAPH OF OXIDATION OF IRON OXIDE OBTAINED FROM TPR TEST 2 WITH AIR, B=20	113
APPENDIX B4.3: TGA GRAPH OF OXIDATION OF IRON OXIDE OBTAINED FROM TPR TEST 2 WITH AIR, B=10	114

APPENDIX B4.4: TGA GRAPH OF OXIDATION OF IRON OXIDE OBTAINED FROM TPR TEST 1 WITH AIR, B=20	115
APPENDIX B4.5: TGA GRAPH OF OXIDATION OF IRON OXIDE OBTAINED FROM TPR TEST 1 WITH AIR, B=10	116
APPENDIX C: MICROSOFT EXCEL SPREAD SHEET	117

LIST OF TABLES

Table 2.1 Literature data on oxygen carriers in chemical looping combustion (Lyngfelt <i>et al.</i> , 2001).....	9
Table 2.2 Crushing strength (N/mm) of metal oxides (Adanez <i>et al.</i> , 2004).	10
Table 2.3 Qualitative estimation of the active oxides (Lyngfelt <i>et al.</i> , 2008).	12
Table 2.4 Possible controlling mechanisms for solid-state reactions (Kanervo, 2003)	15
Table 2.5 Identified reduction mechanisms, activation energies and pre-exponential factors for individual reduction steps (Galvita and Sundmacher 2007).	20
Table 2.6 Activation energies of iron oxide reduction (Mondal <i>et al.</i> , 2004)	23
Table 4.1 TPR test conditions and flow rates	34
Table 4.2 Parameter P for TPR standard condition.....	35
Table 4.3 Recorded temperatures for each run and the average for each peak.	40
Table 4.4 Calculated activation energies.	40
Table 4.5 TGA test conditions	45
Table C.1 Microsoft excel spread sheet for two-dimensional diffusion mechanism	117

LIST OF FIGURES

Figure 1.1 The Keeling Curve of atmospheric CO ₂ concentrations measured at Mauna Loa Observatory (Tans, 2011)	2
Figure 1.2 Global mean surface temperature difference relative to the 1961–1990 average (Hansen <i>et al.</i> , 2006).	2
Figure 2.1 Chemical Looping Combustion (Lyngfelt and Hilmer, 2005).....	4
Figure 2.2 Secondary electron image of: a) unreacted hematite particles, and b) hematite particles that were exposed to six alternating cycles of 180 s CH ₄ and 665 s air. The white marker indicates a length of 300 μm (Mattisson <i>et al.</i> , 2001).....	11
Figure 2.3 Experimental H ₂ -TPR profiles of Fe ₂ O ₃ –Ce _{0.5} Zr _{0.5} O ₂ at three different heating rates (Galvita and Sundmacher, 2007).	18
Figure 2.4 Sample TPR final graph to determine activation energy.	19
Figure 2.5 Comparison of experimental H ₂ -TPR profiles for Fe ₂ O ₃ –Ce _{0.5} Zr _{0.5} O ₂ , Fe ₂ O ₃ and Ce _{0.5} Zr _{0.5} O ₂ samples; heating rate: β=10 °C/min (Galvita and Sundmacher 2007).....	19
Figure 3.1 TPR experimental apparatus	24
Figure 3.2 TPR setup schematic diagram.....	26
Figure 3.3 The Agilent 3000A Micro GC	27
Figure 3.4 Thermometer calibration graph, temperature vs. time	28
Figure 3.5 SDT Q600 simultaneous TGA/DTS.....	29
Figure 4.1 SEM micrographs of iron oxide raw material.....	31
Figure 4.2 SEM micrographs of iron oxide (TPR product).....	32
Figure 4.3 SEM micrographs of iron oxide (TGA product).....	33
Figure 4.4 Experimental CH ₄ TPR profiles of Fe ₂ O ₃ at three different heating rates.....	36
Figure 4.5 Arrhenius plots for TPR of Fe ₂ O ₃ a) for Fe ₂ O ₃ to Fe ₃ O ₄ conversion (first peak) and b) for Fe ₃ O ₄ to FeO conversion (second peak).	38
Figure 4.6 TGA graph of oxidation of iron oxide with air at different temperature rates..	43
Figure 4.7 Arrhenius plots obtained from TGA of iron oxide with air.	44
Figure 4.8 TGA graph of oxidation of iron oxide obtained from TPR test 2 with air, β=15°C/min.....	45
Figure 4.9 Simulated reaction patterns for five reaction mechanisms.	47

Figure 4.10 TPR simulated patterns compared with calculated data.	48
Figure C.1 Simulated graph of two-dimensional diffusion mechanism made by Microsoft Excel.	120

ABSTRACT

Over the past few decades, combustion of fossil fuels has released greenhouse gases such as CO_2 and NO_x into the atmosphere. It has been realized that a mean temperature increase of the Earth, also known as global warming, has resulted from the increase of CO_2 concentration in the air. Hence, there is a growing tendency to establish novel methods of burning fossil fuels in order to mitigate CO_2 concentration. Chemical Looping Combustion (CLC) is a method of burning fuel with inherent separation of CO_2 while curbing the formation of NO_x , typically by circulating an oxygen carrier between an air (oxidation) reactor and a fuel (reduction) reactor. An oxygen carrier, mainly a metal oxide, circulates between the reactors providing the oxygen for conversion of fuel to CO_2 and H_2O . Thus, having a pure CO_2 stream, CO_2 sequestration becomes economically feasible. Fe_2O_3 , due to its availability and properties, could be an apposite oxygen carrier for CLC. Reaction kinetics of reduction of Hematite with methane, in the absence of gaseous oxidant, was studied. Temperature Program Reduction (TPR) experiments were carried out in a fixed bed tubular reactor. Reduction gas was composed of 15% methane and 85% argon. Thermogravimetric Analysis (TGA) was carried out on TPR products using air as the oxidant. Iron oxide samples were analyzed through X-ray diffraction (XRD) analysis and scanning electron microscopy. Two-stage reduction of iron oxide was observed: Fe_2O_3 reduced to Fe_3O_4 and then reduced to FeO . The activation energy of each stage was calculated from Kissinger's method. For the first and second stage of reduction the activation energies were 10.58 ± 0.86 and 25.77 ± 0.83 kJ/mol, respectively. In addition, different kinetic models were assumed and compared to the actual data. A random nucleation mechanism can be assigned to the first stage and a two-dimensional diffusion mechanism can be assigned to the second stage of the reduction.

LIST OF ABBREVIATIONS AND SYMBOLS USED

a.u.	Arbitrary Units
GC	Gas Chromatograph
IOC	iron Ore Company of Canada
LPM	liters per minutes
SEM	Scanning Electronic Microscope
TGA	Thermogravimetric Analysis
TPR	Temperature Program reduction
XRD	X-Ray diffraction
A	pre-exponential factor [s^{-1}]
C_0	Hydrogen concentration [mol/liter]
D_p	particle diameter [mm]
E	the activation energy [kJ/mol]
F	Flow rate[liters/min]
$k(T)$	the temperature-dependent rate coefficient
K	Rate constant
n	the order of reaction
P	parameter P [$^{\circ}K$]
R	the gas constant [J/mol. $^{\circ}K$]
R_0	Oxygen Ratio
S_0	amount of reducible species [mole]
t	time (s)
T	temperature [$^{\circ}K$]
T_{red}	Reduction Temperature [$^{\circ}C$]
T_{ox}	Oxidation Temperature [$^{\circ}C$]
T_0	Initial temperature [$^{\circ}K$]
T_{max}	Maximum Temperature [$^{\circ}K$]

α the degree of conversion

β Heating Rate [$^{\circ}\text{C}/\text{min}$]

ACKNOWLEDGEMENTS

It is a pleasure to thank those who made this thesis possible.

First and foremost I want to thank my supervisor Dr. Michael J. Pegg for his supervision, advice, and guidance from the very early stage of this research. It has been an honor to be his master student. He has taught me how to think big and I appreciate all his contributions of time, ideas, and funding to make my Master's experience productive and stimulating.

Many thanks go in particular to Dr. Stephen Kuzak and Dr. Kevin Plucknett my committee members. I am much indebted to Dr. Plucknett for his supervision in using TGA and also using my committee's precious times to read this thesis and give their critical comments about it.

I gratefully acknowledge Matt Kujath and Ray Dube for their extraordinary assistance and aid in designing, ordering parts and building the reactor. The fixed bed reactor would not have been existed without them.

Where would I be without my family? My parents deserve special mention for their inseparable support and prayers. My father, Hossein Naji, in the first place is the person who put the fundament of my learning character, showing me the joy of intellectual pursuit ever since I was a child. My Mother, Shole, is the one who sincerely raised me with her caring and gently love. I owe my deepest gratitude to my parents for their endless support and encouragement to pursue this degree.

Lastly, I offer my regards and blessings to all of those who supported me in any respect during the completion of the project.

CHAPTER 1: INTRODUCTION

1.1 BACKGROUND

There is considerable evidence to indicate that accumulation of carbon dioxide in the atmosphere significantly increases global warming. Atmospheric CO₂ concentration and the earth's temperature have both been atypically rising in the previous decades (Kessel, 2000), as seen in Figs. 1.1 and 1.2.

Hence, we are trying to decrease CO₂ emissions by curbing the release of more CO₂ into the atmosphere. One of the major sources of CO₂ emissions is a power plant, where fossil fuels are the source of heat. Sequestration of CO₂ under the earth's surface into some appropriate geological storage reservoirs may prove beneficial. On the other hand, sequestration of CO₂ is extremely expensive when the flue gas stream only contains about 8 to 13 percent CO₂ and the rest is nitrogen, water vapor, oxygen, and trace amounts of minor pollutants such as SO_x and NO_x.

Current carbon capture methods are not cost effective. Chemical Looping Combustion (CLC) is a method of burning fuel with inherent separation of CO₂ by using dual reactors; the fuel reactor, where the fuel reduces a metal oxide and the air reactor where the reduced metal oxide burns by air to return to its primary condition. Having a near pure CO₂ stream, CO₂ sequestration becomes more economically feasible. Hematite (Fe₂O₃), due to its availability and properties, may be a suitable candidate to be an oxygen carrier for CLC.

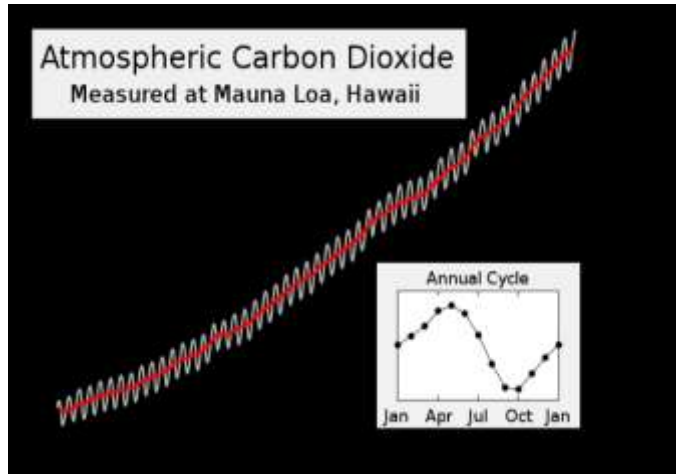


Figure 1.1 The Keeling Curve of atmospheric CO₂ concentrations measured at Mauna Loa Observatory (Tans, 2011)

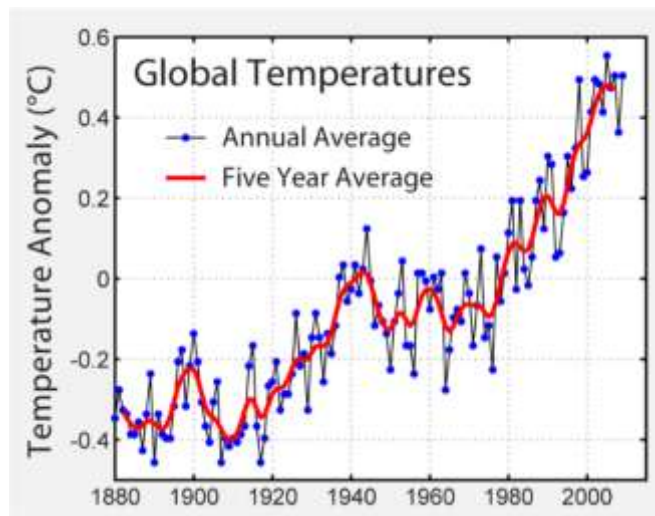


Figure 1.2 Global mean surface temperature difference relative to the 1961–1990 average (Hansen *et al.*, 2006).

1.2 OBJECTIVES

The objectives of this study were to:

- (1) Determine the reaction kinetics of the reduction of Fe_2O_3 with CH_4 .
- (2) Design and construct a fixed bed tubular reactor.
- (3) Carry out Temperature Program Reduction (TPR) on Fe_2O_3 using CH_4 as reducing gas.
- (4) Carry out Thermogravimetric analysis (TGA) on the TPR products using air as the oxidant.
- (5) Assume different kinetic models and compare them with TPR data.
- (6) Determine the best kinetic model for reaction.
- (7) Determine the activation energy.

This thesis consists of four sections. Section 2 summarizes the previous studies about chemical looping combustion, presents former research results regarding kinetic studies of different reactions and outlines different reaction mechanisms that have been proposed by their authors. Section 3 describes the experimental apparatus and explains the applied test methods. Finally, Section 4 presents the activation energies and reaction mechanisms and discusses how the data obtained from experiment is in satisfactory agreement with theory, followed by conclusion and recommendations.

CHAPTER 2: LITERATURE REVIEW

2.1 CHEMICAL LOOPING COMBUSTION (CLC)

The concept of chemical looping reaction was first introduced in 1983 by Richard Knoche. CLC is a novel combustion method with inherent CO_2 separation. A typical CLC unit decomposes the traditional combustion into two reactors as, shown in Fig. 2.1; the fuel reactor, where the fuel reduces an oxygen carrier, and the air reactor where the reduced oxygen carrier burns by air to return to its initial condition. The oxygen carrier is usually a metal oxide (Jernald *et al.*, 2006). The gases produced from the fuel reactor are CO_2 and H_2O . Water can be removed through a condensation process and almost pure CO_2 will be obtained. Carbon dioxide separation without consuming energy makes CLC a distinct separation method (Cho *et al.*, 2004).

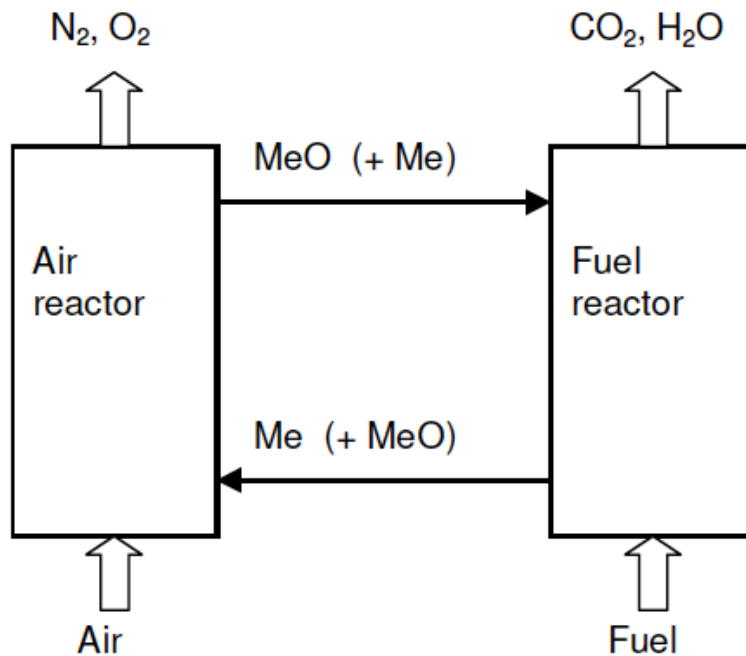
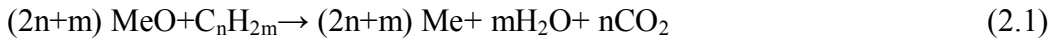


Figure 2.1 Chemical Looping Combustion (Lyngfelt and Hilmer, 2005)

The reaction in the fuel reactor takes place according to the following overall reaction:



where MeO is a metal oxide and Me represents a metal or a reduced form of MeO. This metal or reduced oxide is oxidized in the air reactor through the following reaction:



Reaction between air and the metal oxide is basically exothermic, while reduction of the metal oxide by fuel can be endothermic or exothermic, based on the metal type. The reduced oxygen carrier is introduced to the air reactor and absorbs oxygen and produces heat. The flue gas is mostly N_2 mixed with the remaining oxygen. Then the oxygen carrier is transferred to the fuel reactor to complete its cycle (Lyngfelt *et al.*, 2001). Separation of CO_2 is not the only environmental benefit of this method. Another advantage of this combustion method is the elimination of NO_x formation. This fact can be explained by flameless oxidation of the metal oxide. In fact, oxidation of the metal oxide completely independent of fuel in the air reactor prevents the formation of NO_x (Jin *et al.*, 1998).

Among all reactor types, fluidized bed reactors are mostly used when a perfect contact between fluid and solid particles is needed. Fluidized bed reactors are also applicable in industry when solid particles need to be reactivated, such as catalytic reactions. These two advantages, in spite of all the difficulties and complexities of the fluidized bed reactors, make them the unsurpassed reactor type for CLC reactions (Mattisson *et al.*, 2001).

Back in 1995, chemical looping reaction was found appropriate for several industrial applications. It was basically a cyclic solid-gas reaction which could be used for processes such as catalytic cracking, hydrogen generation, sulphur removal, coal gasification and so on. However, it had not yet been analyzed as an alternative combustion method (Ishida *et al.*, 1995).

One of the first papers was published by Ishida *et al.* (1995) at the Tokyo Institute of Technology investigating NiO as an oxygen carrier and methane as the fuel. Their

research revealed great potential, such that in the future even a power plant will be able to use this method of combustion, instead of the traditional fuel burning, and accordingly can lead to mitigation of greenhouse gases in the atmosphere. In 1998, Ishida *et al.* conducted research regarding carbon deposition on the solid particles, in order to apply chemical looping combustion in power plants. In their paper, the kinetic behaviour of carbon deposition was investigated for different type of oxygen carriers using various gas compositions. The results of their study indicated the conditions in which carbon deposition can be thoroughly controlled. As a result, the idea of using chemical looping combustion in power plants was considered to be feasible.

In addition to CO₂ separation, chemical looping has also been claimed to decrease the fuel exergy devastation which leads to power efficiency improvement. This claim has been examined by Anheden and Svedberg (1998) using two CLC gas turbines. One of them was using methane as fuel and the other one was using a mixture of CO and H₂, which can be assumed as coal gasification products. Fe₂O₃ and NiO were chosen as the oxygen carriers. The results of the study showed reduction of irreversibility caused by combustion compared to the traditional combustion method. It not only showed that the net power efficiency was either similar or higher than the conventional combustion method, but it also mentioned the possibility of increasing the net efficiency even more by enhancing the system to exploit the remaining exergy of the exhaust gas.

CLC researches mostly investigated gaseous fuels, although interest in solid fuels is growing rapidly. Considering coal as a major fossil fuel source in the world, numerous studies have been done on using coal as a solid fuel for CLC. Among those, Jin *et al.* (2004) indicated that using coal gas as the fuel for CLC, instead of natural gas, results in a considerable improvement in reactivity. Ston (2008), in the *overview of Canada's coal sector*, has stated: "The readily available and low-cost makes coal the choice of fuel for electricity production in some provinces such as Alberta and Saskatchewan" and according to the Statistics Canada website, in 2006 for Alberta, Saskatchewan and Nova Scotia, coal share of total electricity generation was 62.4 %, 52.9% and 57.3%, respectively. Of course it will be more inspiring for these provinces, in which coal is the dominant fuel for power plants.

Leion *et al.* (2008) investigated the possibility of using solid fuel in chemical looping combustion. Petroleum coke was used as the fuel and gasification intermediates were conducting the reaction between the oxygen carrier and solid fuel in a laboratory scale fluidized bed reactor. The oxygen carrier consisted of 60% Fe₂O₃ and 40% MgAl₂O₄. In each cycle 0.2 g of solid fuel was used, mixed in with 20 g of oxygen carrier. The gasification process was realized to occur faster at the presence of iron oxide. On the other hand, the iron oxide reaction with the intermediate gasification products, which are mostly CO and H₂, was observed to occur faster. The gasification reaction was determined to be the limiting step due to a slow reaction rate when compared to the iron oxide reaction with gasification products. Addition of SO₂ and steam to the fluidizing gas proved to be effective in terms of increasing the conversion rate. Agglomeration was not observed even after 100 cycles without changing the particles. An earlier paper was published in 2007 by Leion *et al.* using South African coal as the solid fuel. The same results were observed. Ninety five percent conversion was reached at 950 °C within 4 to 25 min, while 80% conversion was accomplished within 2 to 10 min, depending on the fuel. Lyngfelt *et al.* (2001) designed a boiler using the CLC technique. A CLC setup consisting of two fluidized bed interconnected reactors was designed and tested. The reactors were described as high-velocity risers and low-velocity bed reactors. Fe₂O₃ and NiO were used as the oxygen carriers. Reaction rate for both reduction and oxidation reactions was acceptable and the feasibility of this process was concluded.

2.1.1 OXYGEN CARRIERS

In order to apply chemical looping combustion not only at the lab scale but also in the industrial plants, it has been realized that having an appropriate oxygen carrier is critical. As a matter of fact, the circulation rate between reactors and the amount of bed material needed is contingent on the capacity of the oxygen carrier (Hossain and Lasa, 2008). Oxygen carrier recirculates between two reactors and mainly, as its name defines, absorbs and transfers the air's oxygen to the fuel reactor. To calculate the recirculation flow rate it is necessary to have the reaction rate and also the capacity of the oxygen carrier (Lyngfelt *et al.*, 2001). Hence, having the appropriate oxidation and reduction rate appears to be

essential for an oxygen carrier (Jernald *et al.*, 2006). It is also so important for the oxygen carrier to convert the fuel to water and carbon dioxide which, based on previous studies, some metal oxides are not capable of. Furthermore, oxygen carrier should have enough physical strength in order to maintain their particle size due to attrition and fragmentation (Cho *et al.*, 2004).

A number of studies have been conducted in several aspects, such as the oxygen ratio of the oxygen carrier, which is the maximum transported mass of oxygen for the specific mass flow of metal oxide, the melting point and the heat balance for different metal oxides. A perfect candidate for an oxygen carrier should have a number of specifications. It should be highly reactive in both reactions, oxidation by air and reduction by fuel (Mattisson *et al.*, 2001). It also should have excellent physical and chemical stability (Haber, 1991). To be low-priced and easily obtainable would be also a significant consideration. In addition, it should be environmentally friendly and also nontoxic. Lots of metals and their corresponding oxides have been examined in order to determine if they have the aforementioned qualifications. Nevertheless, kinetic results are only available for a few metal oxides for application in CLC including Fe, Ni, Co, Mn and Cu (Lyngfelt *et al.*, 2001). Table 2.1 shows a summary of the previous studies, from 1986 to 1999, on some metal oxides and their oxidation and reduction temperatures.



Many studies have been done on the mechanical strength of the oxygen carriers. Adanez and his colleagues (2004) have compared different metal oxides. A summary of his study is shown in Table 2.2. Based on his work it can be concluded that Fe-based oxygen carriers have great crushing strength value. The preparation is important as well. Al_2O_3 , TiO_2 and ZrO_2 are the best candidates for preparing iron oxide.

Table 2.1 Literature data on oxygen carriers in chemical looping combustion (Lyngfelt *et al.*, 2001)

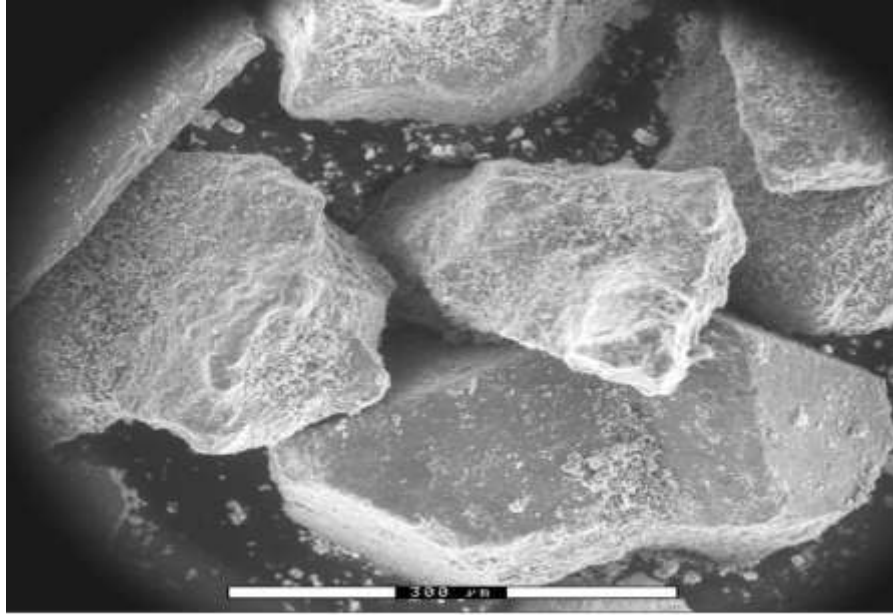
Carrier/support	Carrier/support (continued)	Red. gas	T _{red.} (°C)	T _{ox.} (°C)	D _p (mm)
Fe ₂ O ₃ , Fe ₂ O ₃ /Al ₂ O ₃	Fe ₂ O ₃ /Ni	H ₂ H ₂ /H ₂ O	700–900	800–1000	0.007
NiO/YSZ, NiO	Fe ₂ O ₃ /YSZ Fe ₂ O ₃ /Al ₂ O ₃	H ₂	600,800,1000	700,900,1100	1–3
NiO/YSZ		H ₂	600,800,1000	600,800,1000	1.8
NiO	NiO/YSZ	H ₂	600	1000,1200	2
NiO/YSZ, Fe ₂ O ₃ /YSZ	Co ₃ O ₄ /YSZ, CoO-NiO/YSZ	H ₂ , CH ₄	600	1000	1.8
NiO/YSZ	Fe ₂ O ₃ /YSZ	H ₂ /N ₂	550,600,700		
NiO/Al ₂ O ₃	Fe ₂ O ₃ /Al ₂ O ₃	CO/N ₂	800,900		
NiO/TiO ₂	Fe ₂ O ₃ /TiO ₂	CO/CO ₂ CO/N ₂ /CO ₂ CO/N ₂ /H ₂ O			
NiO/Al ₂ O ₃ , NiO/TiO ₂ , NiO/MgO, CoO/Al ₂ O ₃ , CoO/TiO ₂ , NiO/Al ₂ O ₃	CoO/MgO Fe ₂ O ₃ /Al ₂ O ₃ , Fe ₂ O ₃ /TiO ₂ , Fe ₂ O ₃ /MgO	H ₂ H ₂ O/CH ₄	600 700	1000 1000	2.1,1.8
		H ₂ (TGA) H ₂ /Ar(CR)	900	900	0.07
NiO		CH ₄	400–700		0.07

Table 2.2 Crushing strength (N/mm) of metal oxides (Adanez et al., 2004).

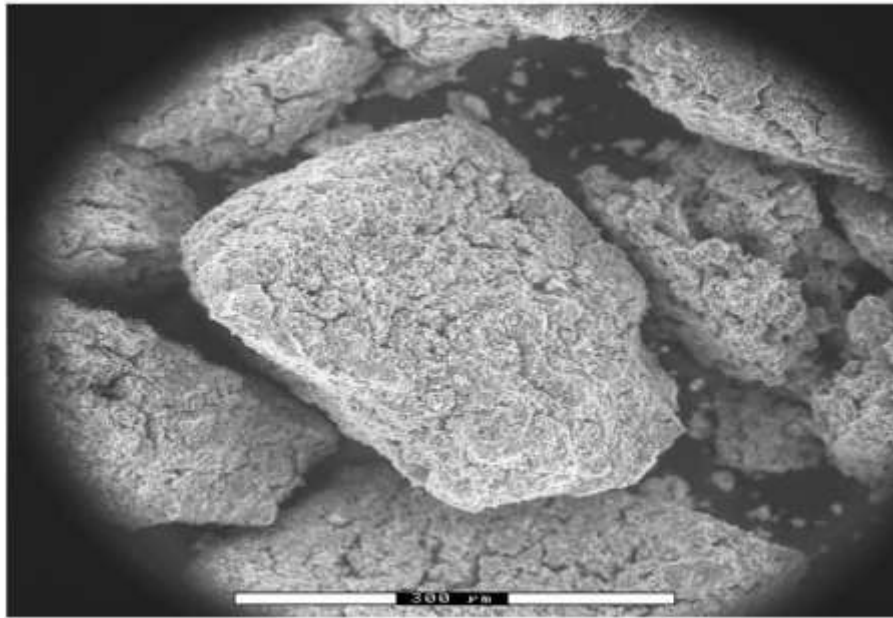
		Metal-based oxygen carriers															
		Cu				Fe				Mn				Ni			
Inert	T _{max} (°C)	950	1100	1200	1300	950	1100	1200	1300	950	1100	1200	1300	950	1100	1200	1300
	MeO(%)																
Al ₂ O ₃	80	3	5			0	13	105	61	0	0	0		0	0	0	0
	60	0	0			0	12	17	57	0	0	0		0	0	0	0
	40	0	0			0	12	22	65	0	3	12		0	2	3	4
Sepiolite	80	4				9	48			1	23*			0	1	4	120
	60	0				7	20			1	12*			1	6	14*	
	40	0				1	14			0	27*			0	3	53	
SiO ₂	80	22				12	60			10	37			0	1	11*	25*
	60	20				15	85			16	28			6	16	32	45
	40	17				10	52			16	22			11	29	35	
TiO ₂	80	66				12	71	111	17	2	57			1	16	42	50
	60	59				21	45	36	11	8	77			4	17	32	48
	40	43				40	94	81	30	13	84			14	23	33	65
ZrO ₂	80	6				3	25	33	76	0	11	37	29	0	2	1	3
	60	2				12	20	29	54	1	16	33	25	0	0	3	5
	40	1				13	19	19	56	2	11	36	27	0	3	13*	11*

 Melt or decompose
 Soft (Values lower than 10 N/mm)
 * Broken after 5 cycles

Mattisson *et al.* (2001) have exposed Fe₂O₃ to several cycles of air and methane to study the hardness of hematite. Hematite was chosen based on its low price and global availability. Figure 2.2 shows a secondary electron image of iron oxide particles before and after six cycles in a fixed bed quartz reactor at 950 °C. As shown in Fig. 2.2, some breakage of particles occurred, which can be due to the chemical reactions between iron oxide and the flow gases. The fractures decrease the efficiency by reducing the bed replacement period. To improve the hardness, Mattisson has suggested synthesizing the iron particles on a carrier matrix, which can be made of Al₂O₃. He also indicated that using such materials as binders can improve the reactivity of the hematite.



a)



b)

Figure 2.2 Secondary electron image of: a) unreacted hematite particles, and b) hematite particles that were exposed to six alternating cycles of 180 s CH₄ and 665 s air. The white marker indicates a length of 300 μm (Mattisson *et al.*, 2001)

As mentioned before, the production of a pure stream of CO₂ is the main advantage of applying the CLC method for burning fuel. Therefore, considerable work has been done to investigate the capability of the oxygen carrier to entirely convert the fuel to CO₂ and H₂O. Among all of the metal oxides, Ni, Mn, Fe, Cu and Co have shown satisfactory conversion rate (Mattisson *et al.*, 2001). However, cobalt is not a suitable candidate due to low conversion rate. The maximum conversion rate for Co is 93% at 1000°C and it is fairly expensive. In addition, cobalt has some health and safety issues which cannot be neglected. Nickel has also been found to be dangerous for human health in spite of its high oxygen ratio (0.21) which eliminates it from the list of proper oxygen carriers (Lyngfelt *et al.*, 2008). Table 2.3 has summarized a comparison among these metal oxides.

Table 2.3 Qualitative estimation of the active oxides (Lyngfelt *et al.*, 2008).

	Fe ₂ O ₃ /Fe ₃ O ₄	Mn ₃ O ₄ /MnO	CuO/Cu	NiO/Ni	comments
R ₀	0.03	0.07	0.20	0.21	Oxygen ratio
Reactivity	←decreasing increasing→				
Cost	←decreasing increasing→				
Health & Environm.				-	
Thermodynamics				-	<99.5% conv. for NiO
Reaction with CH ₄			+		CuO exothermic w. CH ₄
Melting point			-		1085°C for Cu

Lyngfelt *et al.* (2008) have also indicated that if the fuel is CO or H₂, the reaction will be exothermic, although using methane as a fuel makes the reaction endothermic except for Cu. Therefore, using Cu gives the process the advantage of maintaining the temperature of the oxygen carrier, which makes the circulation of metal oxide to the air reactor more efficient. Cho *et al.* (2004) have investigated the feasibility of using a few metal oxides as an oxygen carrier for CLC. The research was conducted on iron, nickel, copper and manganese oxides. Particle size was selected in the range of 125-180 μm. Reduction behaviour of metal oxides was investigated at 950°C, except for copper which was investigated at 850°C. Nickel oxide and copper oxide oxygen carriers showed

significantly high reactivity, while iron oxide also showed a reasonable reactivity. Among the metal oxides, agglomeration has been found in iron and copper oxides, which can be indicated as their disadvantage. The amount of bed mass was determined to be 80, 200 and 330 kg/MW_{th} for nickel, copper and iron oxide, respectively. Palacios (2004) has also conducted some studies on 240 samples of different metal oxides to find the most promising CLC oxygen carriers. Applying thermogravimetric analysis with methane as the reducing gas, the following results were obtained. Cu- based oxygen carriers, prepared with SiO₂ or TiO₂ as inert material, have shown the best properties and the sintering temperature was determined to be 950°C. The best inert material to prepare an iron-based oxygen carrier is claimed to be Al₂O₃ and ZrO₂. For a Ni-based oxygen carrier, TiO₂ was found to be the best inert material. All of the results were obtained based on the crushing strength and the reactivity of the oxygen carriers.

2.2 KINETIC STUDIES

Kinetic study of a reaction is an indispensable stage in order to design a reactor. In kinetic studies the main goal is to obtain the concentration change of the reactant or products as a function of time. In this research, the rate of hematite (Fe₂O₃) reduction with methane (CH₄) and oxidation of FeO and Fe₃O₄ with air will be studied. Kinetic results will provide us with the essential data for precise design of the CLC reactors (Smith 1981).

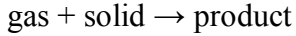
Yu Lin *et al.* (2003) have conducted research on the reduction of iron oxide by hydrogen. In that study, the TPR method has been applied and a two-step reduction was detected. The first step was reduction of Fe₂O₃ to Fe₃O₄ and the second step was further reduction of iron oxide to metallic Fe due to following reaction:



Formation of FeO as an intermediate form of oxide was not observed in the experiment. After calculation of activation energies and simulation of the reaction pattern, Yu Lin (2003) has suggested a unimolecular mechanism for the first step and a two- dimensional mechanism for the second step of the reaction.

2.2.1 KINETIC EQUATIONS

For the following reaction:



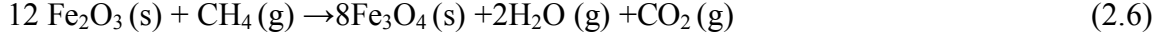
The reaction rate can be described as:

$$\text{rate} = - \frac{d[\text{gas}]}{dt} = k(T)[\text{gas}]^n \quad (2.4)$$

where $[\text{gas}]$ is the gas concentration, n the order of reaction, $k(T)$ the rate constant given by the Arrhenius equation, where T is the temperature (Kelvin), R the gas constant and E is the activation energy (Yu Lin *et al.*, 2003). The Arrhenius equation is given by:

$$k(T) = A e^{-\frac{E}{RT}} \quad (2.5)$$

The following reaction occurs between iron oxide and methane, which is an example of the above mentioned general gas-solid reaction:



The reaction rate can be written as:

$$\frac{d\alpha}{dt} = k(T)f(\alpha) \quad (2.7)$$

where α is the degree of conversion of mobile oxygen in the solid reactant (Yu Lin *et al.*, 2003).

The most commonly related kinetic models can be classified into three groups, which define diffusion controlled processes, boundary-controlled processes, and processes involving random nucleation and subsequent growth of nuclei. Arithmetical expressions for $f(\alpha)$ and $g(\alpha)$ for each of these models are listed in Table 2.4.

Table 2.4 Possible controlling mechanisms for solid-state reactions (Kanervo, 2003)

Mechanisms	$f(x)$	$g(x)$
1 Random nucleation	$(1-x)$	$-\ln(1-x)$
2 Contracting area	$(1-x)^{1/2}$	$2(1-(1-x)^{1/2})$
3 Contracting volume	$(1-x)^{1/3}$	$3(1-(1-x)^{1/3})$
4 1D Avrami-Erofeyev	$2(1-x)(\ln(1-x))^{1/2}$	$(-\ln(1-x))^{1/2}$
5 2D Avrami-Erofeyev	$3(1-x)\ln(1-x)^{2/3}$	$(-\ln(1-x))^{1/3}$
6 3D Avrami-Erofeyev	$4(1-x)(\ln(1-x))^{2/3}$	$(-\ln(1-x))^{1/4}$
7 One-dimensional diffusion	$1/2x$	x^2
8 Three-dimensional diffusion	$3(1-x)^{2/3}/(2(1-(1-x)^{1/3}))$	$(1-(1-x)^{1/3})^2$

The diffusion-controlled mechanism is accurate when the overall rate of the reaction is determined by the movement of one or more reactant species to or a product from a reaction interface inside the material. Phase boundary controlled models are defined as shrinking/unreacted cores or contracting spheres where the reaction is the rate determining step which proceeds topochemically¹. Nucleation-controlled processes involve uniform internal reduction and occur by the initial random removal of lattice oxygen atoms until a critical concentration of vacancies is reached. The vacancies are then annihilated by lattice rearrangement to produce metal nuclei. The nuclei then grow and, as they expand, the reduction process accelerates due to the increasing metal-metal oxide interface which is further increased by the formation of new nuclei (Kanervo, 2003). The Avrami-Erofeyev model is concerned with the nucleation process from the statistical probability perspective. The unimolecular model is expected to be a first order reaction, and the three-dimensional diffusion model is equation that assumes the reaction is proceeding equally for all surfaces of the particles, with the reaction rate diminishing as a consequence of increasing thickness of the barrier layer (Yu Lin *et al.*, 2003).

¹ A topochemical reaction is a reversible or irreversible reaction that involves the introduction of a guest species into a host structure and that results in significant structural modifications to the host. (IUPAC Compendium of Chemical Terminology 2nd Edition (1997))

2.3 KINETIC STUDY METHODS

2.3.1 TEMPERATURE PROGRAM REDUCTION (TPR)

Thermo-analytical techniques are well known for the characterization of solid materials. Temperature-programmed reduction (TPR) is a convenient method for characterizing metal oxides. TPR has been used to gain qualitative information on the reducibility of oxide species (Galvita and Sundmacher, 2007).

For a heating program with a constant rate of heating, β , we will have:

$$\frac{dT}{dt} = \beta \quad (2.8)$$

By combining equations 2.5 and 2.7:

$$\frac{d\alpha}{dT} = \frac{A}{\beta} \cdot \exp\left(-\frac{E}{RT}\right) \cdot f(\alpha) \quad (2.9)$$

The TPR response curve is obtained by integrating the previous equation:

$$\int_0^{\alpha} \frac{d\alpha}{f(\alpha)} = g(\alpha) = \frac{A}{\beta} \int_{T_0}^T \exp\left(\frac{-E}{RT}\right) dT \quad (2.10)$$

The maximum reaction rate can then be calculated following:

$$\left[\frac{d}{dT} \left(\frac{d\alpha}{dT} \right) \right]_{T=T_{\max}} = 0 \quad (2.11)$$

By substitution of Eq. 2.9 into Eq. 2.11 we find:

$$\frac{d}{dT} \left[\frac{A}{\beta} \cdot \exp\left(-\frac{E}{RT}\right) \cdot f(\alpha) \right]_{T=T_{\max}} = 0 \quad (2.12)$$

By solving Eq. 2.12, two important results can be concluded:

$$A = \frac{-E}{RT_{\max}^2} \times \frac{\beta e^{E/RT_{\max}}}{(df(\alpha)/d\alpha)_{T=T_{\max}}} \quad (2.13)$$

$$\ln\left(\frac{\beta}{T_{\max}^2}\right) = \left(-\frac{E}{R}\right)\frac{1}{T_{\max}} - \ln\left(\frac{E}{AR}\right) + C \quad (2.14)$$

From Eq. 2.14 and experimental data, the value A can be determined. By plotting $\ln(\beta/T_{\max}^2)$ vs. $(1/T_{\max})$ the slope of the line will indicate $(-E/R)$ which is concluded from Eq. 2.14. In this method it is necessary to use different values of β and determine the T_{\max} for each β in order to plot the graph and evaluate the activation energy (Fig. 2.3 and 2.4).

As shown in Fig.2.3, Galvita and Sundmacher (2007) have observed two peaks for each test. The first one indicates the conversion of Fe_2O_3 to Fe_3O_4 , which they described as phase boundary controlled reaction and the second one is related to the further reaction of Fe_3O_4 with H_2 that results in the formation of metallic Fe. They described the second reaction mechanism as two-dimensional nucleation reaction. Their experimental results are shown in Fig.2.5 and Table 2.5.

By numerically solving Eq. 2.10, $g(\alpha(T))$ and consequently $f(\alpha(T))$ can be evaluated.

$$g(\alpha) = \frac{AE}{R\beta} e^{-\frac{E}{RT}} \left(1 + \frac{RT}{E}\right) \quad (2.15)$$

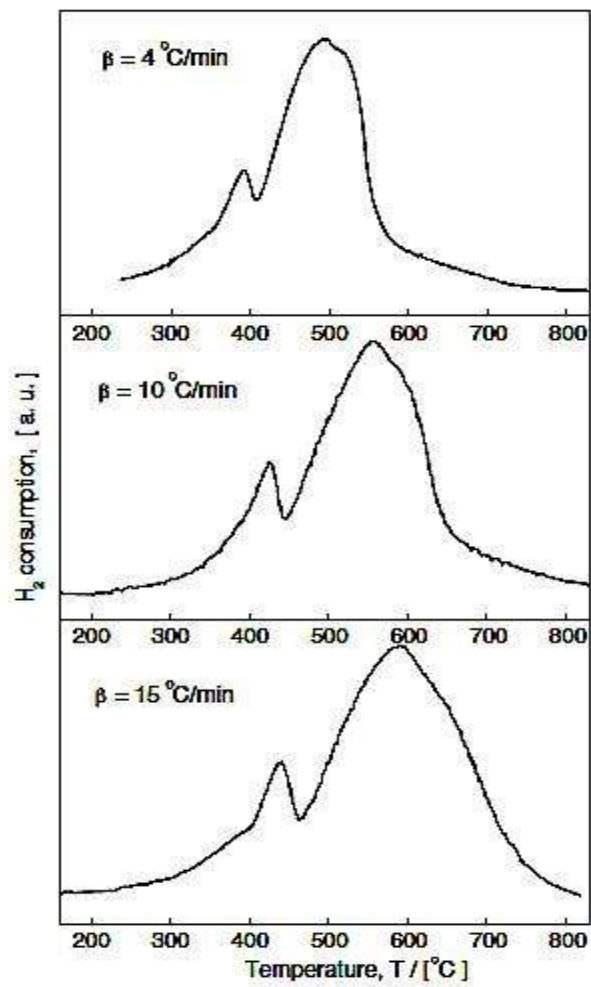


Figure 2.3 Experimental H₂-TPR profiles of Fe₂O₃-Ce_{0.5}Zr_{0.5}O₂ at three different heating rates (Galvita and Sundmacher, 2007).

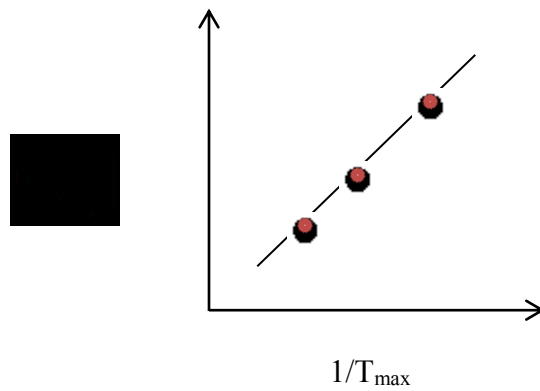


Figure 2.4 Sample TPR final graph to determine activation energy.

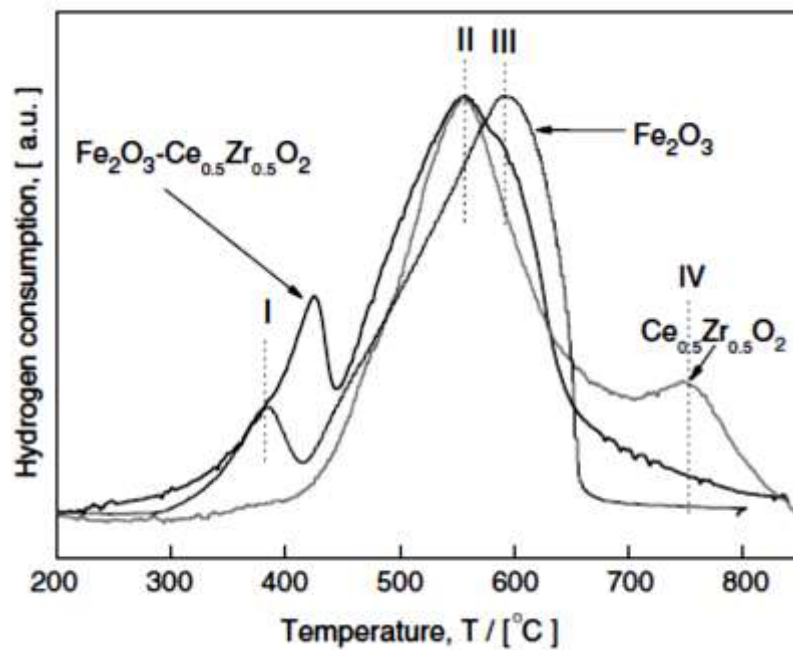


Figure 2.5 Comparison of experimental H₂-TPR profiles for Fe₂O₃ –Ce_{0.5}Zr_{0.5}O₂, Fe₂O₃ and Ce_{0.5}Zr_{0.5}O₂ samples; heating rate: $\beta=10$ °C/min (Galvita and Sundmacher 2007).

Table 2.5 Identified reduction mechanisms, activation energies and pre-exponential factors for individual reduction steps (Galvita and Sundmacher 2007).

Reduction step	Reduction mechanism	A, s^{-1}	$E, kJ/mol$
$Fe_2O_3 \rightarrow Fe_3O_4$ (peak I)	Random nucleation		74–117 96
	Contracting area (= sharp interface controlled reaction)	$1.2 \pm 0.2^* 10^6$	$104 \pm 15^*$
$Fe_3O_4 \rightarrow Fe$ (peak III)	2D Avrami-Erofeyev		70.4 59–69
		330 ± 60	$78 \pm 12^*$
	3D Avrami-Erofeyev		111
$CeO_2 \rightarrow Ce_2O_3$ (peaks II, IV)	Diffusion control		95
	Diffusion control		127
	2DAvrami-Erofeyev (peak II)	$1.45 \pm 0.2^* 10^3$	$83 \pm 15^*$
	Diffusion control (peak IV)	30 ± 7	$66 \pm 13^*$

Yu Lin *et al.* (2003) have applied the TPR method for kinetic study of reduction of iron oxide with hydrogen. Reduction was determined to have been in two stages; first the reduction of Fe_2O_3 to Fe_3O_4 occurs and then the reduction of Fe_3O_4 to Fe. Using the Arrhenius plot the activation energies was calculated for both steps and the result was 89.13 and 70.41 kJ/mol, respectively. The TPR pattern was plotted and the simulation models were compared to the obtained data. The unimolecular model fitted well for the first stage and the two-dimensional nucleation was fitted best for the second stage of the reduction. Jozwia *et al.* (2007) investigated the reduction behaviour of iron oxides using the TPR method. Hydrogen and carbon monoxide mixture was used as reducing agent. Using an in situ X-Ray diffraction (XRD) analysis, three stage reduction of iron oxide was observed; reduction of Fe_2O_3 to Fe_3O_4 then further reduction to FeO, and finally reduction of FeO to Fe.

2.3.1.1 TPR EXPERIMENTAL CONDITIONS

TPR experimental conditions such as the amount of metal oxide, carrier gas and fuel gas flow rates, and heating rate have to be carefully determined. Since the shape of the TPR peaks are noticeably affected by these parameters, choosing an appropriate range for each is critical. Uninformed changes in the experimental conditions can dramatically affect the results. For this purpose, Malet and Caballero (1988) have defined the parameter, **P**, as:

$$P = \beta S_0 / FC_0 \quad (2-16)$$

where S_0 is the amount of reducible species in the sample, F is the gas flow rate and C_0 is the hydrogen concentration in the feed gas to the reactor. The P factor should be set as low as possible and in all cases lower than 20 K. Moreover, for the calculation of activation energy it is preferred to run the test with constant P , using different temperature ramps, in order to obtain the results with more certainty.

2.3.2 THERMO GRAVIMETRIC ANALYSIS (TGA)

One of the most prevalent methods in the study of the kinetics of gas-solid reactions is thermogravimetric analysis (TGA), which can be based on either isothermal or non-isothermal data (Everson *et al.*, 2006). Numerous methods have also been developed in order to evaluate TGA data (Sharp and Wentworth., 1969). Flynn and Wall (1960) have revised five different methods explicitly on TG analysis of polymers. The “integral” method, “differential” method and “difference-differential” method have been compared by Sharp and Wentworth (1969) in their article and the advantages and disadvantages of each of the methods have been pointed out.

In TGA, the solid reactant in the form of a fine powder is placed into a crucible and the gas stream, consisting of an inert carrier gas and the reactant gas, flows above the crucible. The temperature can be set to be constant (isothermal) or be ramped with a certain rate (non-isothermal). As the reaction proceeds, the solid phase will lose or gain weight, based on the nature of the reaction. Evaluation of this weight change and relating it to the rate of the reaction is the main concept of this method.

One way to obtain kinetic factors of a reaction from TGA results is the difference-

differential method. Although this method has several weaknesses, it was commonly used, and both activation energy and the order of the reaction can be evaluated.

Sometimes the corresponding results for the reaction order are meaningless or often have a great value of uncertainty. The integral method, in contrast, is applied to four different orders of reactions, which are 0, 1/2, 2/3 and 1, based on the theoretical explanation of the solid phase reaction. With each of these reaction orders a particular plot can be produced and the best linear plot belongs to the actual reaction rate, which also determines the equivalent activation energy (Sharp and Wentworth, 1969).

In 1966, Achar *et al.* established the differential method for solid phase reactions, which cannot be categorized in terms of an order of reaction. This method applies to all reaction mechanisms as long as the correct reaction mechanism has been already identified. Considering the fact that the correct mechanism of a reaction can be found in prior works, knowing the mechanism of the reaction would no longer be a limitation for this method.

Piotrowski and his research group (2005) have done a comprehensive study on iron oxide reduction using the TGA method. They claimed that the reaction of Fe_2O_3 to Fe_3O_4 is a surface-controlled process and as soon as the first layer of Fe_3O_4 is formed, the reaction mechanism changes to diffusion control to form FeO . They have also indicated that higher temperature results in a higher reaction rate as they chose isothermal TGA experiments with temperature between 700-900 °C.

Hematite reduction, with different reducing gases, has been studied and different activation energies have been obtained. Table 2.6 shows some of the previous study's results.

Table 2.6 Activation energies of iron oxide reduction (Mondal *et al.*, 2004)

Activation energy (kJ/mol)	Reducing agent
74-117	H ₂
57-73	H ₂
35	H ₂
14.6	CO
42.1	H ₂
19.8	CO
96-106	H ₂

CHAPTER 3: EXPERIMENTAL PROCEDURE

3.1 EXPERIMENTAL APPARATUS (TPR)

For this study, a tubular fixed bed reactor has been designed and constructed. The experimental apparatus has been categorized into three main sections namely the supply, reactor and sampling sections. The whole setup is illustrated in Fig 3.1.



Figure 3.1 TPR experimental apparatus

3.1.1 SUPPLY SECTION

The supply section contained two gas lines: argon (Praxair, Grade 5.0, 99.999% pure), which was the carrier gas and methane (Praxair, grade 3.7, 99.97% pure), which was the reactant gas. Two mass flow controllers were used to control the flow rates of the feed; Omega 2600A was used for argon with an accuracy of ± 0.1 liters per minute (LPM), and Omega 2604A was used for methane, with an accuracy of ± 0.01 LPM.

3.1.2 REACTION SECTION

A stainless steel tube (AISI 316 with 7.75 mm inside diameter and total length of 650 mm) was located in an electrical furnace (2238-24-3ZH). The reactor was placed inside a mullite process tube. The mullite tube was designed to protect the reactor from heat loss and maintain a constant heating rate. In order to fix the iron oxide particles inside the tube a chamber consisting of two sintered stainless steel plates (SS-4F-K4-60) was placed 50 mm down from the very top of the reactor. Iron oxide particles were located between the two plates and a K-type thermocouple was placed inside the chamber to measure reaction temperature. The furnace was equipped with two PID temperature controllers (Extech, 48VTR); each was connected to a K-type thermocouple located at the middle of its controlling zone. One of these was controlling the heat rate of the reaction zone (from the top of the tube to the middle) and the other was controlling the heating rate of the preheat zone (from the middle of the tube to the bottom). The temperatures were read through a digital thermometer (Omega, HH21) and were recorded manually. A schematic diagram of the setup is illustrated in Fig. 3.2.

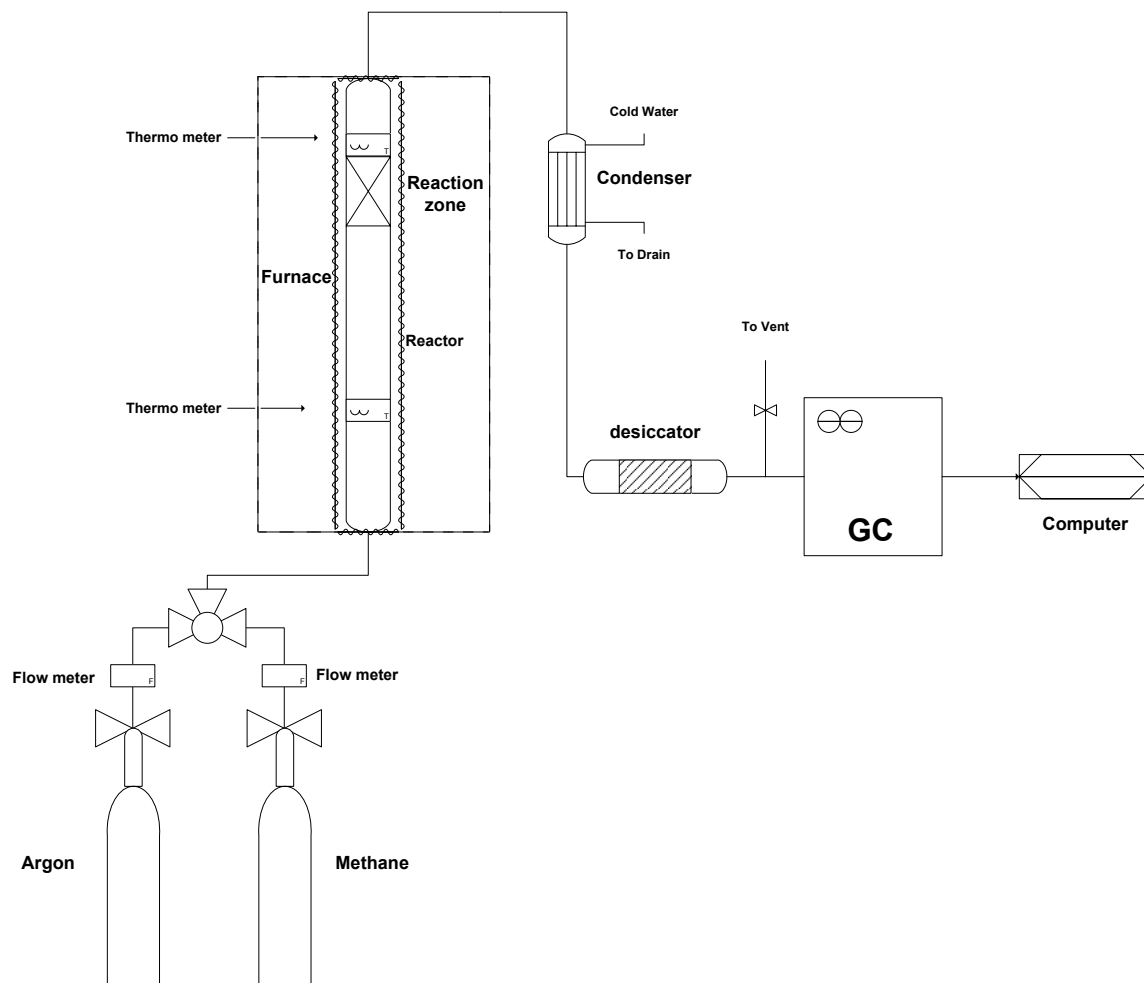


Figure 3.2 TPR setup schematic diagram

3.1.3 SAMPLING SECTION

A gas chromatograph (3000A Micro GC, Agilent) was used (Fig. 3.3) for measuring the composition of the outlet gases. When the gas left the reaction zone, the gas temperature was more than the recommended GC inlet temperature (below 90°C), so a condenser was located in order to cool it down. Cold tap water was used as a cooling fluid. As the exit gas contained water as a product of the reaction, a desiccator was located immediately before the GC entrance in the stream, in order to absorb the water and therefore protect the GC columns from possible moisture damage.



Figure 3.3 The Agilent 3000A Micro GC

3.1.4 PREPARATION STEPS

Preparation steps consisted of a leak test, temperature control calibration and GC calibration. For the leak test, argon was used and the exit valve was closed and 20 psi pressure was applied to ensure all of the couplings and junctions are well sealed, based on the hazardous nature of the experiment. The temperature controller calibration was conducted with different rates of heating, in order to determine the appropriate settings for the temperature ramp. Finally, the GC calibration was performed by flowing different ratios of methane to argon to adjust the GC to recognize the flue gas and reduce possible errors. The first step was calibration of the GC which was performed without heating. The next step was to see if the mixture of methane and argon reacts with anything while passing through the tubes using actual reactor conditions with heating and in high

temperatures (1000 °C). Figure 3.4 shows the calibration data for different heating rates. As the graph shows, the heating ramp was perfectly constant for $\beta=5$ and almost constant for $\beta=10$. For higher heating rates, such as $\beta=15$, the controllers was not able to keep the heating rate constant.

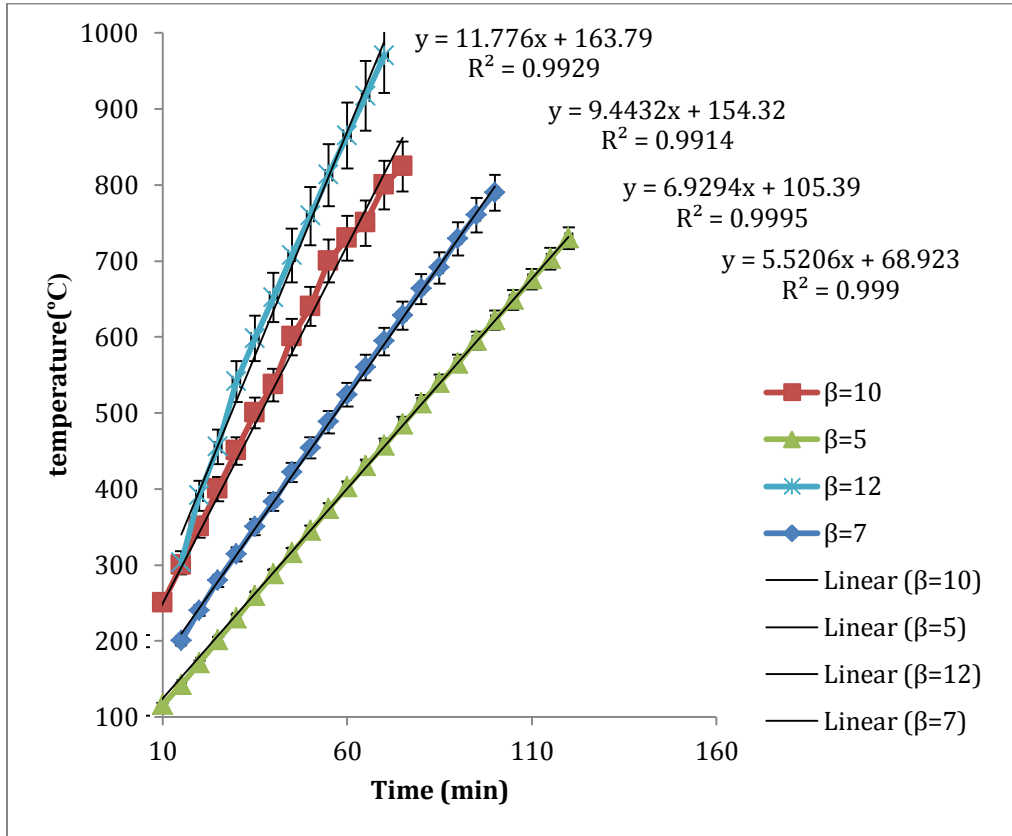


Figure 3.4 Thermometer calibration graph, temperature vs. time

3.2 EXPERIMENTAL APPARATUS (TGA)

In order to complete a cycle in chemical looping combustion, the reduced iron oxide should react with air and return to its primary condition by absorbing oxygen from air. A TA Instruments SDT Q600 TEA system, as shown in Fig 3.5, has been used to evaluate the oxidation of iron with air. Iron oxide samples were placed in an aluminum oxide crucible. The samples were heated up to 1100 °C with three different ramps: 10, 15 and 20 °C/min.



Figure 3.5 SDT Q600 simultaneous TGA/DTS.

CHAPTER 4: RESULTS AND DISCUSSION

4.1 IRON OXIDE CHARACTERIZATION

Iron oxide pellets were ordered from the Iron Ore Company of Canada (IOC). The pellets were then ground and sieved, following a ball mill grinding process. Because of a complementary research on the iron oxide, two particle sizes (75-90 μm and 90-125 μm) were chosen to be suitable as the feed for a pulverized coal burner. The pulverized coal burner has to be designed for the air reactor of the CLC unit. X-ray diffraction (XRD) analysis and scanning electron microscopy (SEM) was performed on the iron oxide. The SEM and XRD test results are attached in Appendix A. The XRD results show only the Fe_2O_3 form of iron oxide in the sample. SEM images of the iron oxide (90-125 μm) as raw material, the product of TPR and the product of TGA are shown in Figs. 4.1, 4.2 and 4.3. Figure 4.1 shows the irregular surface of the iron oxide raw material and the porosity and void spaces between the particles are noticeable. Figure 4.2 shows the microscopic structure of the iron oxide sample after heating up to 1100°C in the fixed bed TPR reactor. The surface became smoother. Figure 4.3 shows the same sample after oxidation with air up to 1100°C. The shape of the surface has noticeably changed. This reduction and oxidation has changed the morphology of the sample. As a result of this temperature treatment there is no sign of void space between the particles and all of them adhered to each other as if it were a single piece. Moreover, the surface is not irregular anymore. However, there is no sign of fracture or breakage in the iron oxide particles. The molar composition of each sample obtained from SEM can also be reviewed in Appendix A. Appendix A1 shows 8.57 weight percent carbon dissolved in the raw sample and it reduced to 7.57 weight percent in the final product. Added carbon improves the hardness of the iron. Therefore, losing carbon could result in reduced strength for the final sample.

As mentioned before, two sets of TPR tests were carried out. The major difference between them was the highest temperature that was reached in the experiment. In test 1 the iron oxide sample was heated up to 800°C, while in test 2 the maximum temperature

was 1100 °C. Based on TGA and XRD analysis of the results of the test 1 product, there was only Fe₃O₄ formation after reduction of the sample with methane, whereas in test 2 samples FeO has also been formed. Galvita and Sundmacher (2007) have mentioned the formation of Fe instead of FeO. Although the method of TPR experiment was almost the same as this study, using H₂ as the reductive gas instead of methane could be one of the reasons why they have not observed FeO formation.

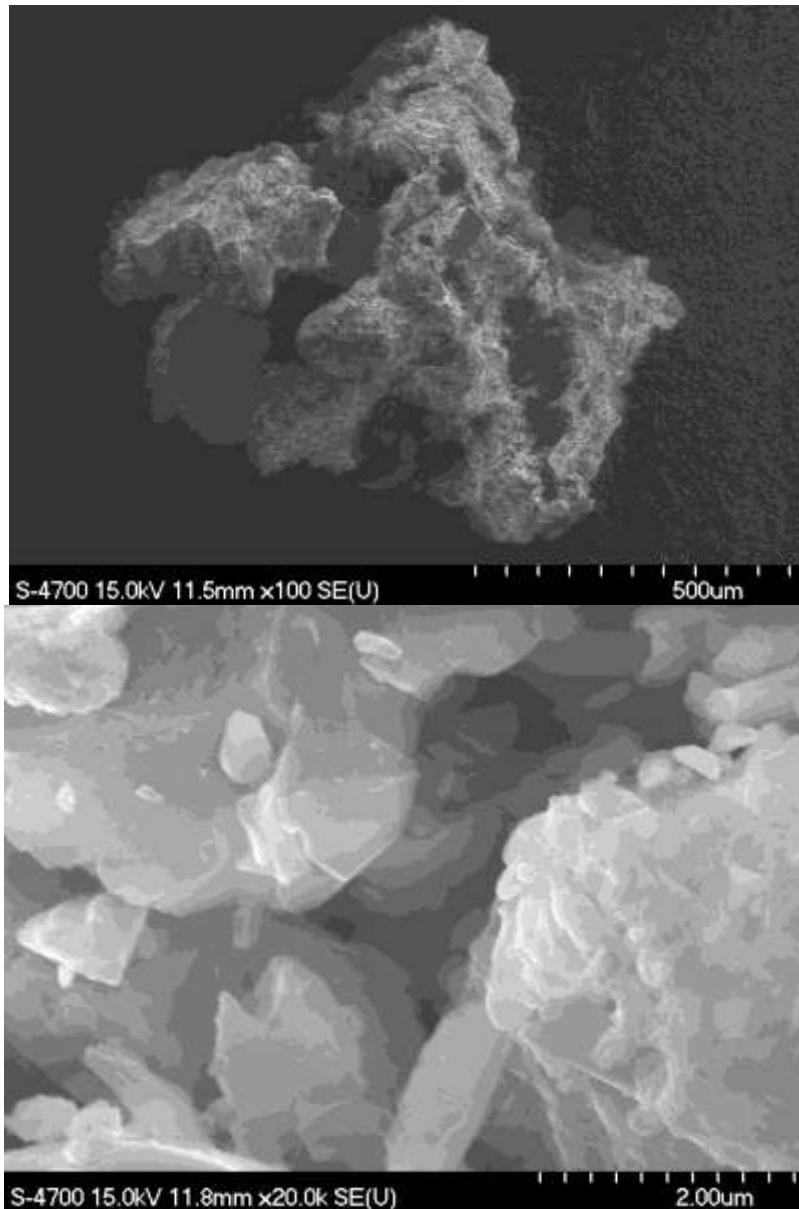


Figure 4.1 SEM micrographs of iron oxide raw material

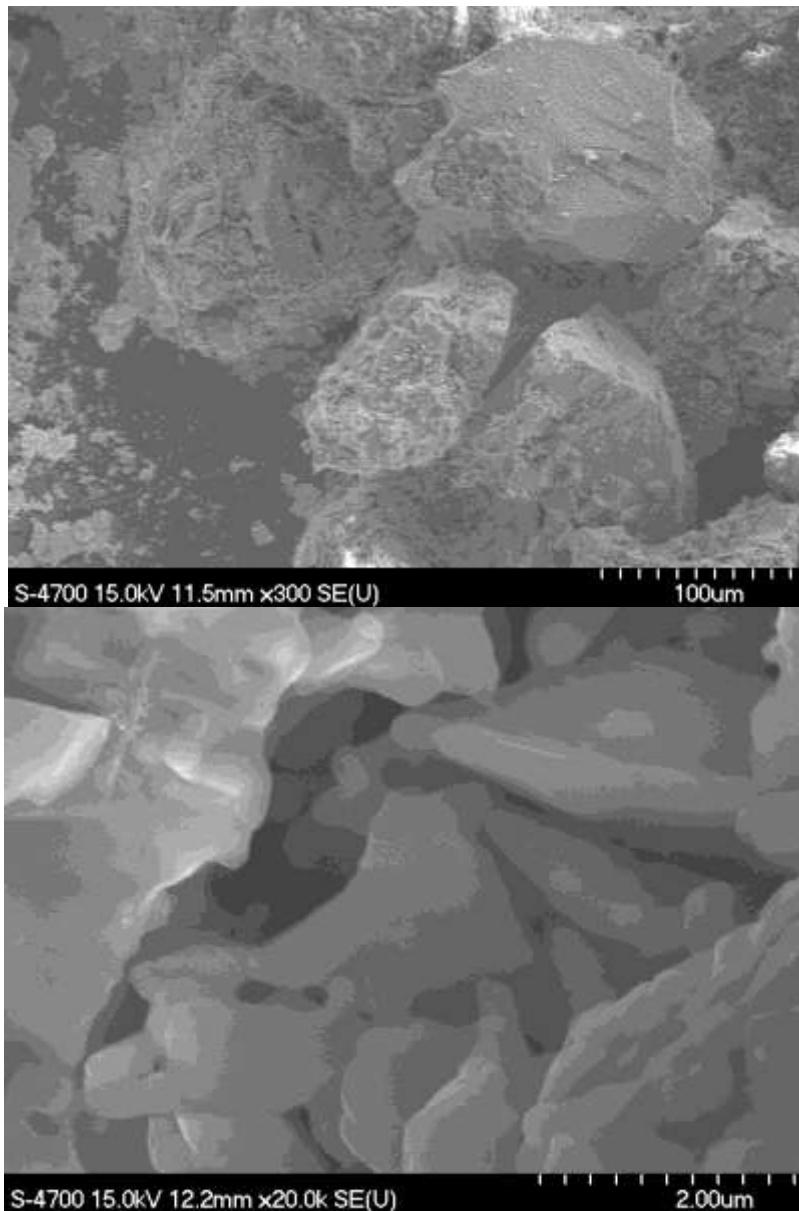


Figure 4.2 SEM micrographs of iron oxide (TPR product)

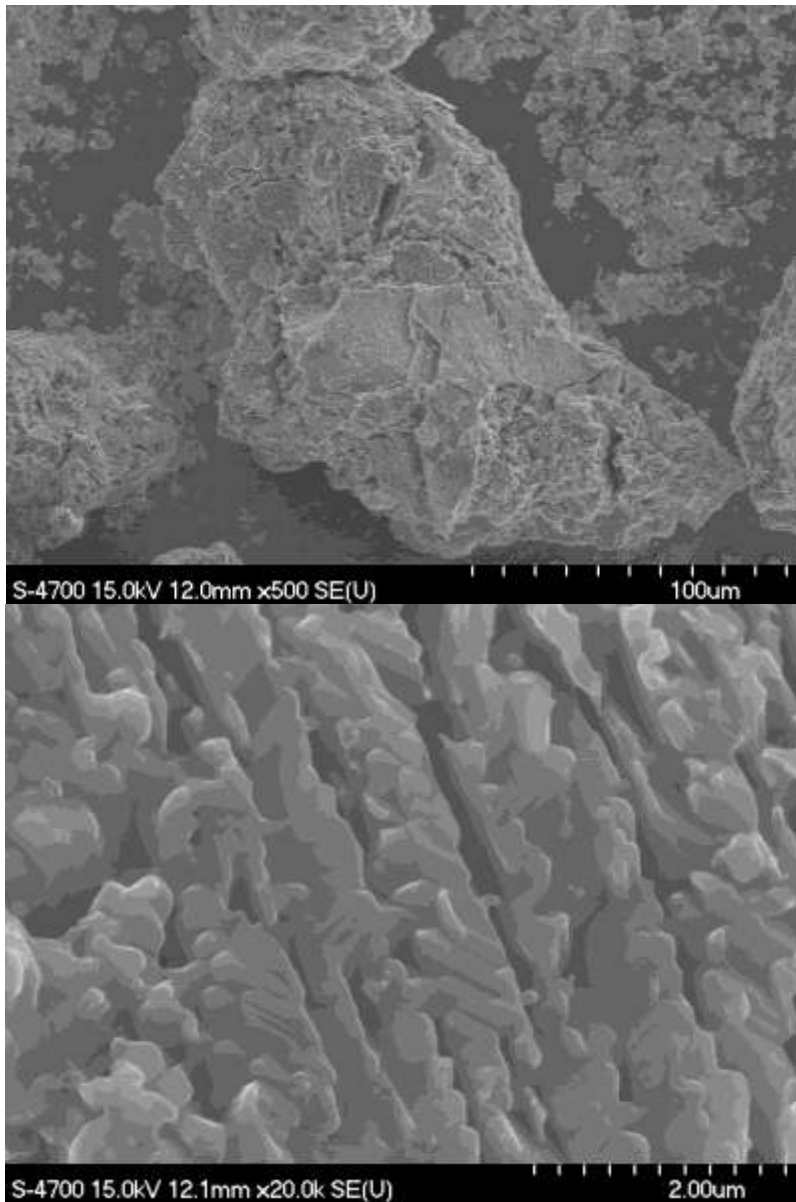


Figure 4.3 SEM micrographs of iron oxide (TGA product)

4.2 TEMPERATURE PROGRAMED REDUCTION RESULTS

Four sets of TPR test, with different operational conditions, have been performed. Table 4.1 shows the summary of test conditions.

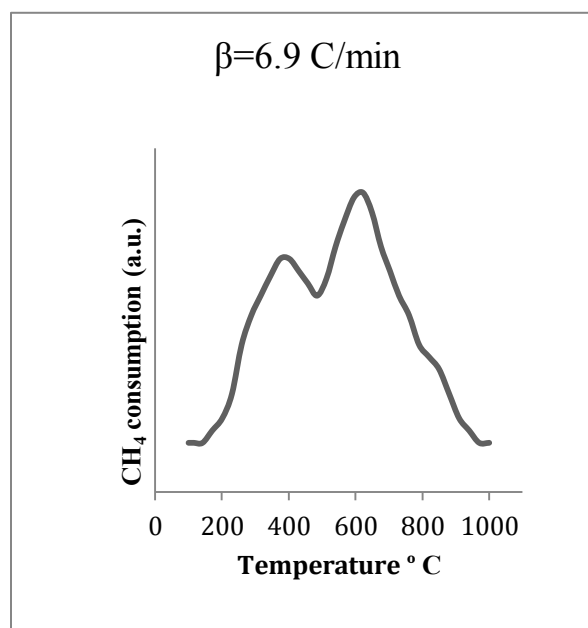
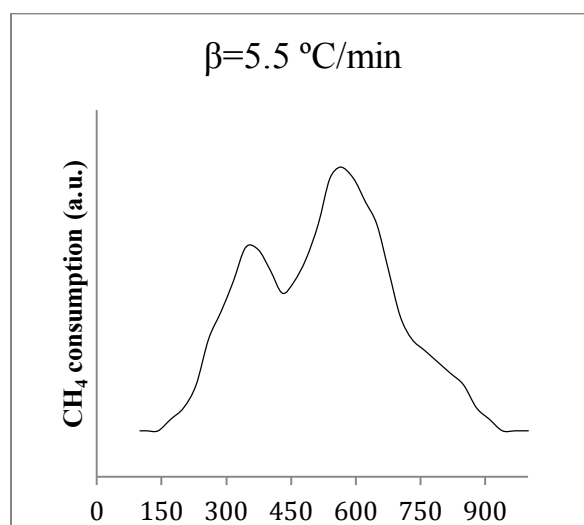
Table 4.1 TPR test conditions and flow rates

	Fe ₂ O ₃	Methane	Argon	Temperature (°C)	Products	β (°C/min)
Test 1	2 g	10 cc/min	100 cc/min	100-800	Fe ₃ O ₄ , CO ₂ , H ₂ O	9.4
Test 2	20 mg	10 cc/min	100 cc/min	100-1100	Fe ₃ O ₄ , FeO, CO ₂ , H ₂ O	5.5
Test 2.1	20 mg	10 cc/min	100 cc/min	100-1100	Fe ₃ O ₄ , FeO, CO ₂ , H ₂ O	6.9
Test 2.2	20 mg	10 cc/min	100 cc/min	100-1100	Fe ₃ O ₄ , FeO, CO ₂ , H ₂ O	9.4
Test 2.3	20mg	10 cc/min	100 cc/min	100-1100	Fe ₃ O ₄ , FeO, CO ₂ , H ₂ O	11.7

The GC reports for the tests are shown in Appendix B. The final results are presented in Fig. 4.4. As shown in Fig 4.4, there are two peaks in each graph which shows a two-step reduction of iron oxide. The first peak can be assigned to the reduction of Fe₂O₃ to Fe₃O₄. This reduction occurs between 350-450 °C, depending on the temperature ramp. The second peak can be assigned to reduction of Fe₃O₄ to FeO. It occurs between 600-800 °C, depending on the temperature ramp. Parameter **P** is calculated for each run, as shown in Table 4.2

Table 4.2 Parameter P for TPR standard condition

	β (°C/min)	S_0 (mole)	FC_0 (mole/min)	P(K)
Test 2	5.5	0.00012	0.0008	0.82
Test 2.1	6.9	0.00012	0.0008	1.03
Test 2.2	9.4	0.00012	0.0008	1.41
Test 2.3	11.7	0.00012	0.0008	1.75



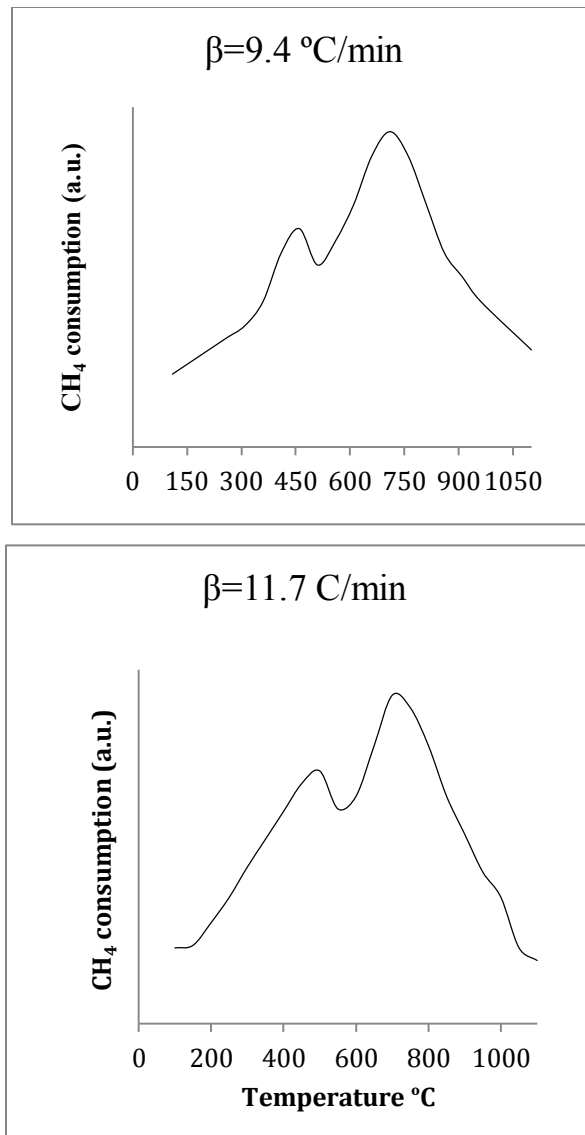


Figure 4.4 Experimental CH₄ TPR profiles of Fe₂O₃ at three different heating rates.

For an accurate result, P should be less than 20 K, and it should be kept as low as possible. It can be concluded that the results became less precise with increasing β . The GC was able to sample every 5 minutes, and a greater value for β results in larger temperature intervals and a smaller number of data points to create the graphs in Fig. 4.4. Figure 4.5a shows an Arrhenius plot based on Kissinger's method extracted from Eq.2.12 and Fig. 4.4 for the first peak while Fig. 4.5b shows the same plot for the second peak. The activation energy for both reactions can be calculated from the trend line of the plot. For the first peak, reduction of Fe₂O₃ to Fe₃O₄, the activation energy was 10.97 (kJ/mol)

and for the second peak, it was 28.43 (kJ/mol). As mentioned before, the activation energy of reduction of Fe_2O_3 to Fe_3O_4 was reported in the literature between 35 and 117 (kJ/mol), if the reducing gas is H_2 and between 14 and 20 (kJ/mol), if the reducing gas is CO (Table 2.6). The iron oxide composition and reducing gas type might be the two main reasons of the difference between the obtained results in different studies. As evident from Fig 4.5b, the Arrhenius plot for the second peak is not as accurate as the one for first peak.

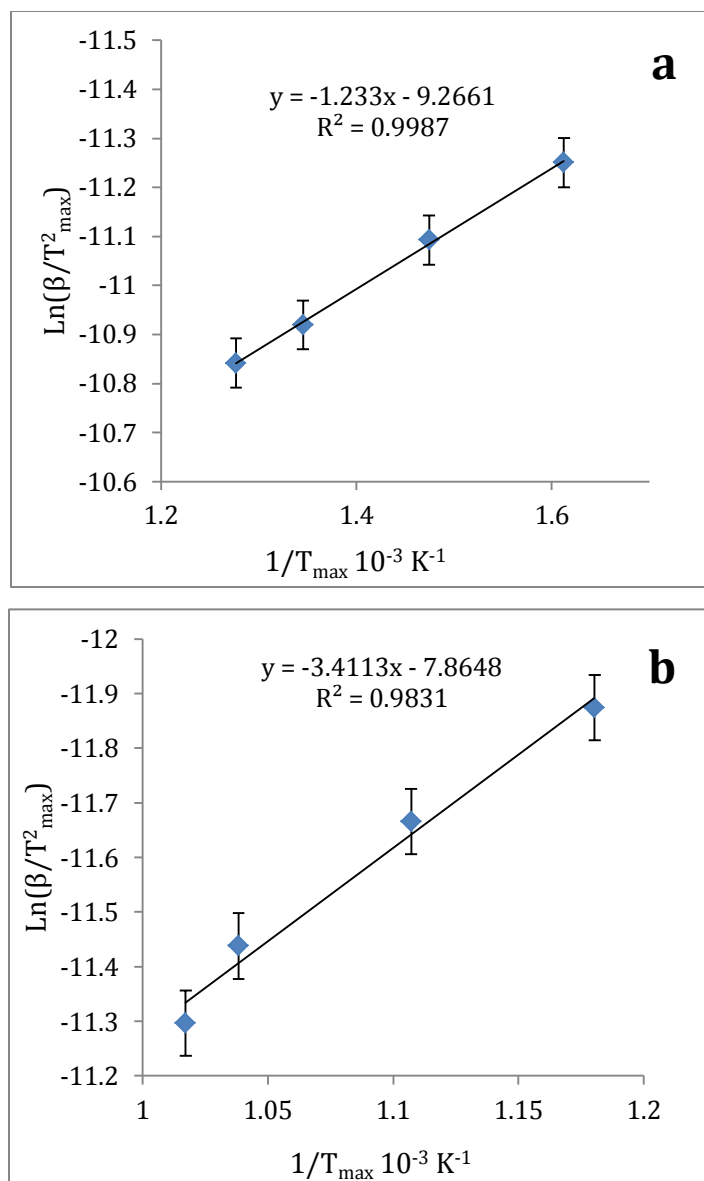


Figure 4.5 Arrhenius plots for TPR of Fe₂O₃ a) for Fe₂O₃ to Fe₃O₄ conversion (first peak) and b) for Fe₃O₄ to FeO conversion (second peak).

4.2.1 EXPERIMENTAL ERROR IN TPR EXPERIMENT

A TPR test has to be performed in a fixed bed reactor. In this experiment, the chamber was designed for 2 g of iron oxide sample. The gas flow for 2g was higher than the GC recommended flow range to analyze the gas mixture properly. This problem required the use of 50 μg of iron oxide and relatively lower flow rates of the gas. However, the chamber should have been designed to be smaller in size, in order to stop the particles from fluidizing. Although the gas flow was too low, and the filters created a significant pressure drop, fixed bed reactor conditions were not fully achieved.

In addition, the inability to maintain a constant temperature ramp, and as a result of that having a fluctuating β instead of a specific β for each experiment provokes further uncertainty in the results (Fig 3.4). Equation 2.7 explains the main concept of this method of kinetic study as assuming a constant β . Inconsistency in the value of β can make a significant difference in the final results.

The conversion rate is calculated by knowing the gas composition at the existing gas temperature. It requires a sampling method in which the gas is analyzed immediately after leaving the reaction zone, where the related gas temperature is recorded. The gas component analyzer of this experiment (GC) was measuring the samples after the gas passed the condenser and desiccator. As a result, the gas related temperature has to be estimated, based on the gas flow rate and the distance between the reaction zone and the GC. Many factors were involved in this estimation which made it almost impossible to be free of errors. It is worth mentioning that by increasing the temperature the accuracy of this estimation was decreased, which explains the difference in the percentage of the error for the first peak and the second peak.

Table 4.3 shows the error calculation chart for this experiment. The maximum error in temperature calculation for TPR test was ± 10 $^{\circ}\text{C}$, which was calculated based on three different runs. Table 4.4 shows calculated activation energies for each run. Based on Table 4.4, the temperature error has resulted different errors in determination of the activation energies. Thus, activation energies of reduction for the first and second stage were determined to be 10.58 ± 0.86 and 25.77 ± 0.83 kJ/mol, respectively.

Table 4.3 Recorded temperatures for each run and the average for each peak.

		Temperature °C		Mean value First peak	Mean value Second peak
		first peak	second peak		
$\beta=5.5$	run1	345	565	343.6	569.6
	run2	339	574		
	run 3	347	570		
$\beta=6.9$	run1	397	621	404	626.3
	run2	405	632		
	run 3	410	626		
$\beta=9.4$	run 1	460	710	462.3	709.3
	run 2	455	701		
	run 3	472	717		
$\beta=11.7$	run 1	499	721	509.6	728.3
	run 2	510	729		
	run 3	520	735		

Table 4.4 Calculated activation energies.

	Activation energy for first peak	Mean	Maximum error	Activation energy for second peak	Mean	Maximum error
Run 1	11.39	10.58	0.86	26.6	25.77	0.83
Run 2	10.64			25.52		
Run 3	9.72			25.19		

4.3 THERMO GRAVIMETRIC ANALYSIS RESULTS

Thermogravimetric Analysis (TGA) was carried out on two samples obtained from the TPR experiments (test 1 and test 2). TGA method characterization is summarized in Table 4.2. For each temperature ramp two different graphs was obtained. One for oxygen consumption vs. temperature and another for weight change percentage vs. temperature. First graph (Fig. 4.6) was used to extract the T_{\max} for each peak. Then Arrhenius plots were obtained (Fig. 4.7) in accordance with Eq.2.11 and Fig. 4.3. The second graph (Fig.4.8) showed evidence for the presence of another kind of iron oxide species for the sample gathered from TPR test 2. The weight percent increase after oxidation can be calculated as follows:

Fe_2O_3 molar weight= 159.6882

Fe_3O_4 molar weight= 231.5356



$$\text{Weight percent change} = \frac{(6 \times 159.6883) - (4 \times 231.5356)}{(4 \times 231.5356)} = 3.45\%$$

It can be concluded from above calculation that the weight percent increase should not be more than 3.45% if the sample contains only Fe_3O_4 , as it did not exceed 3.45% for the iron oxide obtained from TPR test 1. Therefore, XRD was carried out and the result is shown in Appendix A2. The formation of FeO in the sample, in addition to Fe_3O_4 , is evident from the XRD analysis. The weight percent of FeO to Fe_3O_4 can be obtained from the sample's weight gain, shown in Fig.4.8, and also based on the determined stoichiometry of the reactions (Eqs. 4.1 and 4.2). Oxidation of iron oxide happens according to the following reactions:



FeO molar weight= 71.8446

$$\text{Weight percent change} = \frac{(2 \times 231.5356) - (6 \times 71.8446)}{6 \times 71.8446} = 7.4\%$$

Total weight percent change= 4.5% (Fig. 4.8)

$\text{FeO to Fe}_3\text{O}_4 = 4.5 - 3.45 = 1.05\%$ Molar weight change

FeO mass fraction in the feed of TGA: $1.05 \div 7.42 = 0.14$

Regarding the above equations and calculations, the FeO Mass fraction in the sample obtained from TPR test 2 was 0.14. Activation energies were estimated using Fig. 4.7 and Eq.2.11. For the first peak and second peak the activation energies are 14.30 kJ/mol and 86.88 kJ/mol, respectively.

The Fe_3O_4 conversion to FeO occurs in the range of 600 to 800°C, and continues to 1100°C for TPR test 2 conditions and 35 molar percent of the final sample was FeO. It can be concluded that for the TPR test 1, which was completed at 800°C, the amount of FeO in the final sample was negligible. This hypothesis was examined by XRD analysis and the result shows that only Fe_3O_4 was detected in the sample. The TGA weight change percentage graph also shows around 3% weight change, which is reasonable for conversion of Fe_2O_3 to Fe_3O_4 .

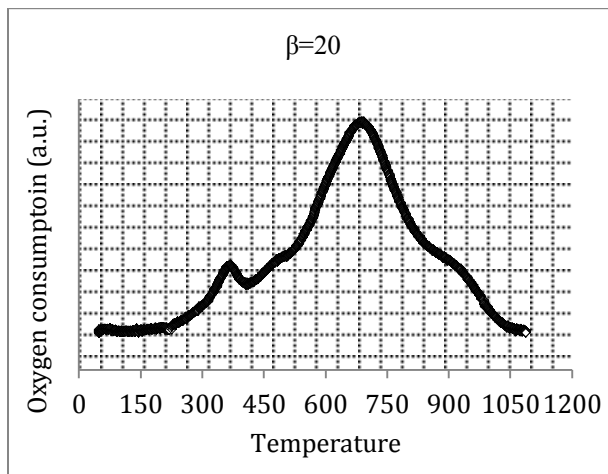
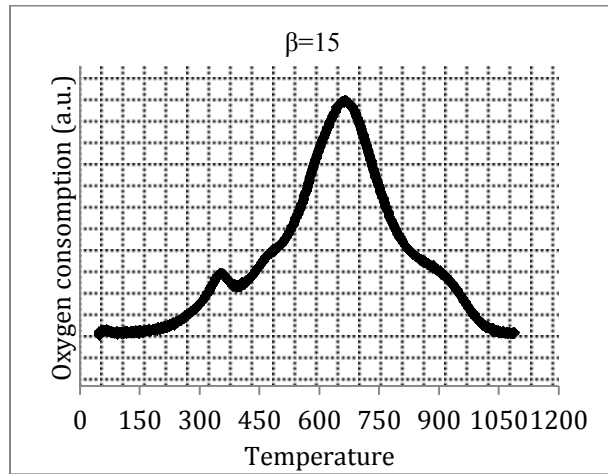
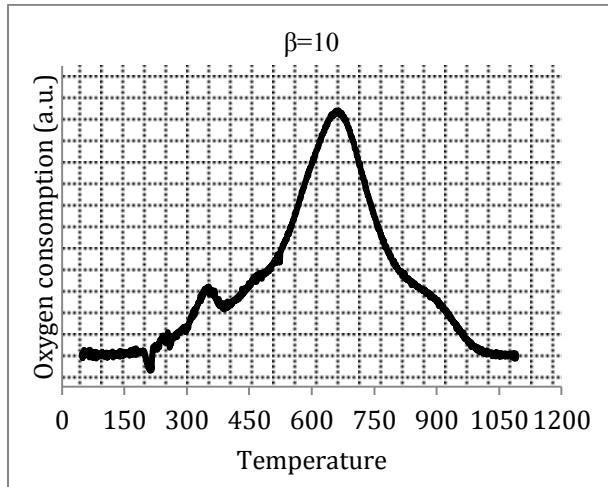


Figure 4.6 TGA graph of oxidation of iron oxide with air at different temperature rates

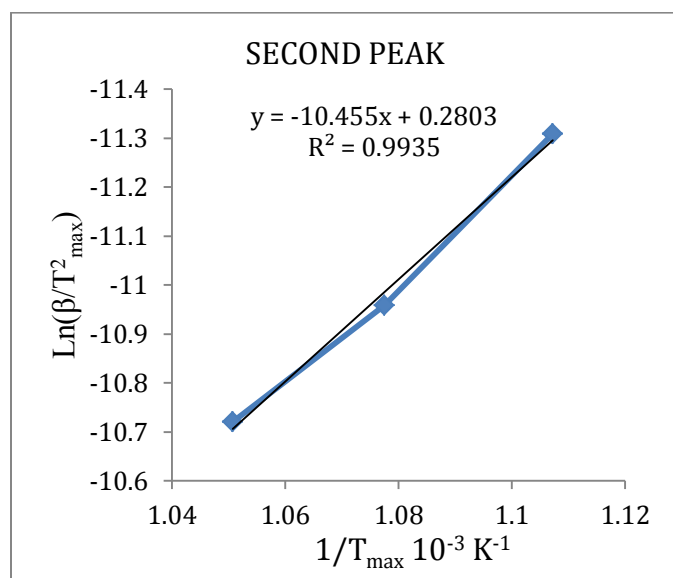
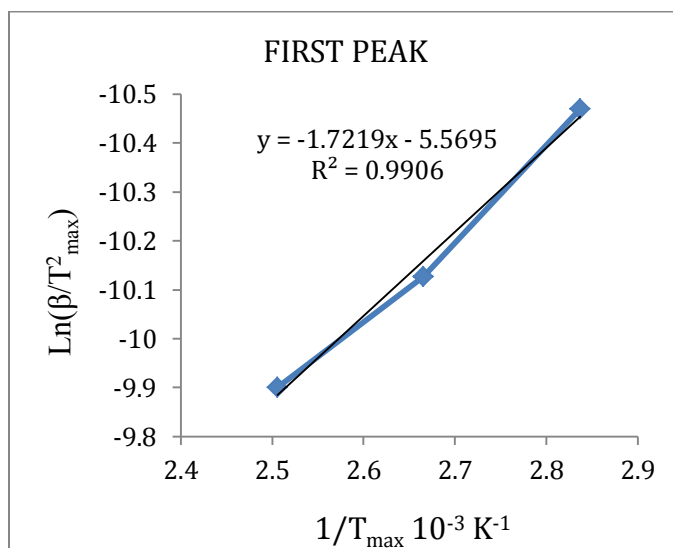


Figure 4.7 Arrhenius plots obtained from TGA of iron oxide with air.

Table 4.5 TGA test conditions

	Iron oxide particle size (µm)	Oxidation gas	Temperature range (°C)	Temperature Ramp(°C/min)
Test1	90-125	Air	50 – 1100	10
Test2	90-125	Air	50 – 1100	15
Test3	90-125	Air	50 – 1100	20

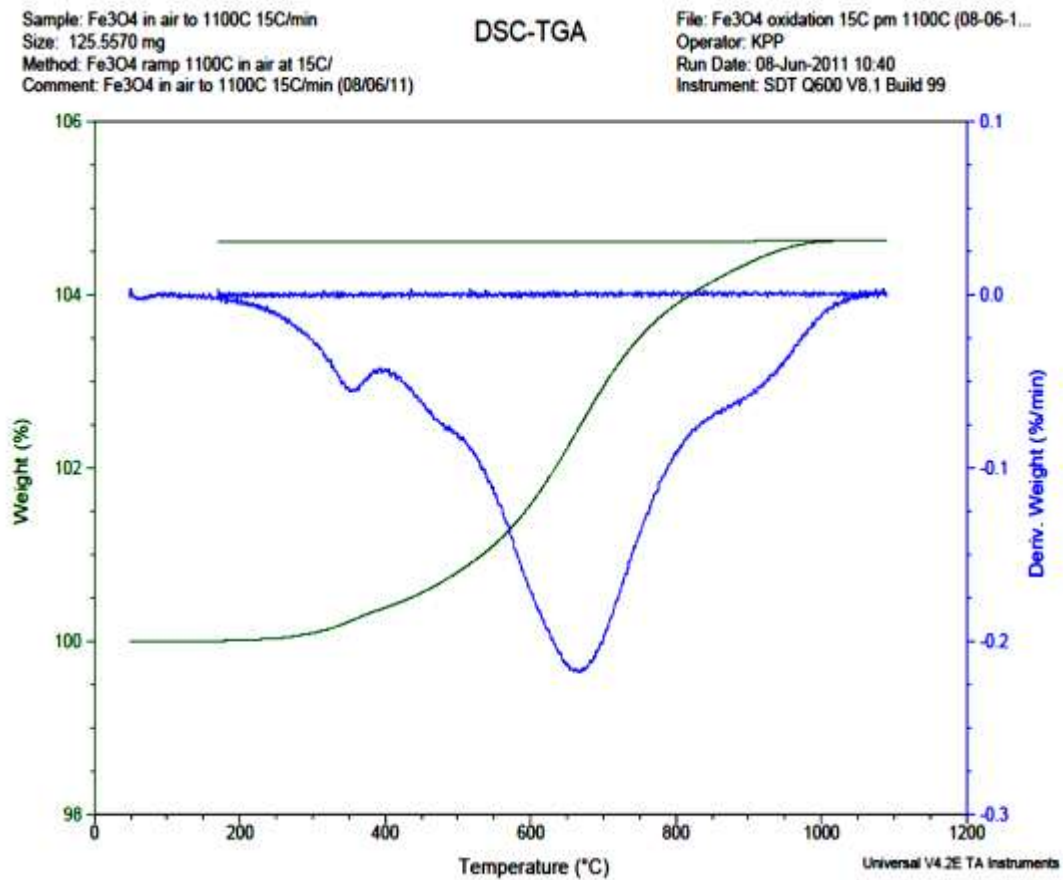


Figure 4.8 TGA graph of oxidation of iron oxide obtained from TPR test 2 with air, $\beta=15^{\circ}\text{C}/\text{min}$

4.4 REACTION MECHANISM

To evaluate the reaction mechanism, integration of Eq. 2.9 should be solved. This integral has been solved numerically using Maple software and the result was:

$$g(\alpha(T)) = \frac{AE}{R\beta} e^{-\frac{E}{RT}} \left(1 + \frac{RT}{E}\right) \quad (2.15)$$

Hence, functions of $g(\alpha(T))$, and consequently $f(\alpha(T))$, are given. Combining the result with Eq. 2.9 and 2.10, simulation of the reaction pattern for different $f(\alpha)$ from Table 2.4 would be possible:

$$\frac{d\alpha}{dT} = \frac{A}{\beta} \cdot \exp\left(-\frac{E}{RT}\right) \cdot f(\alpha(T)) \quad (2.9)$$

Figure 4.9 shows simulated patterns for some of the common solid-gas reaction mechanisms, obtained from a Microsoft Excel spread sheet. The calculations can be seen in Appendix C.

By comparing the simulated reaction patterns with graphs obtained from TGA and TPR, the best mechanism can be assigned for each reaction. The random nucleation mechanism can be assigned to the first peak, reduction of Fe_2O_3 to Fe_3O_4 and two-dimensional diffusion mechanisms can be assigned to the second peak, reduction of Fe_3O_4 to FeO as shown in Fig. 4.10. The same result was achieved for the mechanism of the reactions in the literature, although the flow gas was not the same.

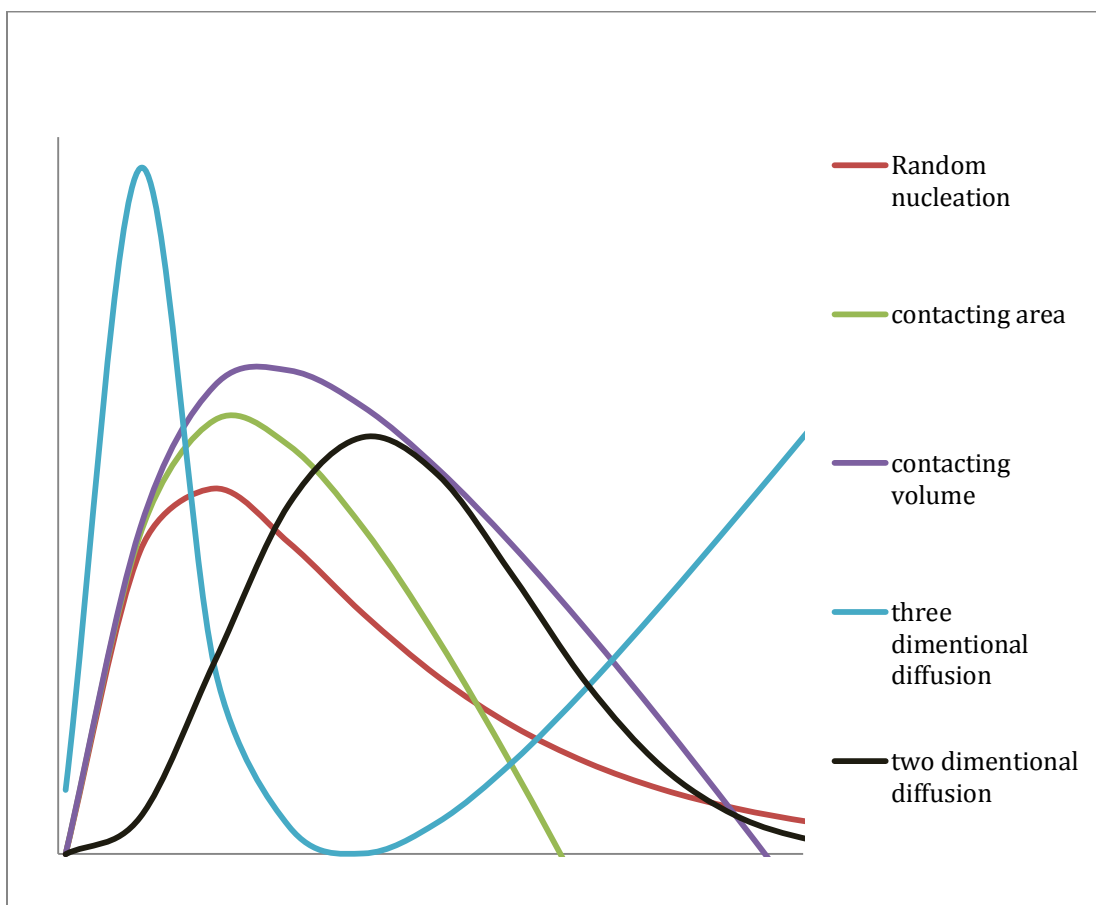


Figure 4.9 Simulated reaction patterns for five reaction mechanisms.

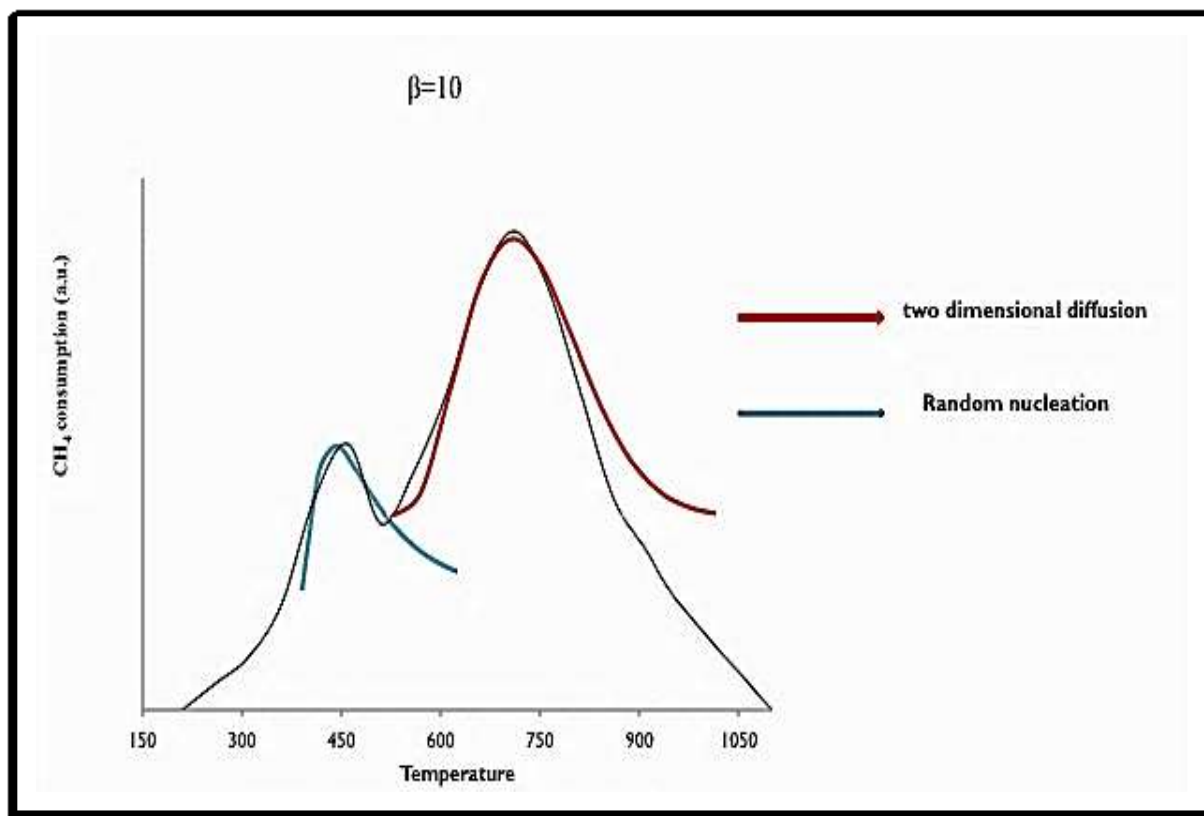


Figure 4.10 TPR simulated patterns compared with calculated data.

CHAPTER 5: CONCLUSIONS

A lab-scale tubular fixed bed reactor was designed and built in order to investigate the kinetics of the reduction of hematite with methane. The temperature program reduction tests were conducted using a gas chromatograph for evaluation of methane consumption. Thermogravimetric analysis was carried out on the reduced iron oxide to return it to its initial state, in order to simulate a CLC cycle condition. Two-stage reduction of iron oxide was observed: Fe_2O_3 reduced to Fe_3O_4 and then reduced to FeO . For the first and second stage of reduction, the activation energies were 10.58 ± 0.86 and 25.77 ± 0.83 kJ/mol, respectively. Integration of the equation for the reaction kinetics was solved using MAPLE 13 and different TPR patterns were calculated. The experimental TPR pattern was compared to the calculated patterns and the random nucleation mechanism was the best fit for the first stage of reduction and the two-dimensional diffusion was the best fit for the second stage of reduction. The calculated activation energies and Arrhenius coefficients were in satisfactory agreement with the previous studies in the literature. By applying the kinetic data gathered in this study, a CLC unit can be modeled and designed for this specific oxygen carrier and fuel. The results of the SEM and XRD tests confirm that the Fe_2O_3 sample did not show any particular change in the shape of the surface after reduction with methane at 1100°C . However, an obvious change in the sample surface was observed after oxidation at 1100°C , with air. In order to use the iron oxide for more than one cycle, the sample should be enhanced by some kind of binder or additive to obtain more heat resistivity. It was also concluded that reduction of Fe_2O_3 at 800°C only formed Fe_3O_4 , and the formation of FeO was observed only at higher temperature.

REFERENCES

- Abdel Halim K. S. (2007). *Isothermal reduction behaviour of Fe₂O₃ /MnO composite materials with solid carbon*. Materials Science and Engineering, **452**:15–22.
- Achar B. N. N., Brindley G. W. Sharp J. H. (1966). Proceedings of the International Clay Conference. Jerusalem, **1**: 67.
- Adanez J., De Diego L. F., Labiano F. G., Gayan P., Abad A. (2004). *Selection of Oxygen Carriers for Chemical-Looping Combustion*. Energy & Fuels, **18**: 371-377.
- Anheden M., Svedberg G. (1998). *Energy analysis of chemical looping combustion systems*. Energy Convers. Mgmt., **39**:1967-1980.
- Cho P., Mattisson T., Lyngfelt A. (2004). *Comparison of iron-, nickel-, copper- and manganese-based oxygen carriers for chemical-looping combustion*. Fuel, **83**: 1215–1225.
- Diego L. F., Labiano F. G., Gayan P., Celaya J., Palacios J. M., Adanez J. (2007). *Operation of a 10 KWth chemical-looping combustor during 200 h with a CuO–Al₂O₃ oxygen carrier*. Fuel, **86**: 1036-1045.
- Everson R. C., Neomagus H. W. J. P., Njapha D. (2006). *Kinetic analysis of non-isothermal thermogravimetric analyser results using a new method for the evaluation of the temperature integral and multi-heating rates*. Fuel, **85**: 418–422.
- Fernandez B., Rueda L., Stefani P. M., Caba K., Mondragin I, Eceiza A. (2007). *Kinetic and thermodynamic studies of the formation of a polyurethane based on 1,6-hexamethylene diisocyanate and poly(carbonate-co-ester)diol*. Thermochemica Acta, **459**: 94–103.
- Flynn G. H., Wall L. A. (1969), Journal of research of the National Bureau of Standards, **70**:487
- Galvita V., Sundmacher K. (2007). *Redox behavior and reduction mechanism of Fe₂O₃-CeZrO₂ as oxygen storage material*, J. Mater Sci., **42**: 9300- 9307.

- Haber J. (1991). *Manual on catalyst characterization*. Pure & App/. Chem., **63**: 1227-1246.
- Hansen J., Sato M., Ruedy R., Lo K., Lea D. W., Elizade M. M. (2006). *Global temperature change*. PNAS, **103**: 39-14293.
- Hossain M. M., Lasa H. I. (2008). *Chemical-looping combustion (CLC) for inherent CO₂ separations—a review*. Chemical Engineering Science, **63**: 4433 – 4451.
- Ishida M., Jin H. (1994). *A novel combustor based on chemical-looping reactions and its reaction kinetics*. Journal of Chemical Engineering of Japan, **27**: 296–301
- Ishida M., Jin H. (1996). *Novel chemical-looping combustor without NO_x formation*. Industrial and Engineering Chemistry Research, **35**: 2469–2472.
- Ishida M., Jin H., Okamoto T. (1995). *A Fundamental Study of a New Kind of Medium Material for Chemical-Looping Combustion*. Energy & Fuels, **10**: 958-963.
- Ishida M., Jin H., Okamoto T. (1998). *Kinetic Behaviour of Solid Particle in Chemical-looping Combustion: Suppressing Carbon Deposition in Reduction*. Energy & Fuels, **12**: 223-229.
- Ishida M., Yamamoto M., Ohba T. (2002). *Experimental results of chemical-looping combustion with NiO/NiAl₂O₄ particle circulation at 1200 °C*. Energy Conversion and Management, **43**: 1469–1478.
- Ishida M., Yamamoto M., Saito Y. (1999). *Experimental works on innovative chemical-looping combustor*. ECOS'99, International conference on efficiency, costs, optimization, simulation and environmental aspects of energy systems, Tokyo, June 8–10: 306–310.
- Jernald E., Mattisson T., Lyngfelt A. (2006). *Thermal analysis of chemical looping combustion*. Chemical Engineering Research and Design, **84**: 795–806
- Jin H. Ishida M. (2004). *A new type of coal gas fueled chemical-looping combustion*. Fuel, **83**: 2411–2417.

Jin H., Okamoto T., Ishida M. (1998). *Development of a Novel Chemical-Looping Combustion: Synthesis of a Looping Material with a Double Metal Oxide of CoO-NiO*. Energy & Fuels, **12**: 1272-1277.

Jin, H., Okamoto T., Ishida M. (1999). *Development of a novel chemical-looping combustion: Synthesis of a solid looping material of NiO/NiAl₂O₄*. Industrial and Engineering Chemistry Research, **38**: 126–132.

Jozwiak W. K., Kaczmarek E., Maniecki T.P., Ignaczak W., Maniukiewicz W. (2007). *Reduction behavior of iron oxides in hydrogen and carbon monoxide atmospheres*. Applied Catalysis, **326**: 17–27.

Kessel D. G. (2000). *Global warming- facts, assessment, countermeasures*. Journal of Petroleum Science and Engineering, **26**: 157–168.

Kanervo J.M. (2003). *Kinetic analysis of temperature-programmed reaction*. Industrial Chemistry publication Series, **16**: 70

Kok M. V., Okanda E. (1995). *Kinetic analysis of in situ combustion processes with Thermogravimetric and differential thermogravimetric analysis and reaction tube experiments*. Journal of analytical and applied pyrolysis, **31**: 63-73.

Leion H., Mattisson T., Lyngfelt A. (2007). *The use of petroleum coke as fuel in chemical-looping combustion*. Fuel, **86**: 1947–1958.

Leion H., Mattisson T., Lyngfelt A. (2008). *Solid fuels in chemical-looping combustion*. international journal of greenhouse gas control, **2**: 180 – 193.

Li K., Wang W., Wei Y., Yan D. (2010). *Direct conversion of methane to synthesis gas using lattice oxygen of CeO₂-Fe₂O₃ complex oxides*. Chemical Engineering Journal, **156**: 512–518.

Lyngfelt A., Johansson M., Mattisson T. (2008). *Chemical looping combustion- Status of development*. 9th International Conference on Circulating Fluidized Beds (CFB-9).

- Lyngfelt A., Leckner B., Mattisson T. (2001). *A fluidized-bed combustion process with inherent CO₂ separation; application of chemical-looping combustion*. Chemical Engineering Science, **56**: 3101–3113.
- Lyngfelt A., Hilmer T. (2005). *Construction and 100 h of operational experience of a 10-kW chemical looping combustor, The CO₂ Capture and Storage Project (CCP) for Carbon Dioxide Storage in Deep Geologic Formations For Climate Change Mitigation*. Volume 1 – Capture and Separation of Carbon Dioxide from Combustion Sources, Chapter 36.
- Malet P., Caballero A. (1988). *The Selection of Experimental Conditions in Temperature programmed Reduction Experiments*. J. Chem. Soc. Faraday Trans. I, **84**: 2369-2375.
- Mattisson T., Johansson M., Lyngfelt A. (2004). *Multi cycle Reduction and Oxidation of Different Types of Iron Oxide Particles Application to Chemical-Looping Combustion*. Energy & Fuels, **18**: 628-637.
- Mattisson T., Lyngfelt A., Cho P. (2001). *The use of iron oxide as an oxygen carrier in chemical looping combustion of methane with inherent separation of CO₂*. Fuel, **80**: 1953-1962.
- Mattisson T., Lyngfelt A. (2001). *Capture of CO₂ using chemical-looping combustion*. In Scandinavian Nordic Section of Combustion Institute. Goteborg.
- Mondal K., Lorethova H., Hippo E., Wiltowski T., Lalvani S. B. (2004). *Reduction of iron oxide in carbon monoxide atmosphere—reaction controlled kinetics*. Fuel Processing Technology, **86**: 33– 47.
- Nakano Y., Iwamoto S., Maeda T., Ishida M., Akehata T. (1986). *Characteristics of reduction and oxidization cyclic process by use of α -Fe₂O₃ medium*. Iron & Steel Journal of Japan, **72**: 1521–1527.
- Pineau A., KAnari N., Gaballah I. (2006). *Kinetics of reduction of iron oxides by H₂ Part I: Low temperature reduction of hematite*. Thermochimica Acta, **447**: 89–100.

Piotrowski K., Mondal K., Lorethova H., Stonawski L., Szymanski T., Wiltowski T. (2005). *Effect of gas composition on the kinetics of iron oxide reduction in a hydrogen production process*. International Journal of Hydrogen Energy, **30**: 1542-1554.

Ptacek P., Kubatova D., havilca J., Brandstetr J., Soukal F., Opravil T. (2010). *The non-isothermal kinetic analysis of the thermal decomposition of kaolinite by thermogravimetric analysis*. Powder Technology, **204**: 222–227.

Ryu H. J., Bae D. H., Han K. H., Lee S. Y. (2001). *Oxidation and Reduction Characteristics of Oxygen Carrier Particles and Reaction Kinetics by Unreacted Core Model*. Korean J. Chem. Eng., **18**: 831-837.

Sanchez M. E., Otero M., Gomez X., Moran A. (2009). *Thermogravimetric kinetic analysis of the combustion of biowastes*. Renewable Energy, **34**: 1622–1627.

Sharp J. H., Wentworth S. A. (1969). *Kinetic Analysis of Thermogravimetric Data*. Analytical chemistry, **41**(14).

Smith J. M. (1981). *Chemical engineering kinetics*. McGraw-Hill, 3rd edition.

Tans P. (2011). Retrieved from NOAA/ESRL (www.esrl.noaa.gov/gmd/ccgg/trends/).

Yu Lin H., Chen Y. W., Li C. (2003). *The mechanism of reduction of iron oxide by hydrogen*. Thermochimica Acta, **400**: 61–67.

APPENDIX A1: SCANNING ELECTRON MICROSCOPE (SEM) ANALYSIS

Chemical looping combustion

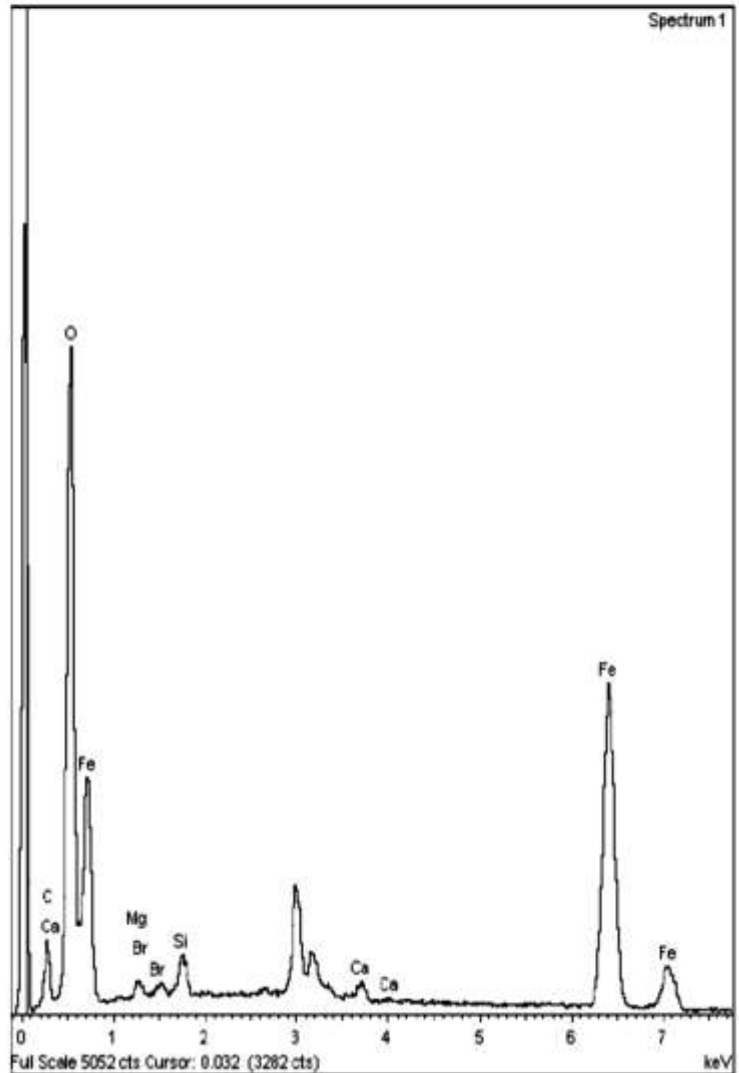
Sample: Iron oxide raw material
Type: Default
ID:

Spectrum processing:
Peaks possibly omitted: 2.635, 2.987, 3.174 keV

Processing option: All elements analyzed
(Normalized)
Number of iterations = 4

Standard:
C CaCO₃ 1-Jun-1999 12:00 AM
O SiO₂ 1-Jun-1999 12:00 AM
Mg MgO 1-Jun-1999 12:00 AM
Si SiO₂ 1-Jun-1999 12:00 AM
Ca Wollastonite 1-Jun-1999 12:00 AM
Fe Fe 1-Jun-1999 12:00 AM
Br KBr 1-Jun-1999 12:00 AM

Element	Weight%	Atomic%
C K	8.57	19.04
O K	30.53	50.92
Mg K	0.60	0.66
Si K	1.10	1.05
Ca K	0.82	0.54
Fe L	57.65	27.55
Br L	0.74	0.25
Totals	100.00	



Chemical looping combustion

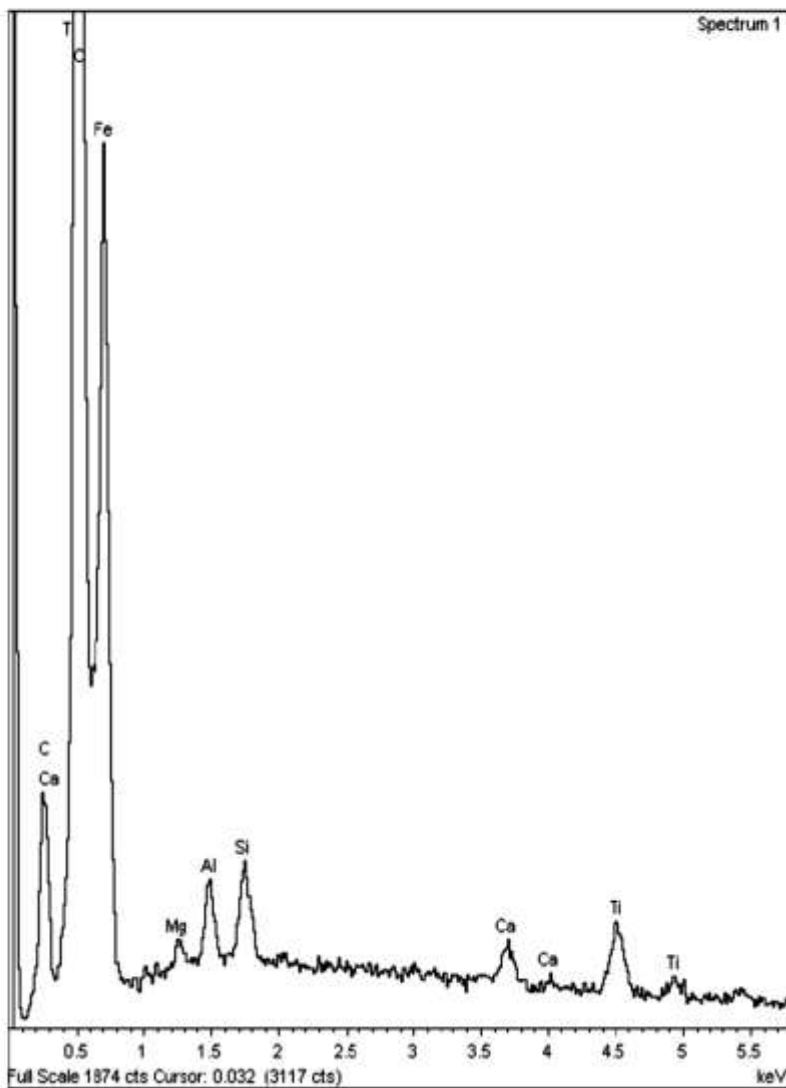
Sample: Iron oxide TGA product
 Type: Default
 ID:

Spectrum processing:
 Peak possibly omitted: 5.435 keV

Processing option : All elements analyzed
 (Normalized)
 Number of iterations = 4

Standard:
 C CaCO₃ 1-Jun-1999 12:00 AM
 O SiO₂ 1-Jun-1999 12:00 AM
 Mg MgO 1-Jun-1999 12:00 AM
 Al Al₂O₃ 1-Jun-1999 12:00 AM
 Si SiO₂ 1-Jun-1999 12:00 AM
 Ca Wollastonite 1-Jun-1999 12:00 AM
 Ti Ti 1-Jun-1999 12:00 AM
 Fe Fe 1-Jun-1999 12:00 AM

Element	Weight%	Atomic%
C K	7.57	17.54
O K	28.38	49.34
Mg K	0.32	0.36
Al K	0.78	0.80
Si K	0.78	0.77
Ca K	0.52	0.36
Ti K	1.55	0.90
Fe L	60.10	29.93
Totals	100.00	



Chemical looping combustion

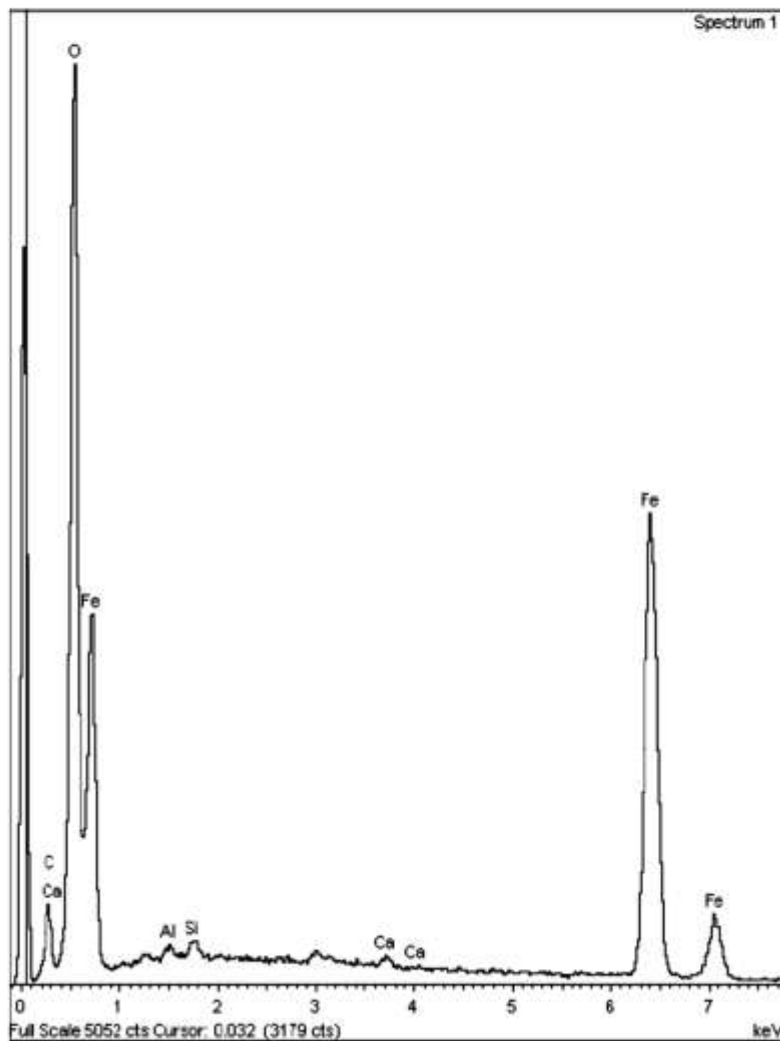
Sample: Iron oxide TPR product
Type: Default
ID:

Spectrum processing :
Peak possibly omitted : 2.985 keV

Processing option : All elements analyzed
(Normalised)
Number of iterations = 4

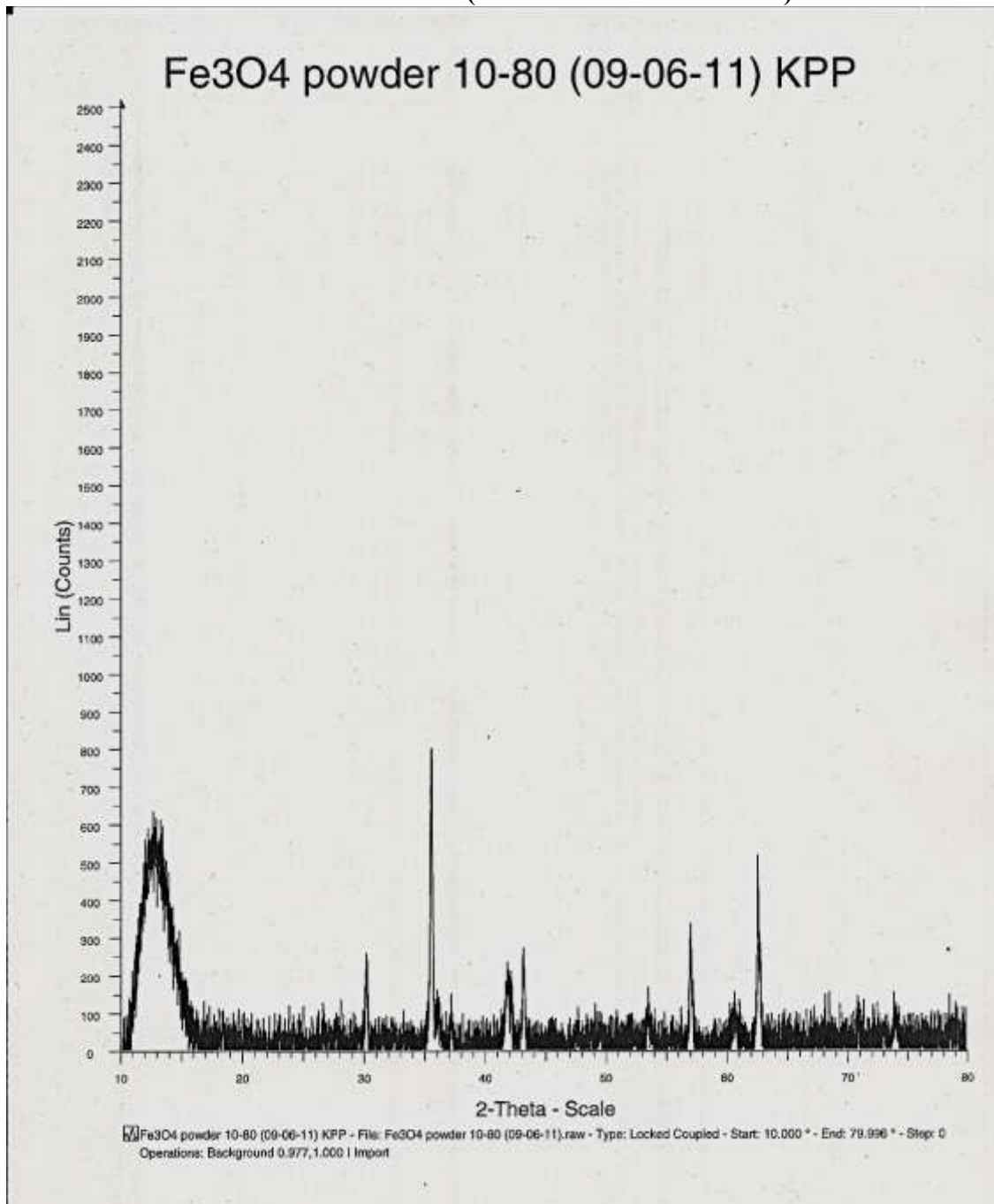
Standard :
C CaCO₃ 1-Jun-1999 12:00 AM
O SiO₂ 1-Jun-1999 12:00 AM
Al Al₂O₃ 1-Jun-1999 12:00 AM
Si SiO₂ 1-Jun-1999 12:00 AM
Ca Wollastonite 1-Jun-1999 12:00 AM
Fe Fe 1-Jun-1999 12:00 AM

Element	Weight%	Atomic%
C K	6.32	14.92
O K	29.37	52.05
Al K	0.23	0.25
Si K	0.36	0.37
Ca K	0.34	0.24
Fe L	63.37	32.18
Totals	100.00	



APPENDIX A2: X-RAY DIFFRACTION ANALYSIS (XRD)

APPENDIX A2.1: XRD SPECTRUM (TGA TEST 2 PRODUCT)



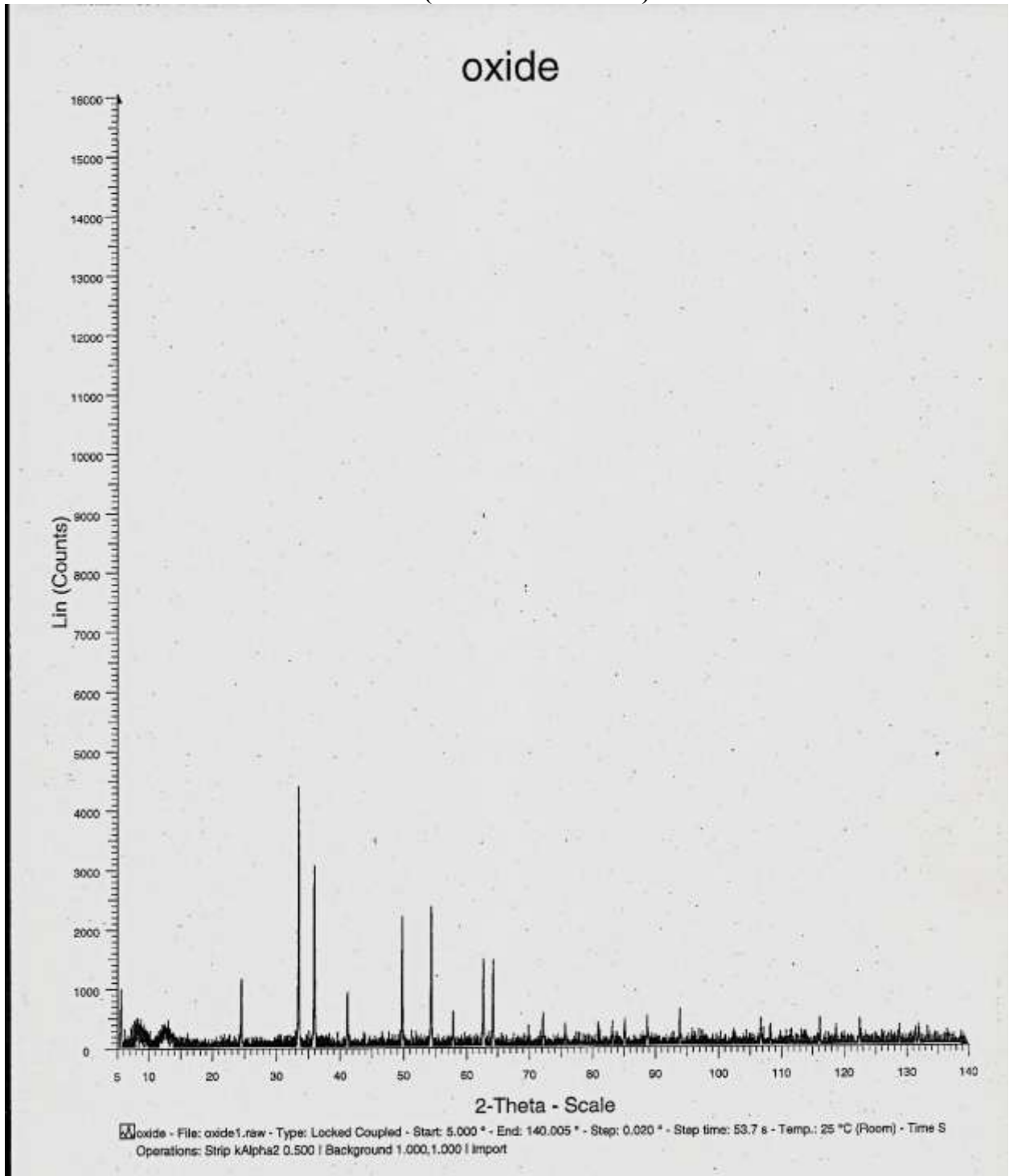
APPENDIX A2.2: XRD ANALYSIS SHOWING THE PRESENCE OF FEO IN TGA TEST 2 SAMPLE

Pattern : 01-089-0687		Radiation = 1.540600		Quality : High	
FeO		d (Å)	<i>h</i>	<i>k</i>	<i>l</i>
		2.49762	680	1	1
		2.16300	999	2	0
		1.52947	466	2	2
Iron Oxide		1.30434	165	3	1
Wustite, syn		1.24881	115	2	2
Lattice : Face-centered cubic		Mol. weight = 71.85			
S.G. : Fm-3m (225)		Volume (Å ³) = 80.96			
a = 4.32000		Dx = 5.095			
Z = 4		R _{int} = 5.01			
<p>Calculated Pattern Original Remarks: REM NDP. Test from ICSD: At least one TF missing. ICSD Collection Code: 82233. Temperature of Data Collection: 298 K. Note: Rietveld profile refinement applied. ANX: AX. Wyckoff Sequence: b a (FM3-M). Unit Cell Data Source: Rietveld or profile fit analysis. Data collection flag: Ambient.</p>					
<p>Calculated from ICSD using POWD-12++ Fjellvag, H., Gronvold, F., Stolen, S., Hauback, B., J. Solid State Chem., volume 124, page 52 (1996)</p>					
Radiation : CuKα1		Filter :			
Lambda : 1.54060		d-sp : Calculated spacings			
SS/POW : FS=1000(0.0000,5)					

APPENDIX A2.3: XRD ANALYSIS SHOWING THE PRESENCE OF Fe_3O_4 IN TGA TEST 2 SAMPLE

Pattern : 03-065-3107		Radiation = 1.540600		Quality : Indexed	
Fe_3O_4		<i>d</i> (Å)	<i>h</i>	<i>k</i>	<i>l</i>
Iron Oxide		4.84426	57	1	1
		2.96649	285	2	2
		2.52983	999	3	1
		2.42213	75	2	2
		2.09763	205	4	0
		1.92491	11	3	3
		1.71270	84	4	2
		1.61475	254	5	1
		1.48324	360	4	4
		1.41825	6	3	3
		1.32685	28	6	2
		1.27954	68	5	3
		1.26492	28	6	2
		1.21106	22	4	4
		1.17491	3	7	1
		1.12123	26	6	4
		1.09235	102	7	3
		1.04881	37	8	0
		1.02506	1	7	3
		0.98883	12	8	2
		0.96885	51	7	5
		0.96246	11	6	6
		0.93809	24	8	4
		0.92098	2	9	1
		0.89443	6	6	6
		0.87956	35	9	3
		0.86635	84	8	4
		0.84328	1	7	7
		0.82276	16	10	2
		0.81114	47	9	5
		0.80738	11	10	2
Lattice : Face-centered cubic S.G. : Fd-3m (227) a = 8.39050 Z = 8		Mol. weight = 231.54 Volume [CD] = 590.70 Dx = 5.207 Mcor = 5.23			
Temperature Factor: IB-Fe ₃ O ₄ . Minor Warning: No e.s.d reported/abstracted on the cell dimension. No R factor reported/abstracted. NIST Collection Code: N AL3917. Data collection flag: Ambient.					
Calculated from NIST using POWD-12++ N.Tombs, Acta Crystallogr., volume 4, page 474 (1951)					
Radiation : CuKα1 Lambda : 1.54060 SS/FOM : F30=1000(0.0000,33)		Filter : d-sp : Calculated spacings			

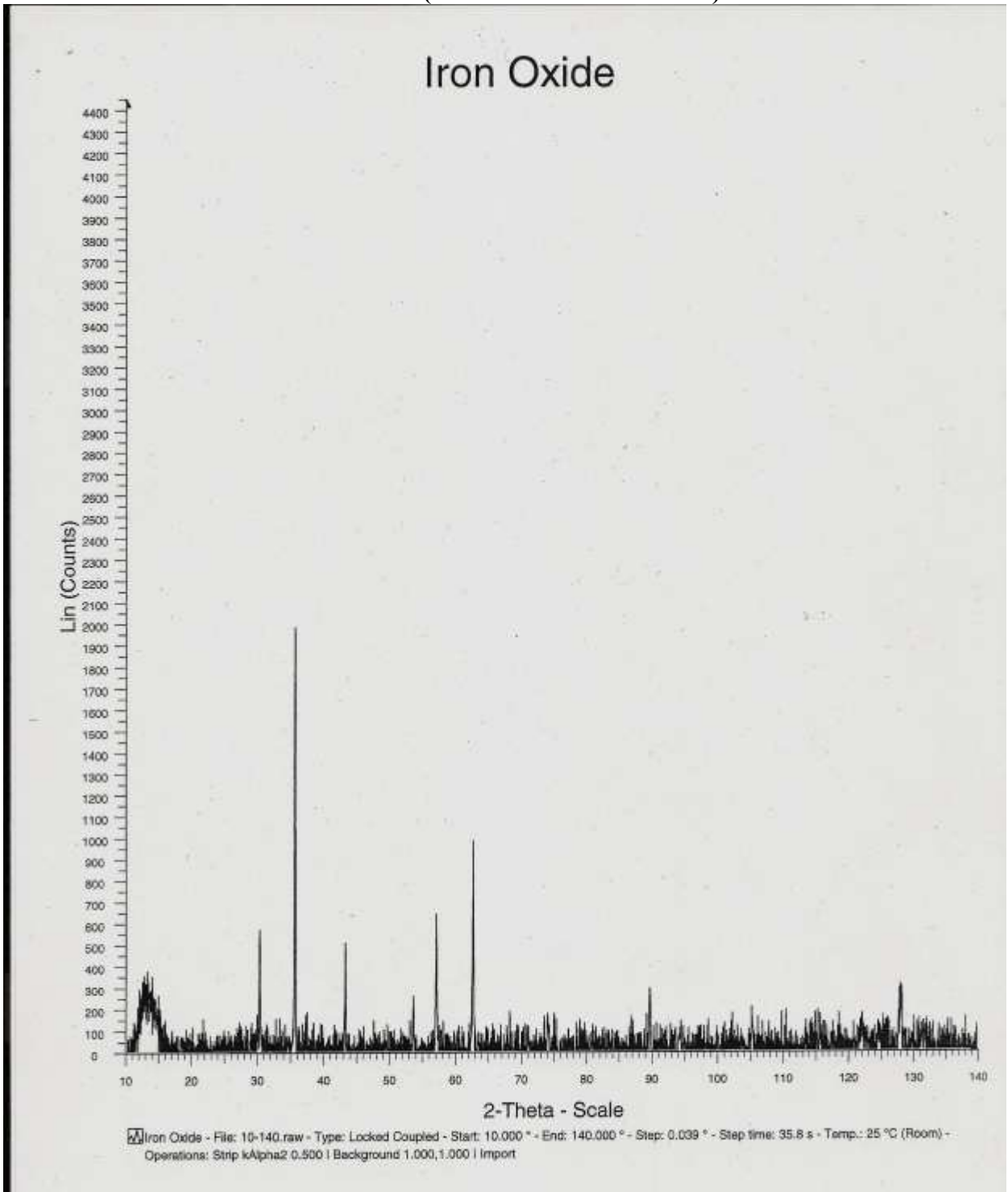
APPENDIX A2.4: XRD SPECTRUM (RAW MATERIAL)



APPENDIX A2.5: XRD ANALYSIS SHOWING THE PRESENCE OF Fe_2O_3 IN RAW MATERIAL

Pattern : 01-089-8104		Radiation = 1.540600		Quality : High		
<p>Fe_2O_3</p> <p>Iron Oxide Also called: diiron(III) oxide, Hematite, syn</p>		d (Å)	l	h	k	i
		3.67278	313	0	1	2
		2.69197	999	1	0	4
		2.51150	704	1	1	0
		2.28467	20	0	0	6
		2.20095	190	1	1	3
		2.07314	17	2	0	2
		1.83639	341	0	2	4
		1.69002	410	1	1	6
		1.63245	5	2	1	1
		1.59981	23	1	2	2
		1.59427	85	0	1	8
		1.48239	254	2	1	4
		1.45002	245	3	0	0
		1.41004	2	1	2	5
		1.34599	25	2	0	8
		1.30742	92	1	0	10
		1.30233	22	1	1	9
		1.26920	3	2	1	7
		1.25575	51	2	2	0
		1.22426	19	0	3	6
		1.21086	9	2	2	3
		1.20184	1	1	3	1
		1.18822	14	3	1	2
		1.18635	34	1	2	8
		1.15969	44	0	2	10
		1.14233	2	0	0	12
		1.13802	60	1	3	4
		1.10047	56	2	2	6
<p>Lattice : Rhombohedral</p> <p>S.G. : R-3c (167)</p> <p>$a = 5.02900$</p> <p>$c = 13.70800$</p> <p>$Z = 6$</p>		<p>Mol. weight = 159.69</p> <p>Volume [CD] = 299.52</p> <p>$Dx = 5.312$</p> <p>$Mcor = 3.26$</p>				
<p>Additional Patterns: See PDF 01-089-8103. ICSD Collection Code: 88418. Temperature Factor: ATF, ANX: A2X3. Wyckoff Sequence: e c (R3-CF). Data collection flag: Ambient.</p>						
<p>Calculated from ICSD using POWD-12++ Yu, S.-C., Lee, J.-S., Tung, S.-F., Lan, C.-L., J. Geol. Soc. China, volume 42, page 349 (1999)</p>						
<p>Radiation : CuKα1</p> <p>Lambda : 1.54060</p> <p>SS/FOM : F28=1000(0.0000,29)</p>		<p>Filter :</p> <p>d-sp : Calculated spacings</p>				

APPENDIX A2.6: XRD SPECTRUM (TGA TEST 1 PRODUCT)



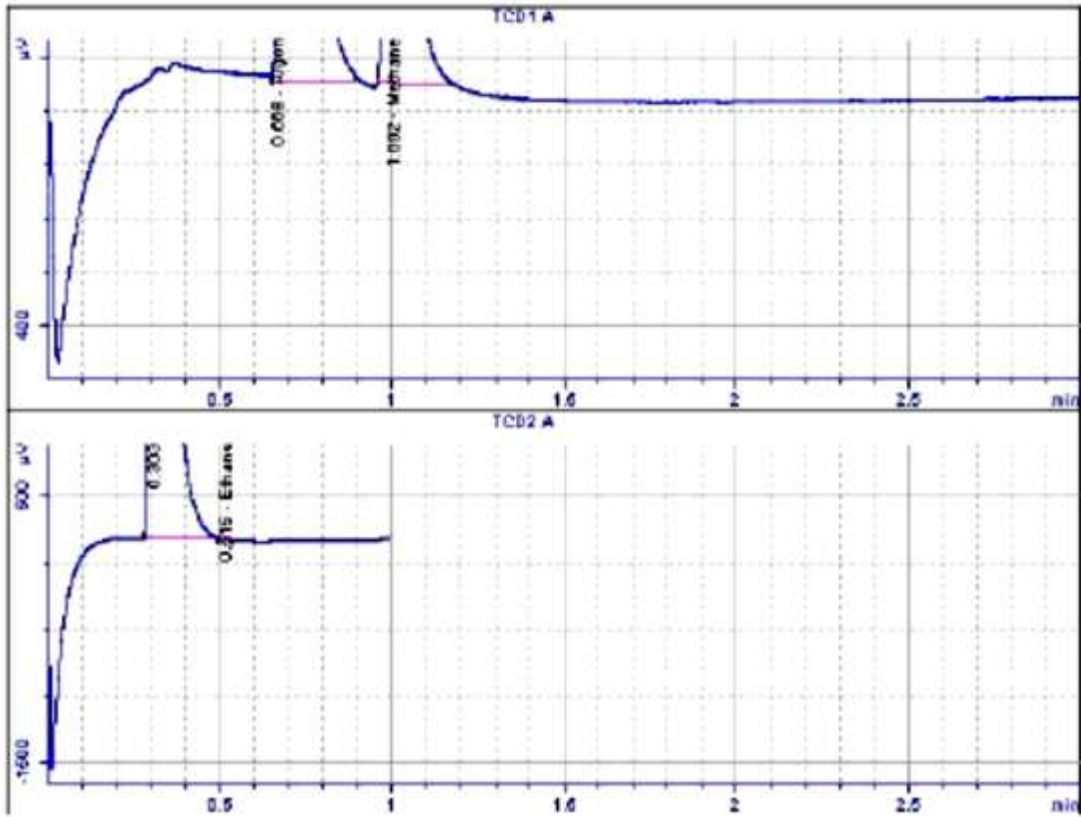
APPENDIX A2.7: XRD ANALYSIS SHOWING THE PRESENCE OF Fe_3O_4 IN TGA TEST 1 PRODUCT

Pattern : 03-065-3107		Radiation = 1.540630		Quality : Indexed		
Fe_3O_4		<i>d</i> (Å)	<i>i</i>	<i>h</i>	<i>k</i>	<i>l</i>
Iron Oxide		4.84426	67	1	1	1
		2.96649	285	2	2	0
		2.52983	999	3	1	1
		2.42213	75	2	2	2
		2.09763	205	4	0	0
		1.92491	11	3	3	1
		1.71270	84	4	2	2
		1.61475	254	5	1	1
		1.48324	360	4	4	0
		1.41825	6	5	3	1
		1.32665	28	6	2	0
		1.27954	68	5	3	3
		1.26492	28	6	2	2
		1.21106	22	4	4	4
		1.17491	3	7	1	1
		1.12123	28	6	4	2
		1.09235	102	7	3	1
		1.04881	37	8	0	0
		1.02506	1	7	3	3
		0.98683	12	8	2	2
		0.96885	51	7	5	1
		0.96246	11	6	6	2
		0.93909	24	8	4	0
		0.92098	2	9	1	1
		0.89443	6	6	6	4
		0.87958	35	9	3	1
		0.85635	84	8	4	4
		0.84328	1	7	7	1
		0.82276	16	10	2	0
		0.81114	47	9	5	1
		0.80738	11	10	2	2
<p>Temperature Factor: IB=Fe₃O₄. Minor Warning: No e.s.d reported/abstracted on the cell dimension. No Rfactor reported/abstracted. NIST Collection Code: N AL3917. Data collection flag: Ambient.</p>						
<p>Calculated from NIST using POWD-12++ N.Tombs, Acta Crystallogr., volume 4, page 474 (1951)</p>						
<p>Radiation : CuKα1 Lambda : 1.54060 SS/FOM : F30=1000(0.0000,33)</p>		<p>Filter : d-sp : Calculated spacings</p>				

APPENDIX B1: GAS CHROMATOGRAPH FILES OF TPR

(B=5)

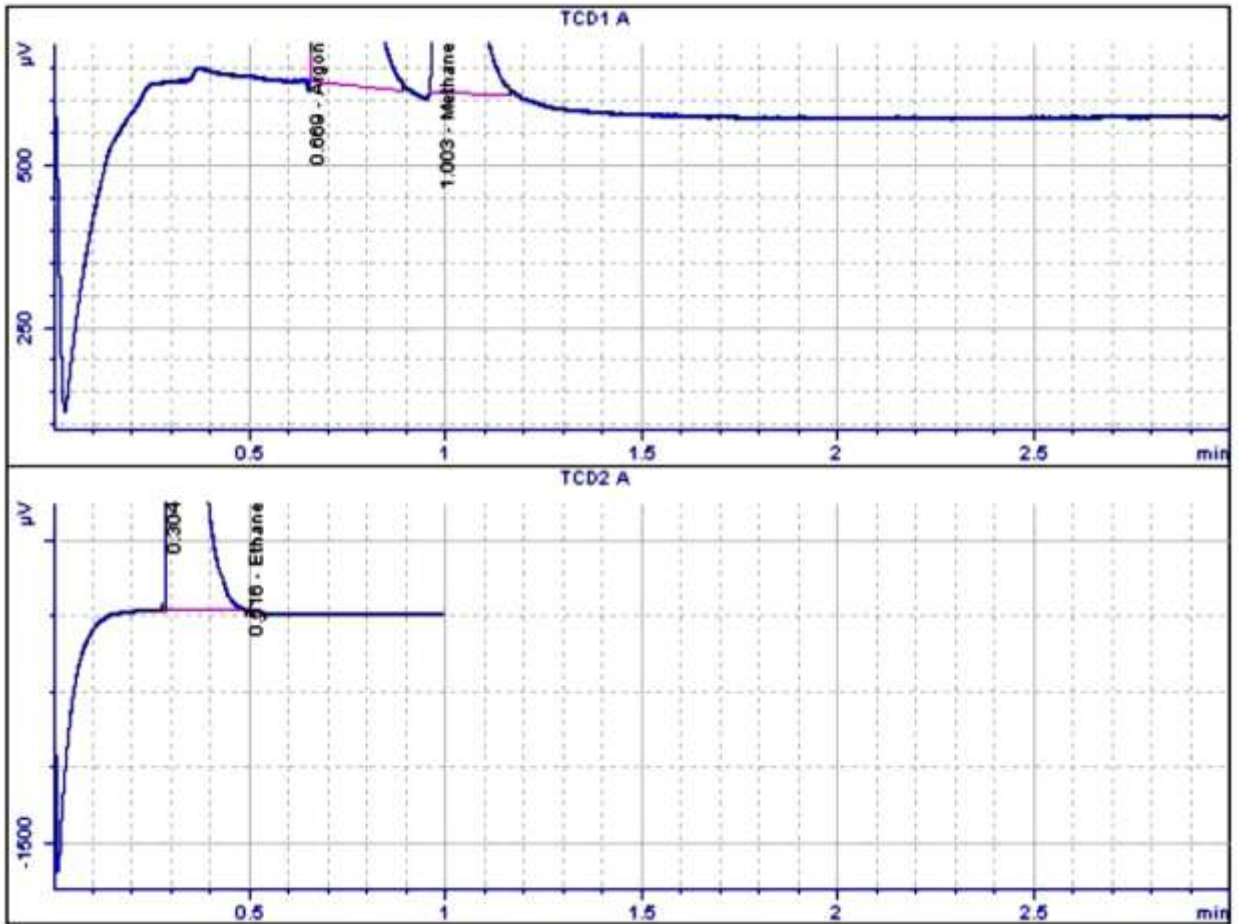
First run



Signal	Retention Time [min]	Type	Area [$\mu V \cdot s$]	Amt/Area	Norm %	Name
1	0.574		-	-	-	Neon
1	0.668	PB	9.7921e+005	7.61245e-005	91.024650	Argon
1	0.717		-	-	-	Oxygen
1	0.866		-	-	-	Nitrogen
1	1.002	BB	5.6571e+004	1.29910e-004	8.974140	Methane
1	1.187		-	-	-	Carbon Dioxide
1	1.465		-	-	-	Carbon Monoxide
2	0.303	BBOS	6.0000e+039	0.00000e+000	0.000000	
2	0.469		-	-	-	Ethylene
2	0.515	PBA	16.74334	5.91779e-005	0.001210	Ethane
2	0.671		-	-	-	Acetylene

Total norm percent = 100.00000

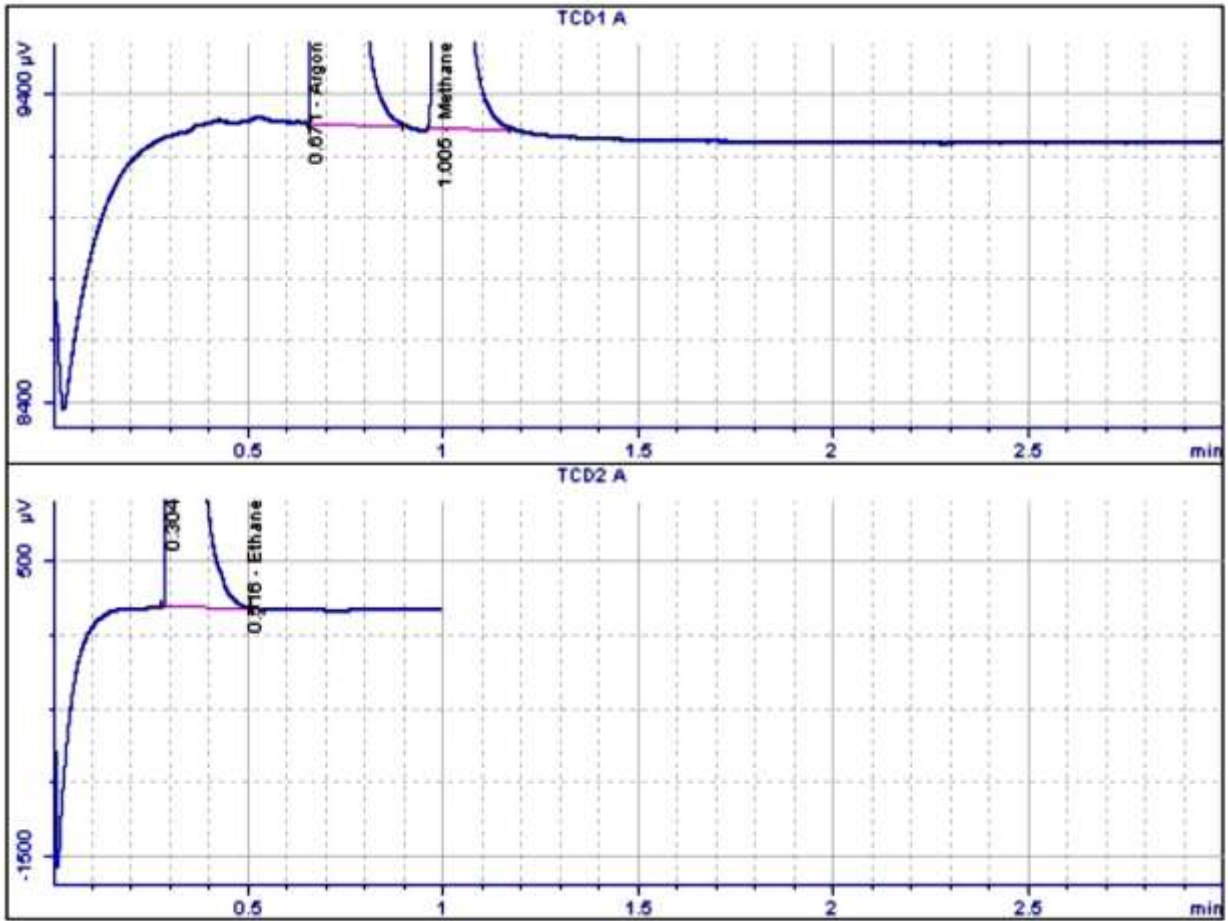
Second run, after 5 minutes



Signal	Retention Time [min]	Type	Area [µV*s]	Amt/Area	Norm %	Name
1	0.574		-	-	-	Neon
1	0.669	BB	9.7630e+005	7.61245e-005	90.987371	Argon
1	0.717		-	-	-	Oxygen
1	0.866		-	-	-	Nitrogen
1	1.003	BB	5.6661e+004	1.29910e-004	9.011515	Methane
1	1.187		-	-	-	Carbon Dioxide
1	1.465		-	-	-	Carbon Monoxide
2	0.304	BBOS	6.2000e+039	0.00000e+000	0.000000	
2	0.469		-	-	-	Ethylene
2	0.516	PBA	15.37632	5.91779e-005	0.001114	Ethane
2	0.671		-	-	-	Acetylene

Total norm percent = 100.00000

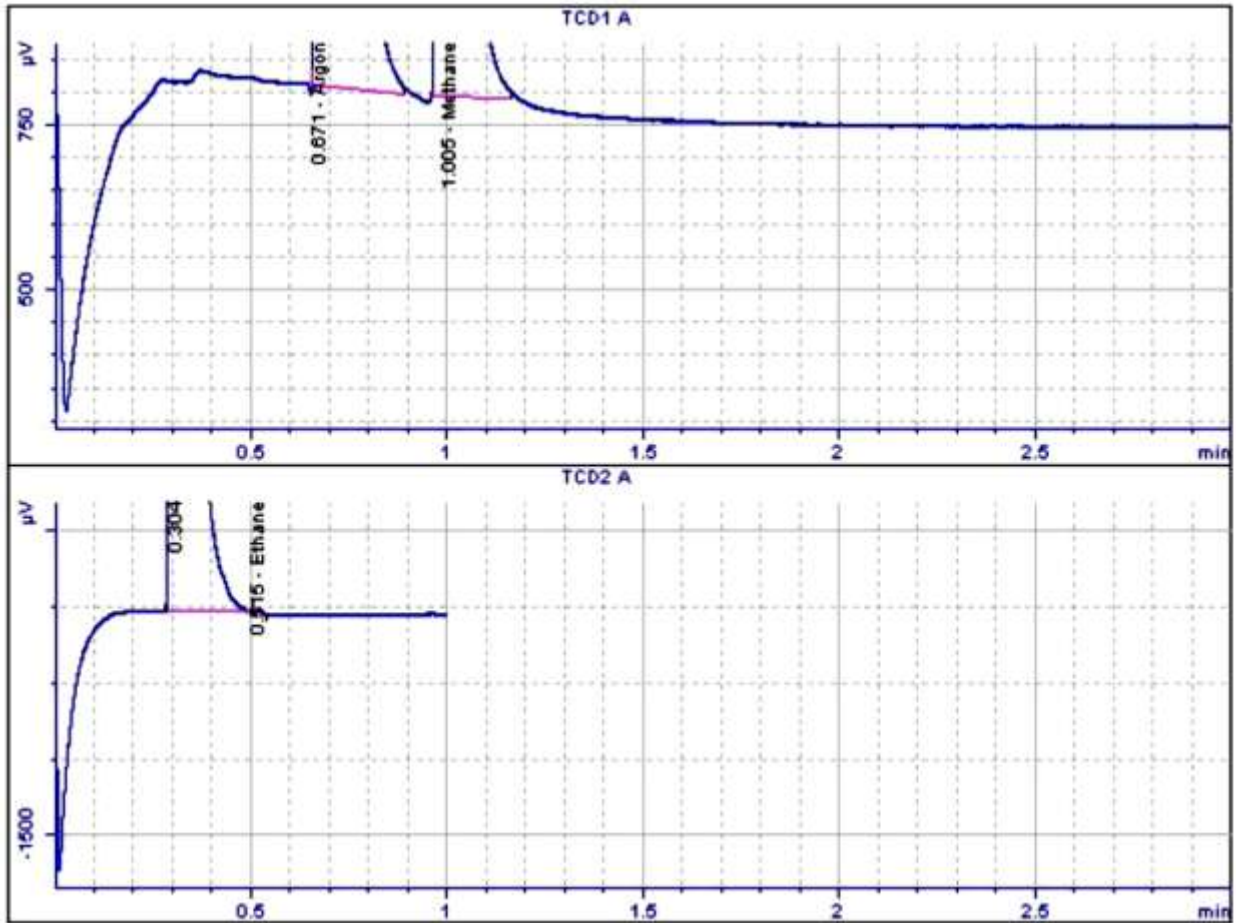
Third run, after 10 minutes



Signal	Retention Time [min]	Type	Area [$\mu\text{V}\cdot\text{s}$]	Amt/Area	Norm %	Name
1	0.574		-	-	-	Neon
1	0.671	PB	9.7206e+005	7.61245e-005	91.001804	Argon
1	0.717		-	-	-	Oxygen
1	0.866		-	-	-	Nitrogen
1	1.005	BB	5.6317e+004	1.29910e-004	8.997317	Methane
1	1.187		-	-	-	Carbon Dioxide
1	1.465		-	-	-	Carbon Monoxide
2	0.304	BBOS	6.2000e+039	0.00000e+000	0.000000	
2	0.469		-	-	-	Ethylene
2	0.516	BBA	12.08604	5.91779e-005	0.000880	Ethane
2	0.671		-	-	-	Acetylene

Total norm percent = 100.00000

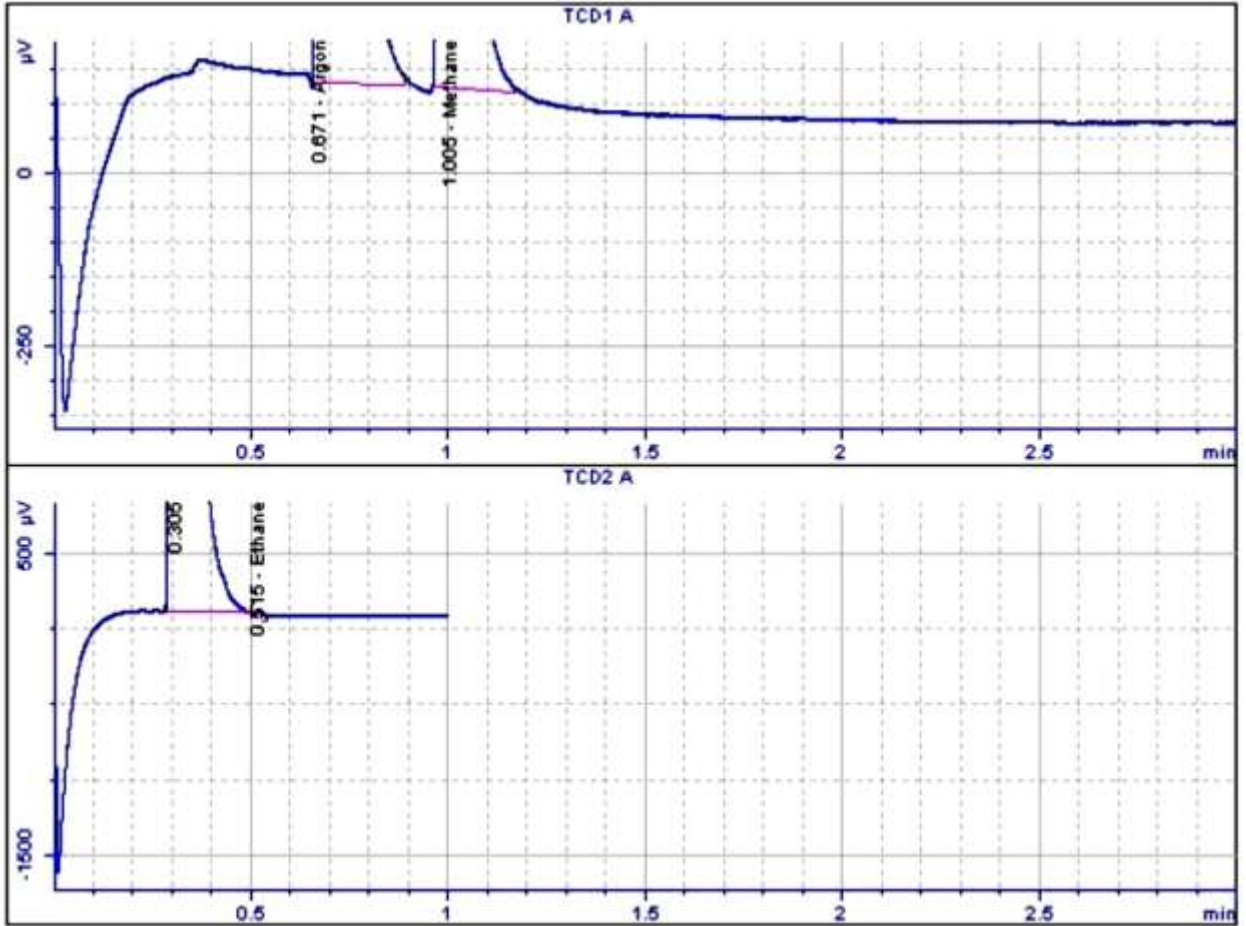
Forth run, after 15 minutes



Signal	Retention Time [min]	Type	Area [µV*s]	Amt/Area	Norm %	Name
1	0.574		-	-	-	Neon
1	0.671	BB	9.7320e+005	7.61245e-005	91.013587	Argon
1	0.717		-	-	-	Oxygen
1	0.866		-	-	-	Nitrogen
1	1.005	BB	5.6302e+004	1.29910e-004	8.985525	Methane
1	1.187		-	-	-	Carbon Dioxide
1	1.465		-	-	-	Carbon Monoxide
2	0.304	BBOS	6.0000e+039	0.00000e+000	0.000000	
2	0.469		-	-	-	Ethylene
2	0.515	BBA	12.22058	5.91779e-005	0.000888	Ethane
2	0.671		-	-	-	Acetylene

Total norm percent = 100.00000

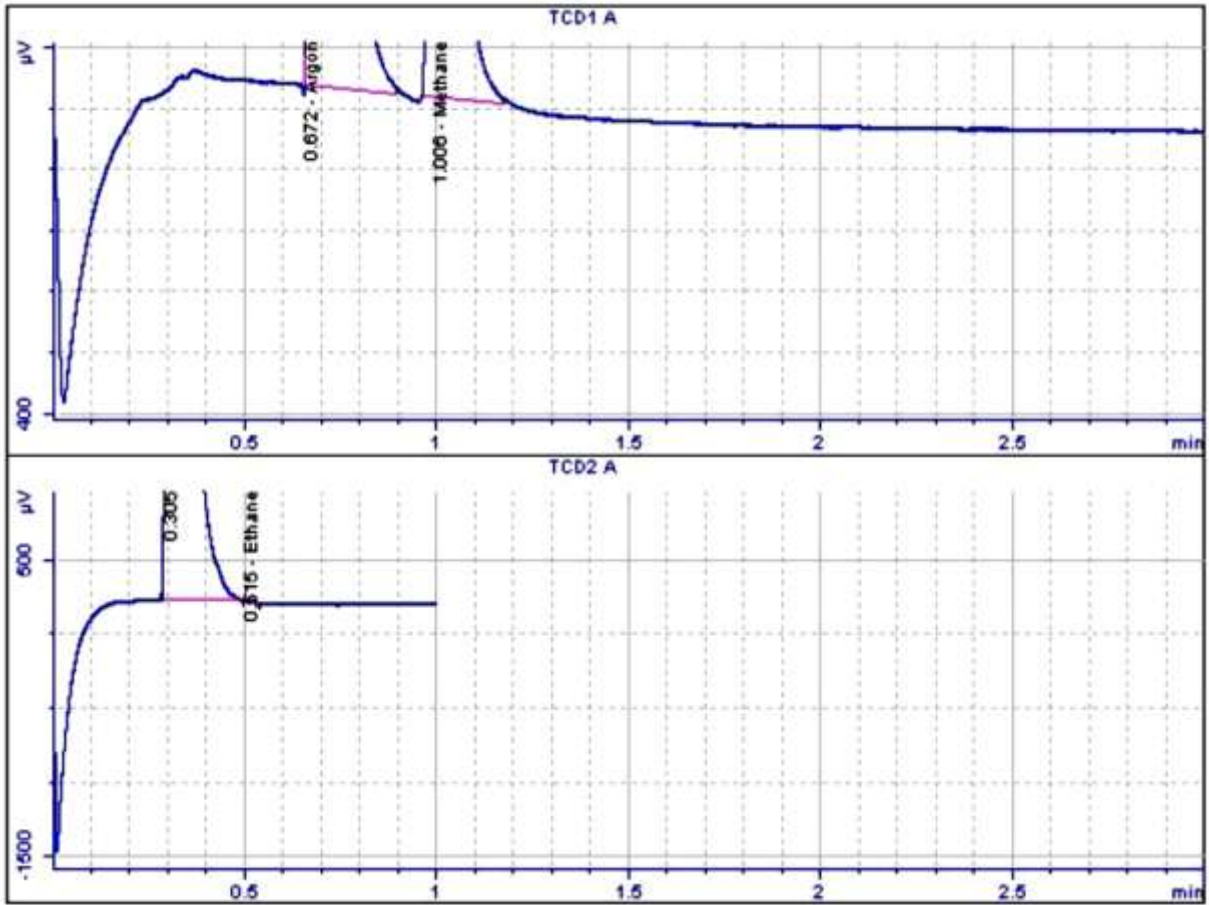
Fifth run, after 20 minutes



Signal	Retention Time [min]	Type	Area [µV*s]	Amt/Area	Norm %	Name
1	0.574		-	-	-	Neon
1	0.671	PB	9.7194e+005	7.61245e-005	91.048446	Argon
1	0.717		-	-	-	Oxygen
1	0.866		-	-	-	Nitrogen
1	1.005	BB	5.5988e+004	1.29910e-004	8.950505	Methane
1	1.187		-	-	-	Carbon Dioxide
1	1.465		-	-	-	Carbon Monoxide
2	0.305	BBOS	6.0000e+039	0.00000e+000	0.000000	
2	0.469		-	-	-	Ethylene
2	0.515	BBA	14.41002	5.91779e-005	0.001049	Ethane
2	0.671		-	-	-	Acetylene

Total norm percent = 100.00000

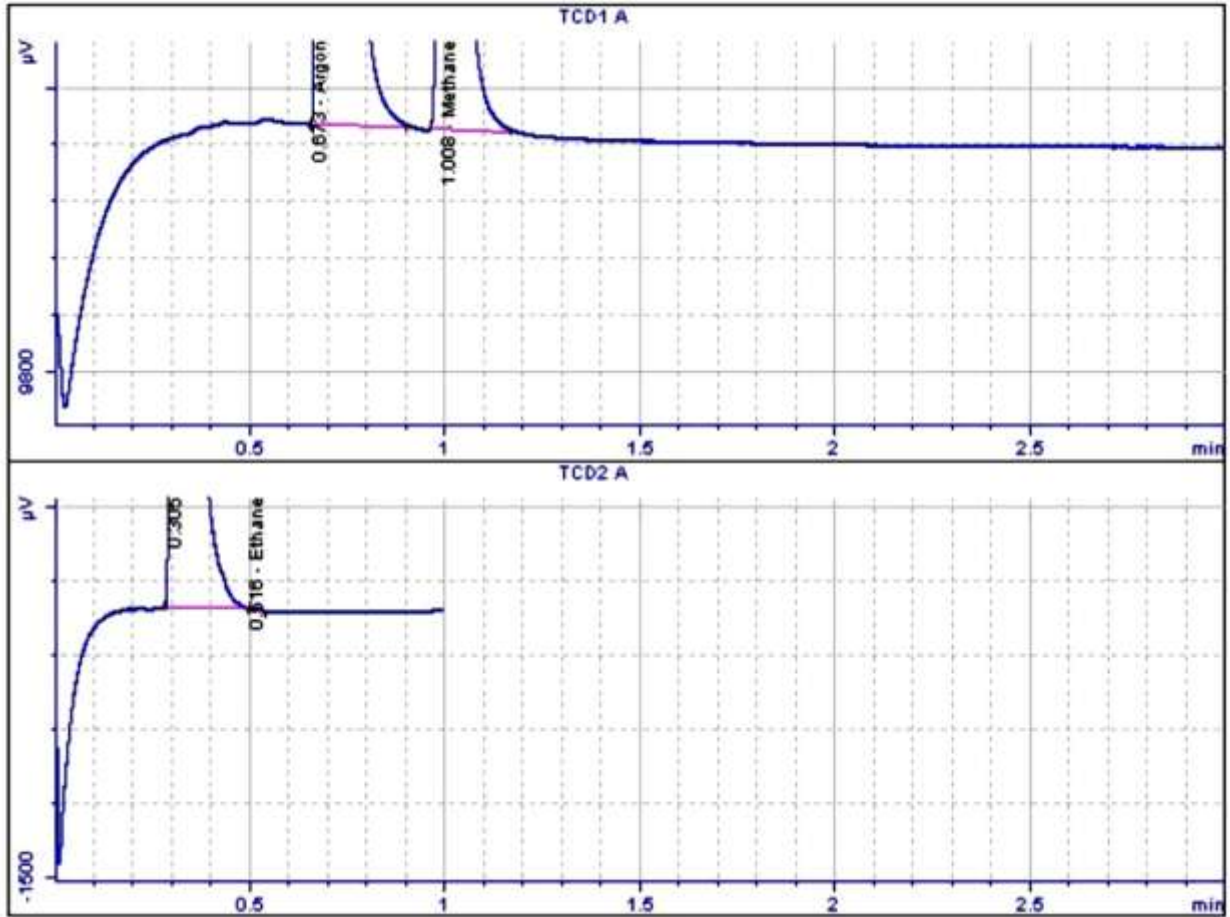
Sixth run, after 25 minutes



Signal	Retention Time [min]	Type	Area [µV*s]	Amt/Area	Norm %	Name
1	0.574		-	-	-	Neon
1	0.672	BB	9.6962e+005	7.61245e-005	91.028499	Argon
1	0.717		-	-	-	Oxygen
1	0.866		-	-	-	Nitrogen
1	1.006	BB	5.5991e+004	1.29910e-004	8.970410	Methane
1	1.187		-	-	-	Carbon Dioxide
1	1.465		-	-	-	Carbon Monoxide
2	0.305	BBOS	6.0000e+039	0.00000e+000	0.000000	
2	0.469		-	-	-	Ethylene
2	0.515	PBA	14.95103	5.91779e-005	0.001091	Ethane
2	0.671		-	-	-	Acetylene

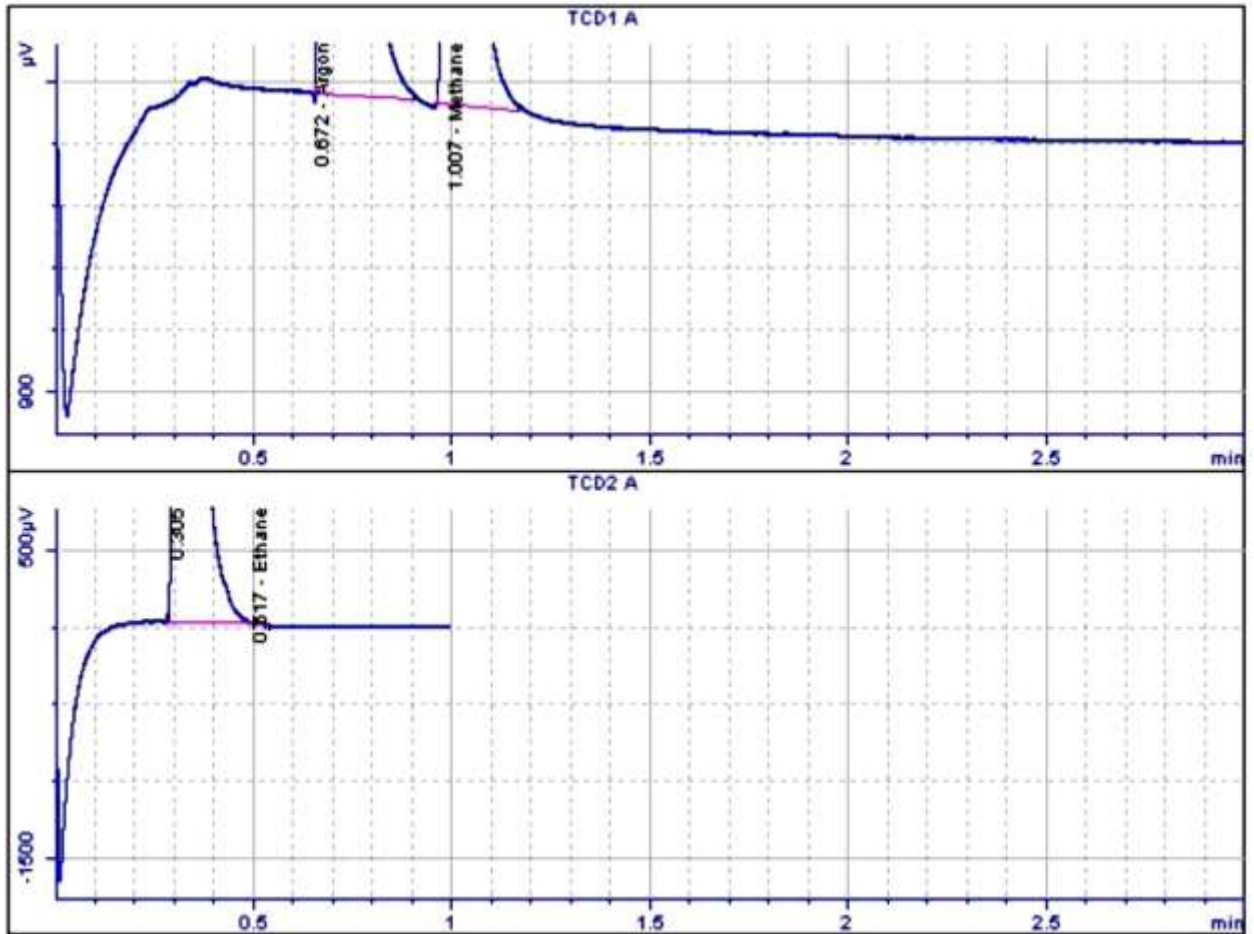
Total norm percent = 100.00000

Seventh run, after 30 minutes



Signal	Retention Time [min]	Type	Area [μV*s]	Amt/Area	Norm %	Name
1	0.574		-	-	-	Neon
1	0.673	PB	9.6642e+005	7.61245e-005	91.092942	Argon
1	0.717		-	-	-	Oxygen
1	0.866		-	-	-	Nitrogen
1	1.008	BB	5.5367e+004	1.29910e-004	8.906037	Methane
1	1.187		-	-	-	Carbon Dioxide
1	1.465		-	-	-	Carbon Monoxide
2	0.305	BBOS	6.2000e+039	0.00000e+000	0.000000	
2	0.469		-	-	-	Ethylene
2	0.516	BBA	13.93573	5.91779e-005	0.001021	Ethane
2	0.671		-	-	-	Acetylene

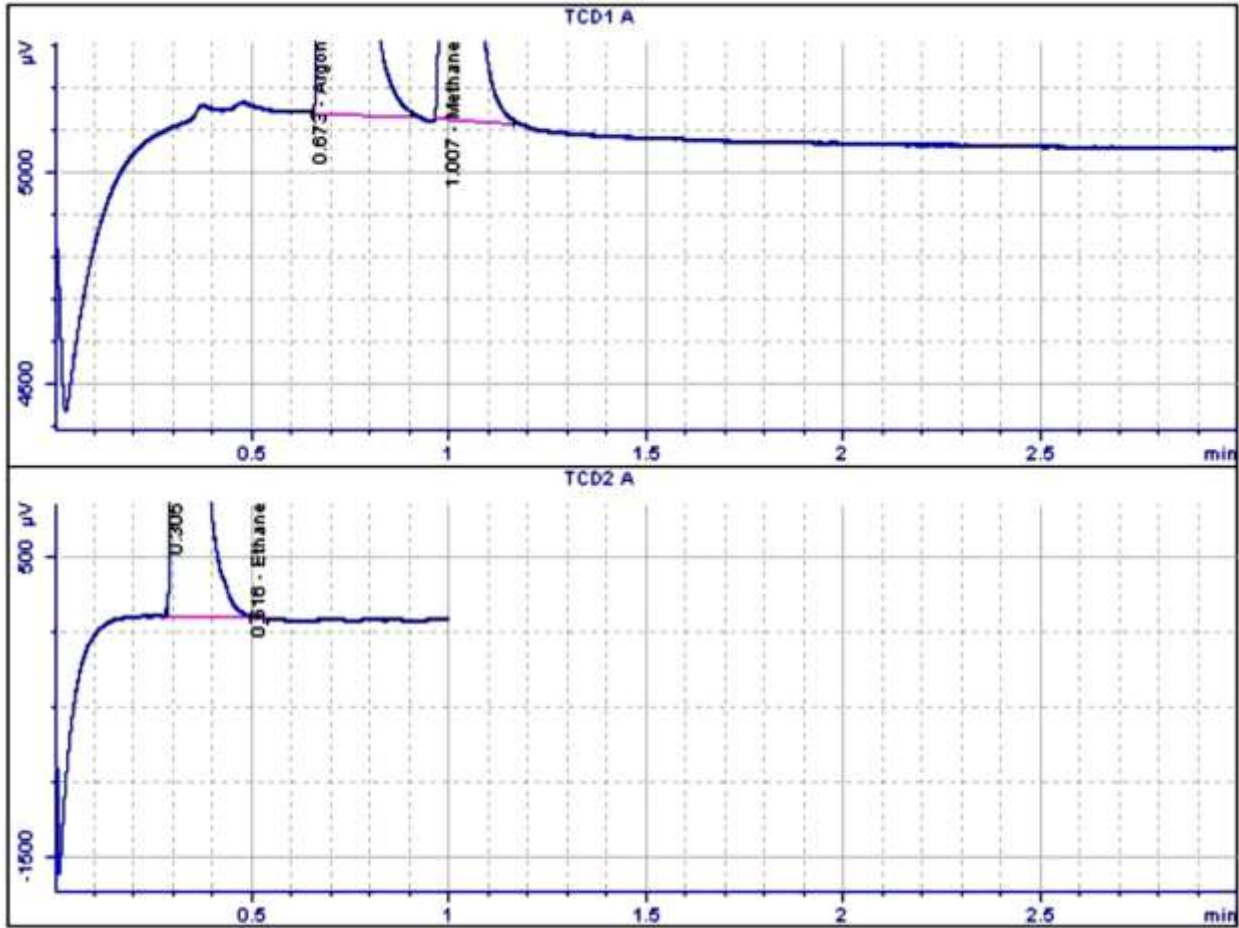
Eighth run, after 35 minutes



Signal	Retention Time [min]	Type	Area [µV*s]	Amt/Area	Norm %	Name
1	0.574		-	-	-	Neon
1	0.672	BB	9.6909e+005	7.61245e-005	91.057960	Argon
1	0.717		-	-	-	Oxygen
1	0.866		-	-	-	Nitrogen
1	1.007	BB	5.5760e+004	1.29910e-004	8.941068	Methane
1	1.187		-	-	-	Carbon Dioxide
1	1.465		-	-	-	Carbon Monoxide
2	0.305	BBOS	6.0000e+039	0.00000e+000	0.000000	
2	0.469		-	-	-	Ethylene
2	0.517	BBA	13.30884	5.91779e-005	0.000972	Ethane
2	0.671		-	-	-	Acetylene

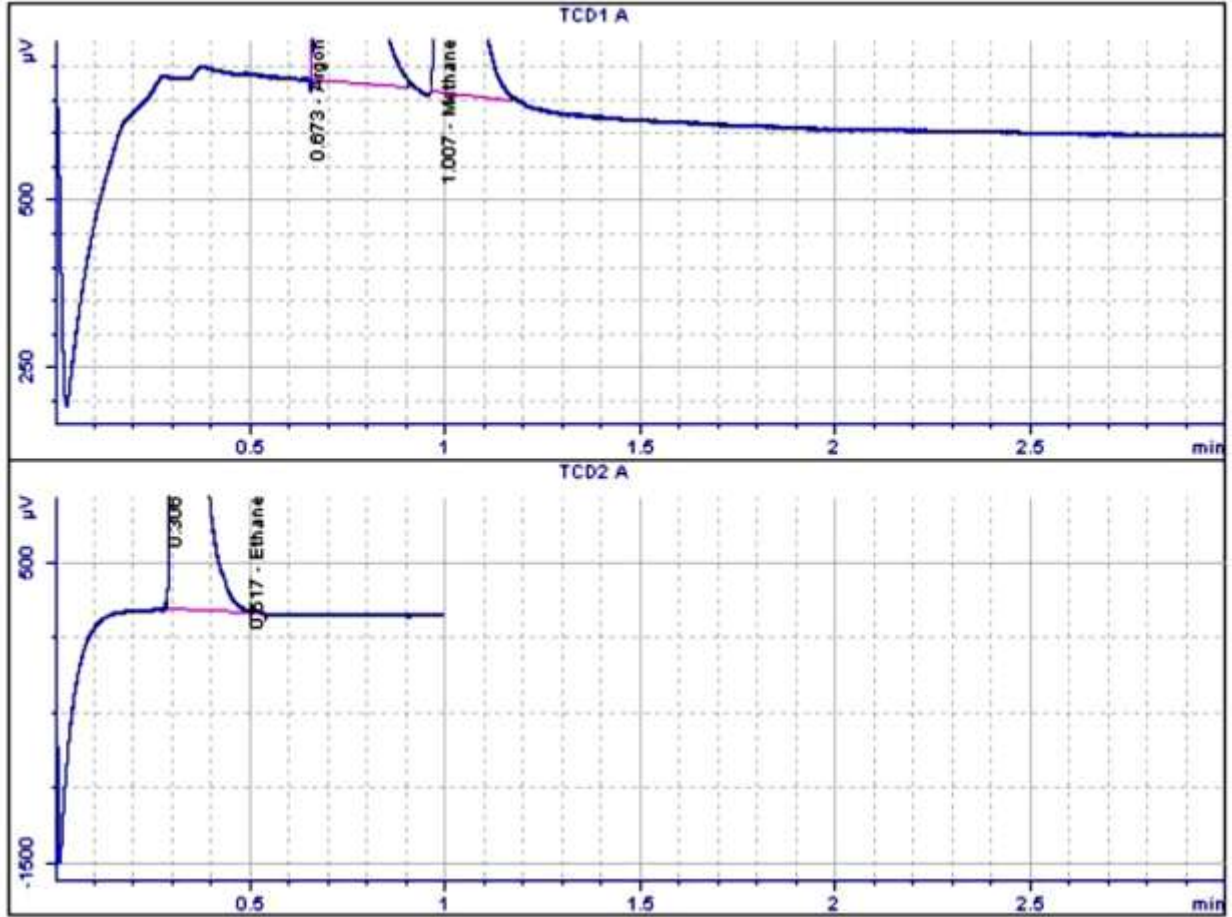
Total norm percent = 100.00000

Ninth run, after 40 minutes



Signal	Retention Time [min]	Type	Area [µV*s]	Amt/Area	Norm %	Name
1	0.574		-	-	-	Neon
1	0.673	PB	9.6704e+005	7.61245e-005	91.038190	Argon
1	0.717		-	-	-	Oxygen
1	0.866		-	-	-	Nitrogen
1	1.007	BB	5.5776e+004	1.29910e-004	8.960824	Methane
1	1.187		-	-	-	Carbon Dioxide
1	1.465		-	-	-	Carbon Monoxide
2	0.305	BBOS	6.0000e+039	0.00000e+000	0.000000	
2	0.469		-	-	-	Ethylene
2	0.516	PBA	13.46628	5.91779e-005	0.000986	Ethane
2	0.671		-	-	-	Acetylene

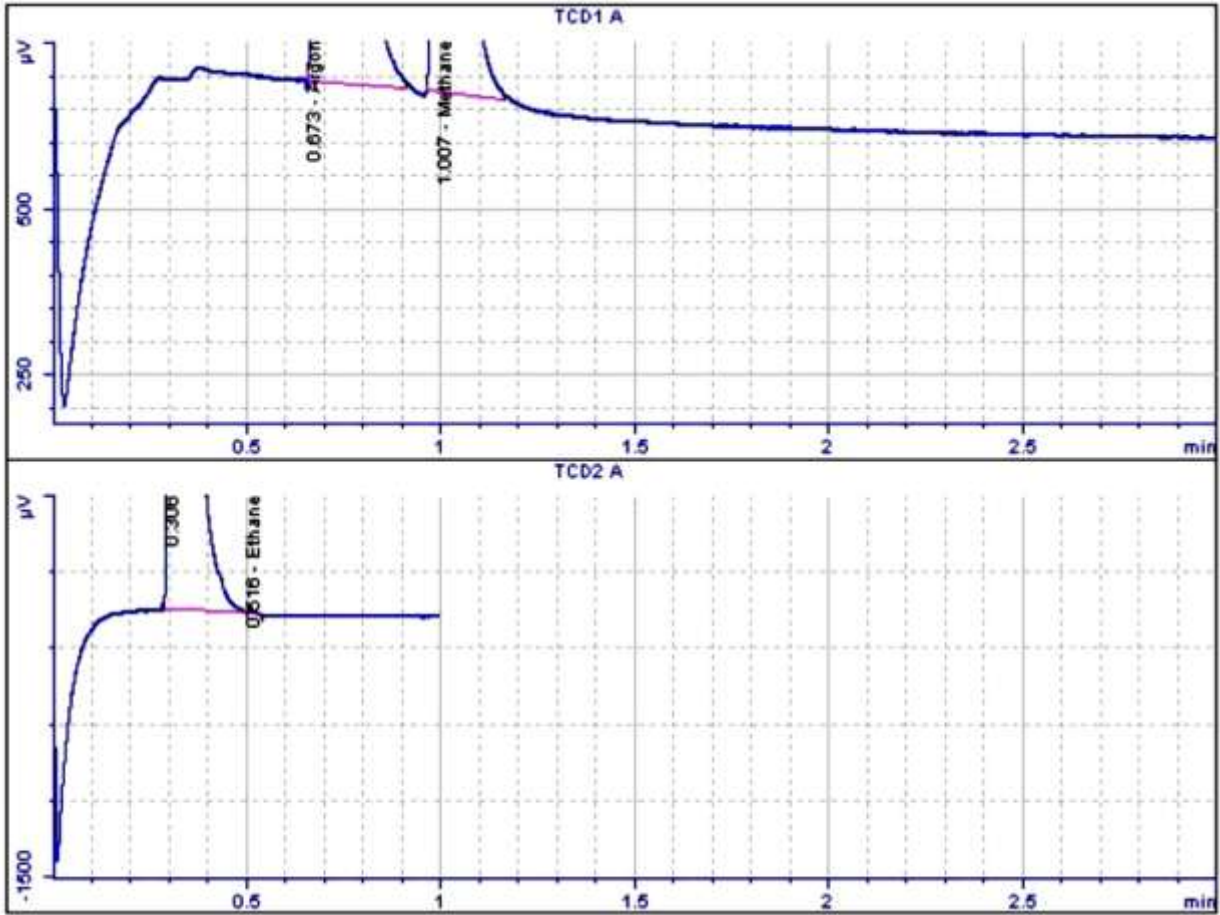
Tenth run, after 45 minutes



Signal	Retention Time [min]	Type	Area [$\mu\text{V}\cdot\text{s}$]	Amt/Area	Norm %	Name
1	0.574		-	-	-	Neon
1	0.673	BB	9.6734e+005	7.61245e-005	91.077635	Argon
1	0.717		-	-	-	Oxygen
1	0.866		-	-	-	Nitrogen
1	1.007	BB	5.5525e+004	1.29910e-004	8.921482	Methane
1	1.187		-	-	-	Carbon Dioxide
1	1.465		-	-	-	Carbon Monoxide
2	0.306	BBOS	6.2000e+039	0.00000e+000	0.000000	
2	0.469		-	-	-	Ethylene
2	0.517	BBA	12.06186	5.91779e-005	0.000883	Ethane
2	0.671		-	-	-	Acetylene

Total norm percent = 100.00000

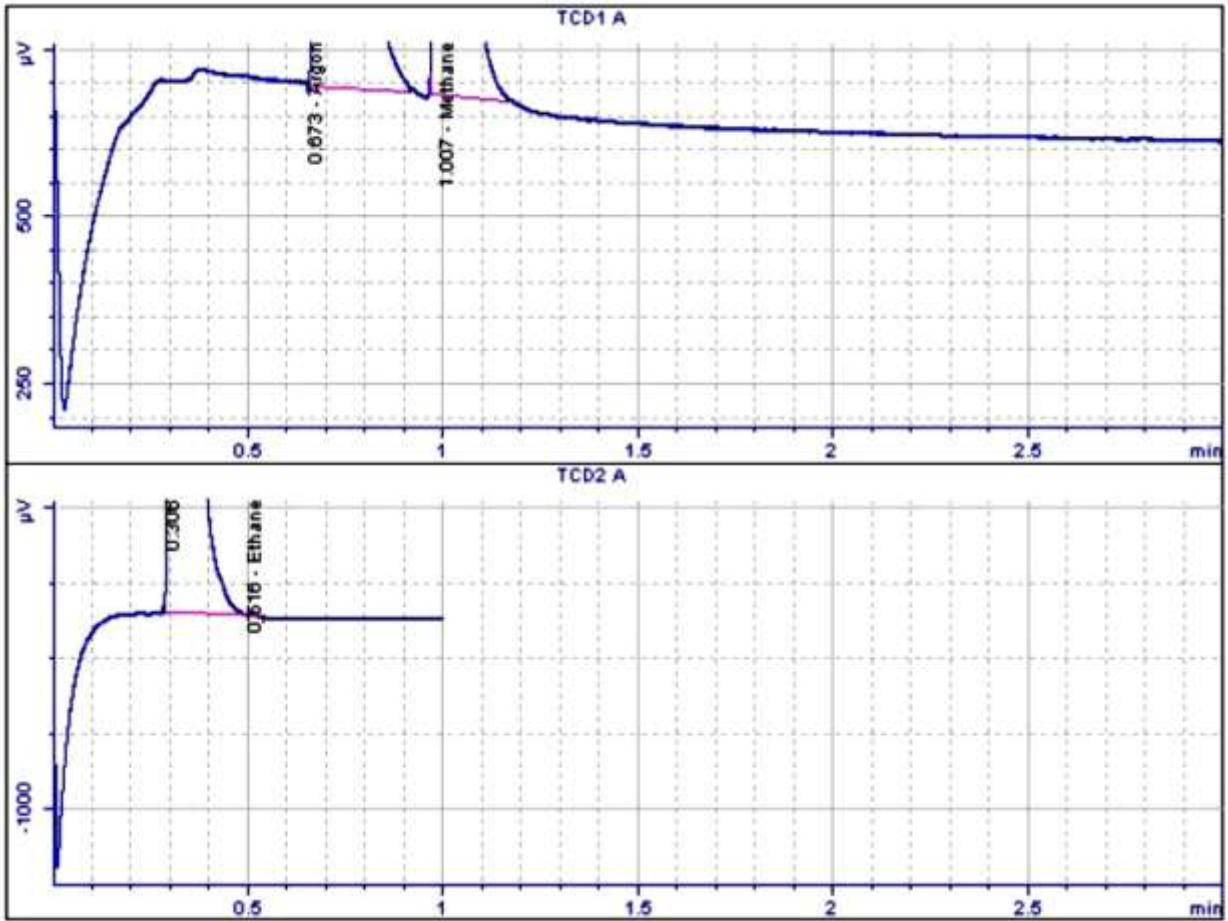
Eleventh run, after 50 minutes



Signal	Retention Time [min]	Type	Area [µV*s]	Amt/Area	Norm %	Name
1	0.574		-	-	-	Neon
1	0.673	BB	9.6623e+005	7.61245e-005	91.105812	Argon
1	0.717		-	-	-	Oxygen
1	0.866		-	-	-	Nitrogen
1	1.007	BB	5.5268e+004	1.29910e-004	8.893154	Methane
1	1.187		-	-	-	Carbon Dioxide
1	1.465		-	-	-	Carbon Monoxide
2	0.306	BBOS	6.0000e+039	0.00000e+000	0.000000	
2	0.469		-	-	-	Ethylene
2	0.516	PBA	14.10592	5.91779e-005	0.001034	Ethane
2	0.671		-	-	-	Acetylene

Total norm percent = 100.00000

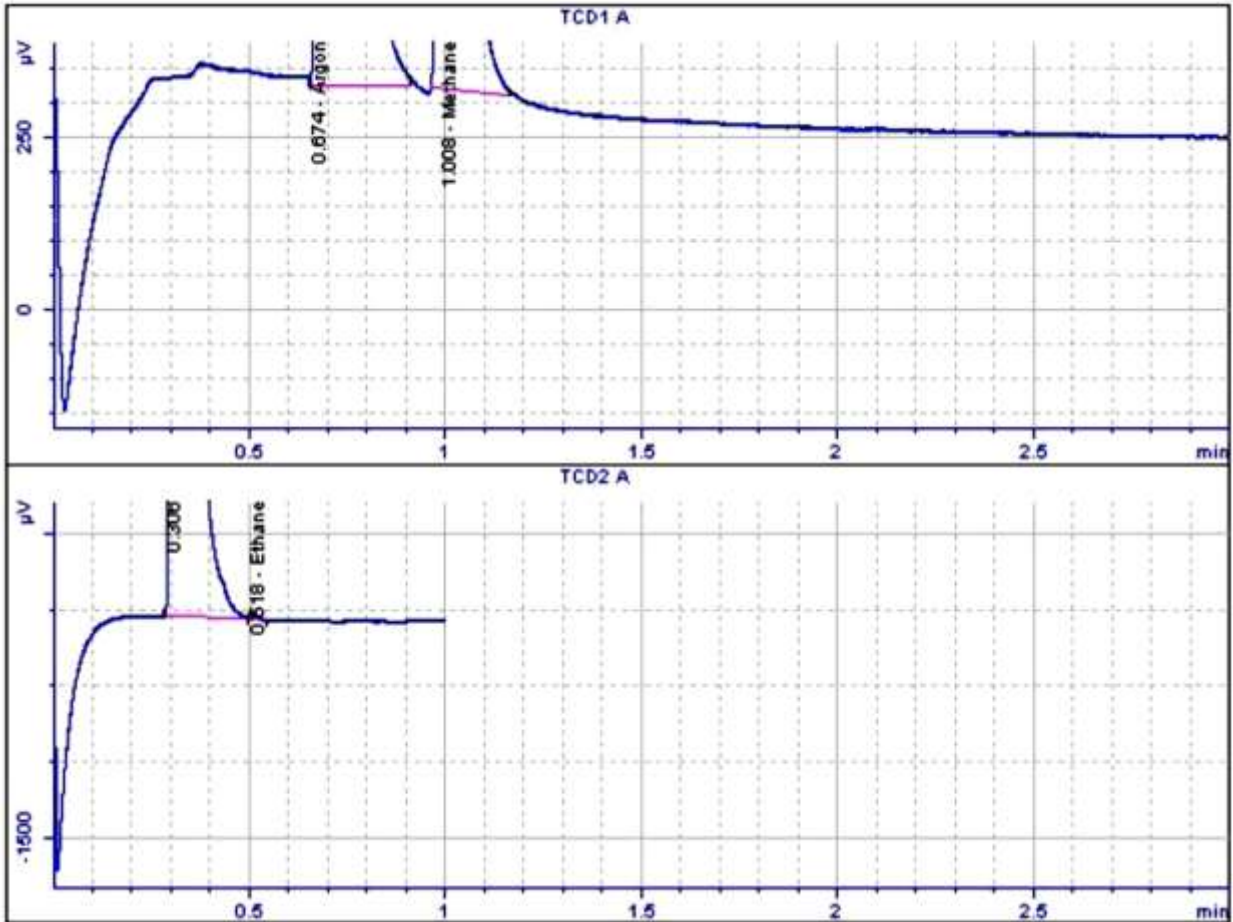
Twelvth run, after 55 minutes



Signal	Retention Time [min]	Type	Area [µV*s]	Amt/Area	Norm %	Name
1	0.574		-	-	-	Neon
1	0.673	PB	9.6649e+005	7.61245e-005	91.137794	Argon
1	0.717		-	-	-	Oxygen
1	0.866		-	-	-	Nitrogen
1	1.007	BB	5.5064e+004	1.29910e-004	8.861119	Methane
1	1.187		-	-	-	Carbon Dioxide
1	1.465		-	-	-	Carbon Monoxide
2	0.306	BBOS	6.2000e+039	0.00000e+000	0.000000	
2	0.469		-	-	-	Ethylene
2	0.516	BBA	14.83378	5.91779e-005	0.001087	Ethane
2	0.671		-	-	-	Acetylene

Total norm percent = 100.00000

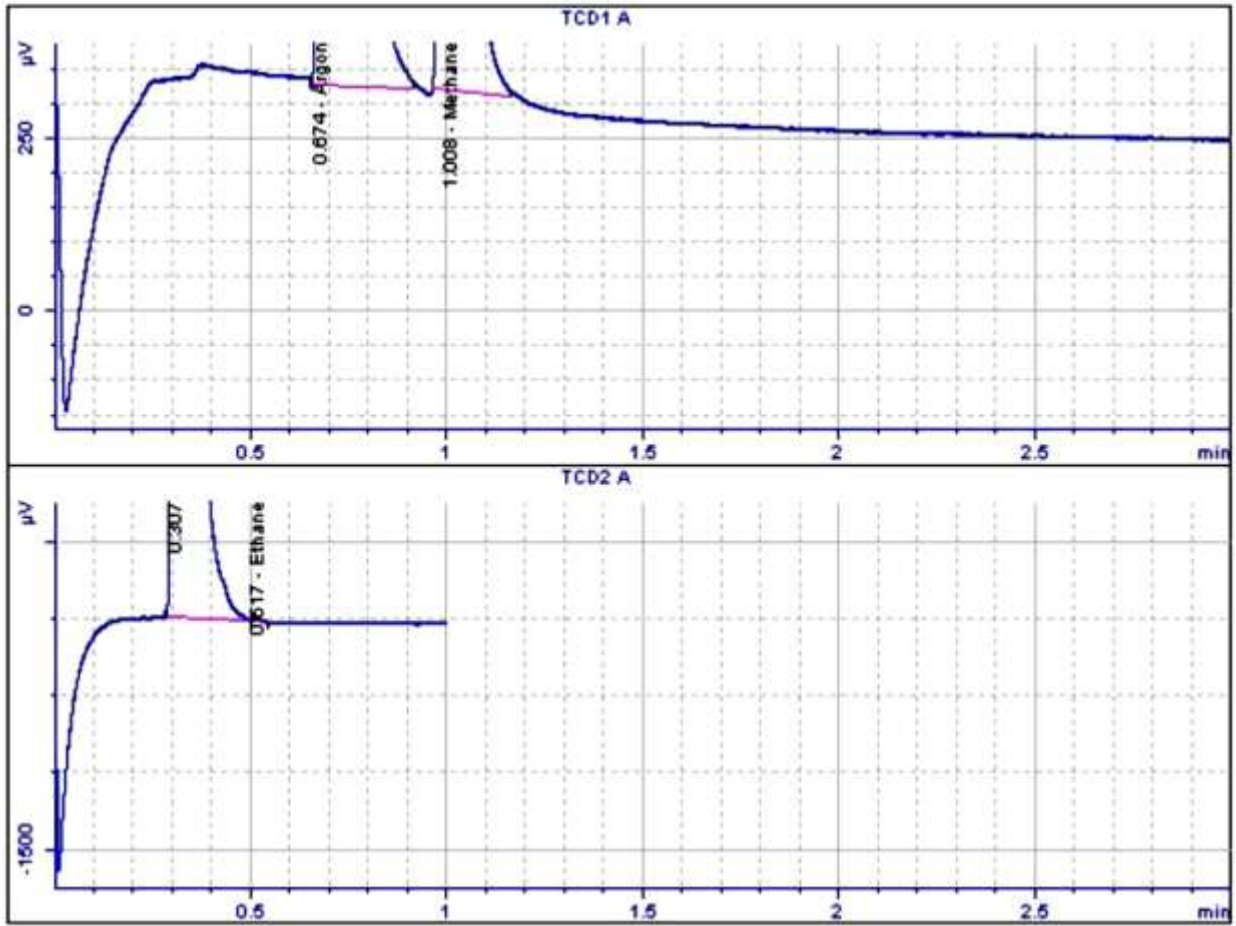
Thirteenth run, after 60 minutes



Signal	Retention Time [min]	Type	Area [µV*s]	Amt/Area	Norm %	Name
1	0.574		-	-	-	Neon
1	0.674	PB	9.6513e+005	7.61245e-005	91.119110	Argon
1	0.717		-	-	-	Oxygen
1	0.866		-	-	-	Nitrogen
1	1.008	BB	5.5115e+004	1.29910e-004	8.879873	Methane
1	1.187		-	-	-	Carbon Dioxide
1	1.465		-	-	-	Carbon Monoxide
2	0.306	BBOS	6.0000e+039	0.00000e+000	0.000000	
2	0.469		-	-	-	Ethylene
2	0.518	BBA	13.85640	5.91779e-005	0.001017	Ethane
2	0.671		-	-	-	Acetylene

Total norm percent = 100.00000

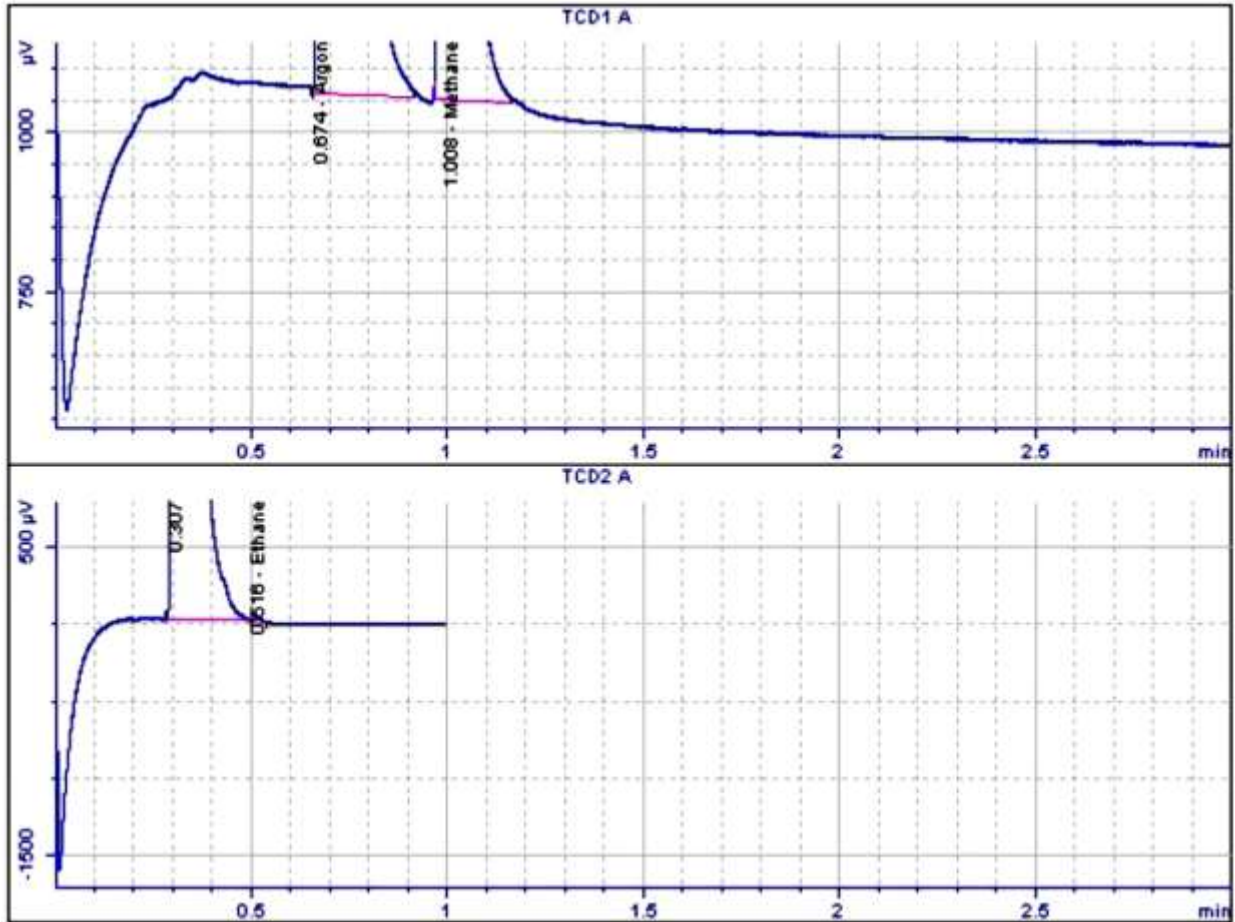
Fourteenth run, after 65 minutes



Signal	Retention Time [min]	Type	Area [µV*s]	Amt/Area	Norm %	Name
1	0.574		-	-	-	Neon
1	0.674	PB	9.6511e+005	7.61245e-005	91.190346	Argon
1	0.717		-	-	-	Oxygen
1	0.866		-	-	-	Nitrogen
1	1.008	BB	5.4625e+004	1.29910e-004	8.807965	Methane
1	1.187		-	-	-	Carbon Dioxide
1	1.465		-	-	-	Carbon Monoxide
2	0.307	BBOS	6.0000e+039	0.00000e+000	0.000000	
2	0.469		-	-	-	Ethylene
2	0.516	PBA	22.99406	5.91779e-005	0.001689	Ethane
2	0.671		-	-	-	Acetylene

Total norm percent = 100.00000

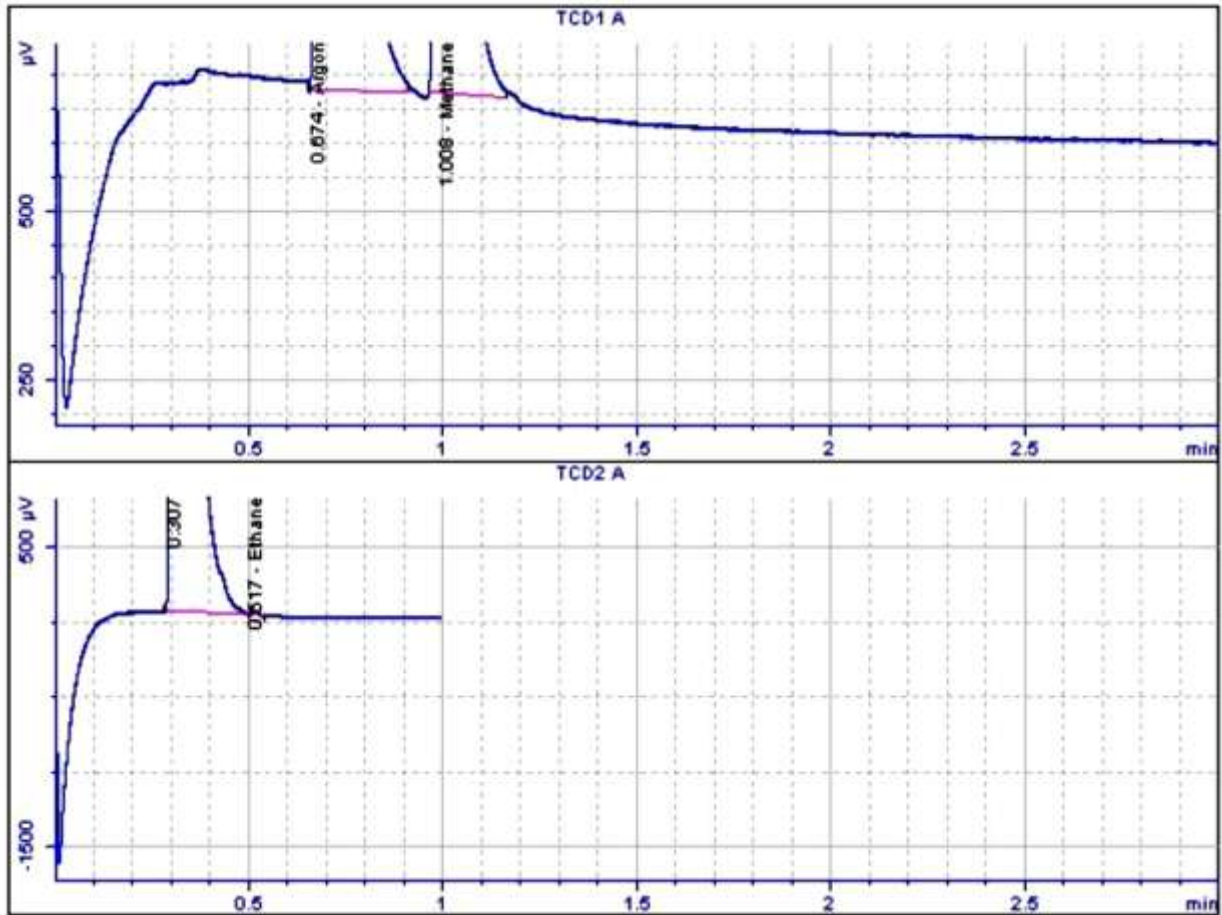
Fifteenth run, after 70 minutes



Signal	Retention Time [min]	Type	Area [µV*s]	Amt/Area	Norm %	Name
1	0.574		-	-	-	Neon
1	0.674	PB	9.6538e+005	7.61245e-005	91.137809	Argon
1	0.717		-	-	-	Oxygen
1	0.866		-	-	-	Nitrogen
1	1.008	BB	5.5000e+004	1.29910e-004	8.860953	Methane
1	1.187		-	-	-	Carbon Dioxide
1	1.465		-	-	-	Carbon Monoxide
2	0.307	BBOS	6.2000e+039	0.00000e+000	0.000000	
2	0.469		-	-	-	Ethylene
2	0.517	BBA	16.87573	5.91779e-005	0.001239	Ethane
2	0.671		-	-	-	Acetylene

Total norm percent = 100.00000

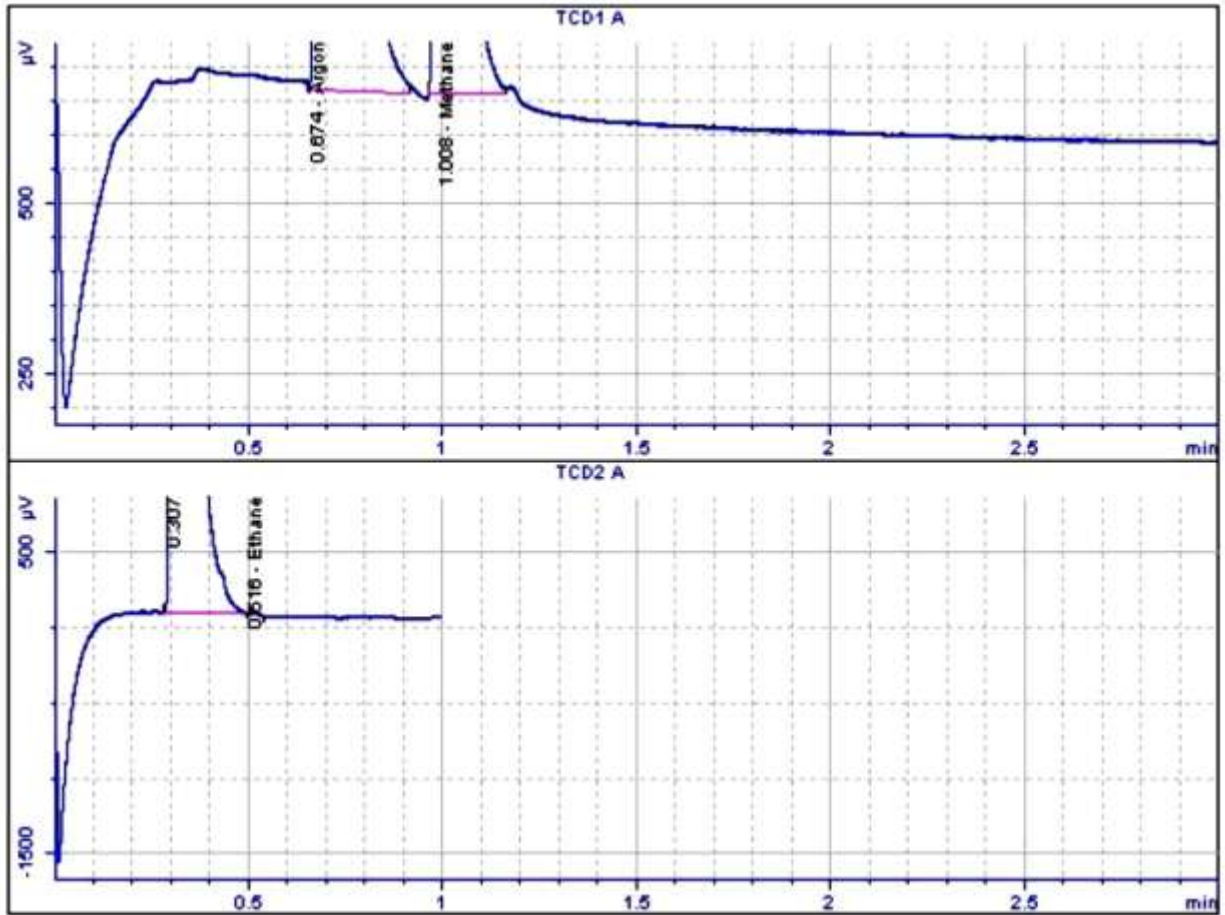
Sixteenth run, after 75 minutes



Signal	Retention Time [min]	Type	Area [μV*s]	Amt/Area	Norm %	Name
1	0.574		-	-	-	Neon
1	0.674	PB	9.6411e+005	7.61245e-005	91.126747	Argon
1	0.717		-	-	-	Oxygen
1	0.866		-	-	-	Nitrogen
1	1.008	BB	5.5004e+004	1.29910e-004	8.872109	Methane
1	1.187		-	-	-	Carbon Dioxide
1	1.465		-	-	-	Carbon Monoxide
2	0.307	BBOS	6.0000e+039	0.00000e+000	0.000000	
2	0.469		-	-	-	Ethylene
2	0.517	BBA	15.57319	5.91779e-005	0.001144	Ethane
2	0.671		-	-	-	Acetylene

Total norm percent = 100.00000

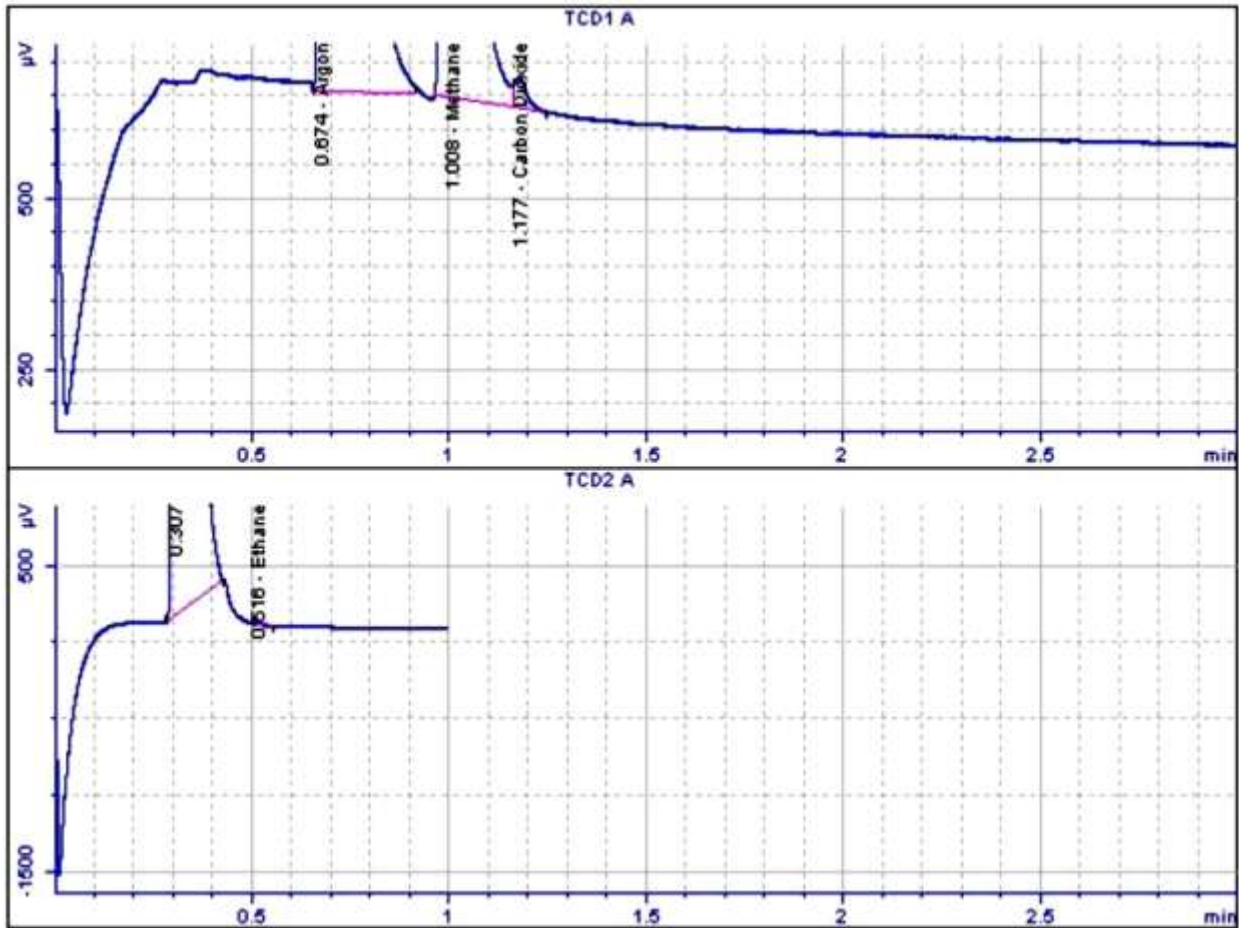
Seventeenth run, after 80 minutes



Signal	Retention Time [min]	Type	Area [µV*s]	Amt/Area	Norm %	Name
1	0.574		-	-	-	Neon
1	0.674	PB	9.6362e+005	7.61245e-005	91.120435	Argon
1	0.717		-	-	-	Oxygen
1	0.866		-	-	-	Nitrogen
1	1.008	BB	5.5019e+004	1.29910e-004	8.878526	Methane
1	1.187		-	-	-	Carbon Dioxide
1	1.465		-	-	-	Carbon Monoxide
2	0.307	BBOS	6.0000e+039	0.00000e+000	0.000000	
2	0.469		-	-	-	Ethylene
2	0.516	BBA	14.12829	5.91779e-005	0.001039	Ethane
2	0.671		-	-	-	Acetylene

Total norm percent = 100.00000

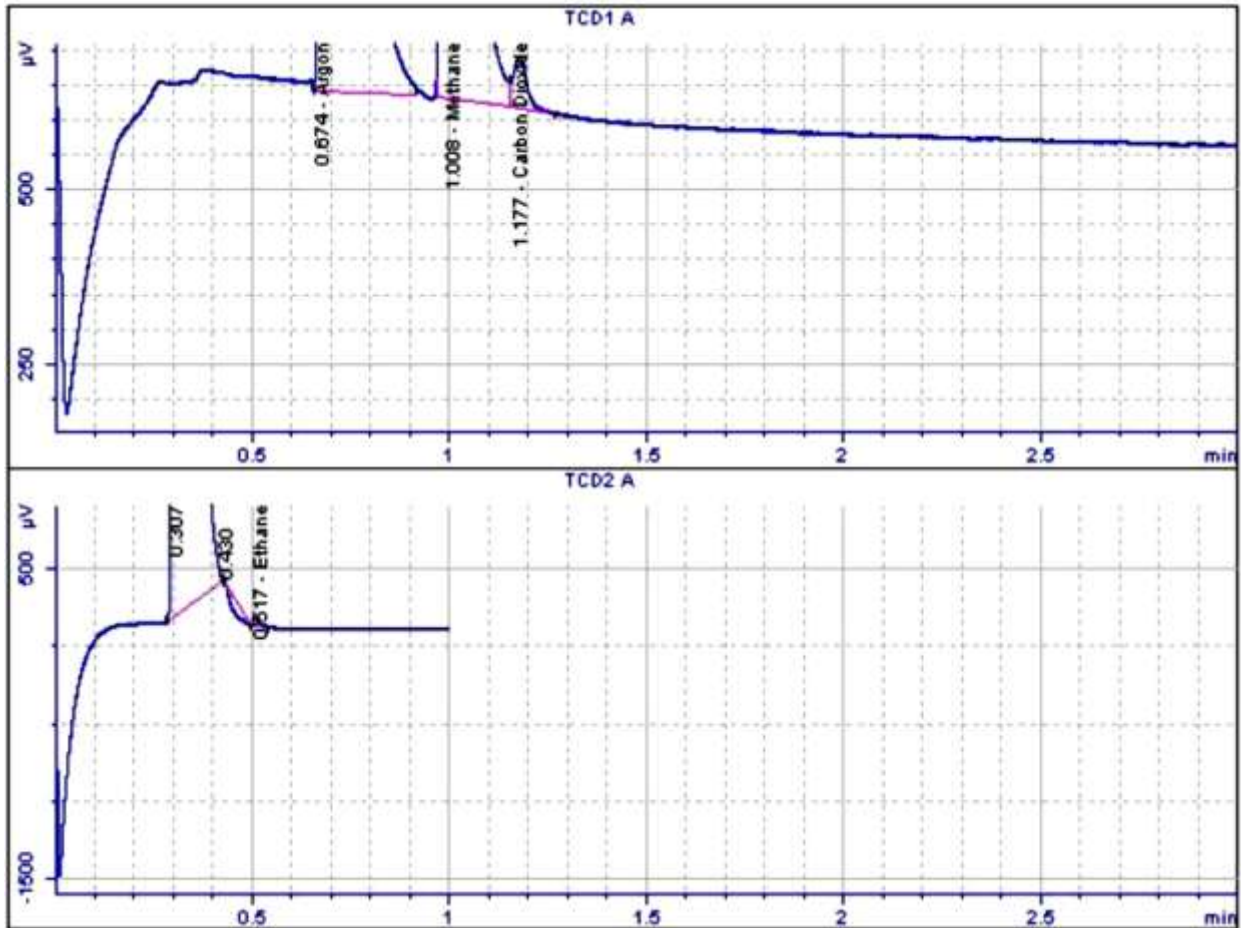
Eighteenth run, after 85 minutes



Signal	Retention Time [min]	Type	Area [$\mu\text{V}\cdot\text{s}$]	Amt/Area	Norm %	Name
1	0.574		-	-	-	Neon
1	0.674	PB	9.6317e+005	7.61245e-005	91.117629	Argon
1	0.717		-	-	-	Oxygen
1	0.866		-	-	-	Nitrogen
1	1.008	BB	5.4992e+004	1.29910e-004	8.878075	Methane
1	1.177	BB	99.57531	3.01494e-005	0.003731	Carbon Dioxide
1	1.465		-	-	-	Carbon Monoxide
2	0.307	PBOS	6.2000e+039	0.00000e+000	0.000000	
2	0.469		-	-	-	Ethylene
2	0.516	PBA	7.68226	5.91779e-005	0.000565	Ethane
2	0.671		-	-	-	Acetylene

Total norm percent = 100.00000

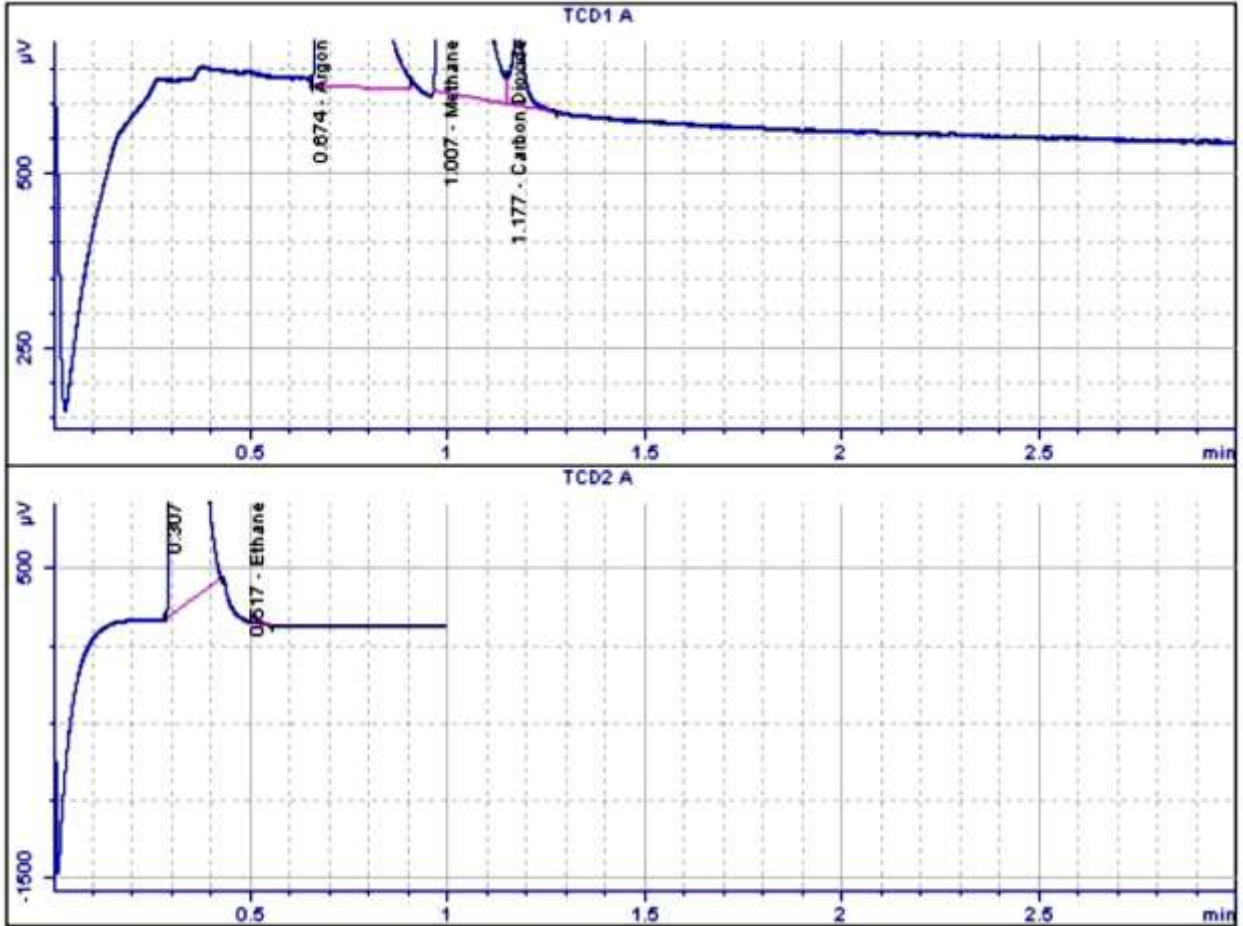
Nineteenth run, after 90 minutes



Signal	Retention Time [min]	Type	Area [µV*s]	Amt/Area	Norm %	Name
1	0.574		-	-	-	Neon
1	0.674	PB	9.6253e+005	7.61245e-005	91.102874	Argon
1	0.717		-	-	-	Oxygen
1	0.866		-	-	-	Nitrogen
1	1.008	BV	5.5033e+004	1.29910e-004	8.889188	Methane
1	1.177	VB	180.07467	3.01494e-005	0.006750	Carbon Dioxide
1	1.465		-	-	-	Carbon Monoxide
2	0.307	PBOS	6.0000e+039	0.00000e+000	0.000000	
2	0.430	BBA	-206.20100	0.00000e+000	0.000000	
2	0.469		-	-	-	Ethylene
2	0.517	BBA	16.14540	5.91779e-005	0.001188	Ethane
2	0.671		-	-	-	Acetylene

Total norm percent = 100.00000

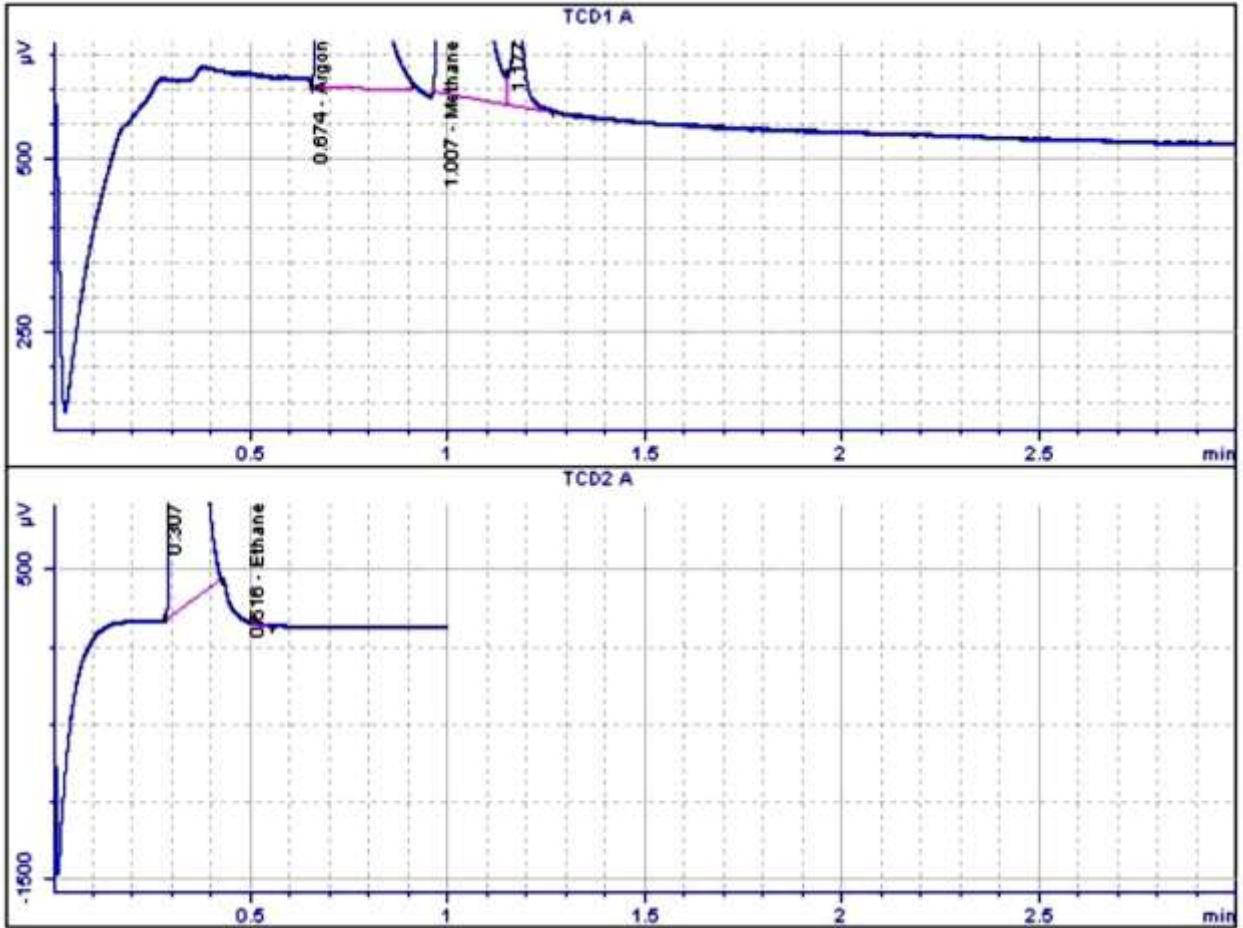
Twentieth run, after 95 minutes



Signal	Retention Time [min]	Type	Area [µV*s]	Amt/Area	Norm %	Name
1	0.574		-	-	-	Neon
1	0.674	PB	9.6285e+005	7.61245e-005	91.156206	Argon
1	0.717		-	-	-	Oxygen
1	0.866		-	-	-	Nitrogen
1	1.007	BV	5.4676e+004	1.29910e-004	8.833707	Methane
1	1.177	VB	245.37086	3.01494e-005	0.009200	Carbon Dioxide
1	1.465		-	-	-	Carbon Monoxide
2	0.307	PBOS	6.0000e+039	0.00000e+000	0.000000	
2	0.469		-	-	-	Ethylene
2	0.517	PBA	12.05770	5.91779e-005	0.000887	Ethane
2	0.671		-	-	-	Acetylene

Total norm percent = 100.00000

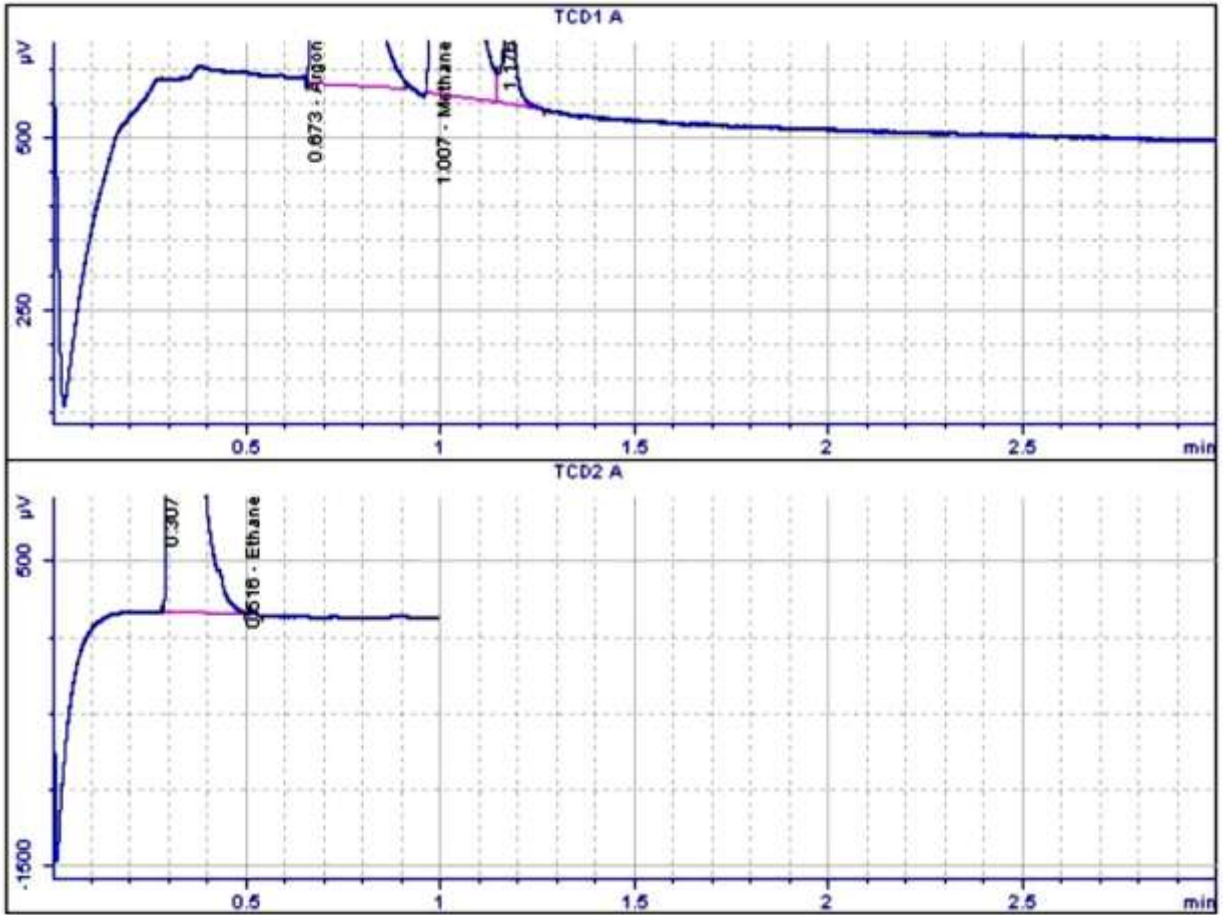
Twentyfirst run, after 100 minutes



Signal	Retention Time [min]	Type	Area [$\mu\text{V}\cdot\text{s}$]	Amt/Area	Norm %	Name
1	0.574		-	-	-	Neon
1	0.674	PB	9.6220e+005	7.61245e-005	91.157967	Argon
1	0.717		-	-	-	Oxygen
1	0.866		-	-	-	Nitrogen
1	1.007	BV	5.4685e+004	1.29910e-004	8.841359	Methane
1	1.177	VB	289.05965	0.00000e+000	0.000000	
1	1.465		-	-	-	Carbon Monoxide
2	0.307	PBOS	6.0000e+039	0.00000e+000	0.000000	
2	0.424		-	-	-	Carbon Dioxide
2	0.469		-	-	-	Ethylene
2	0.516	PBA	9.15568	5.91779e-005	0.000674	Ethane
2	0.671		-	-	-	Acetylene

Total norm percent = 100.00000

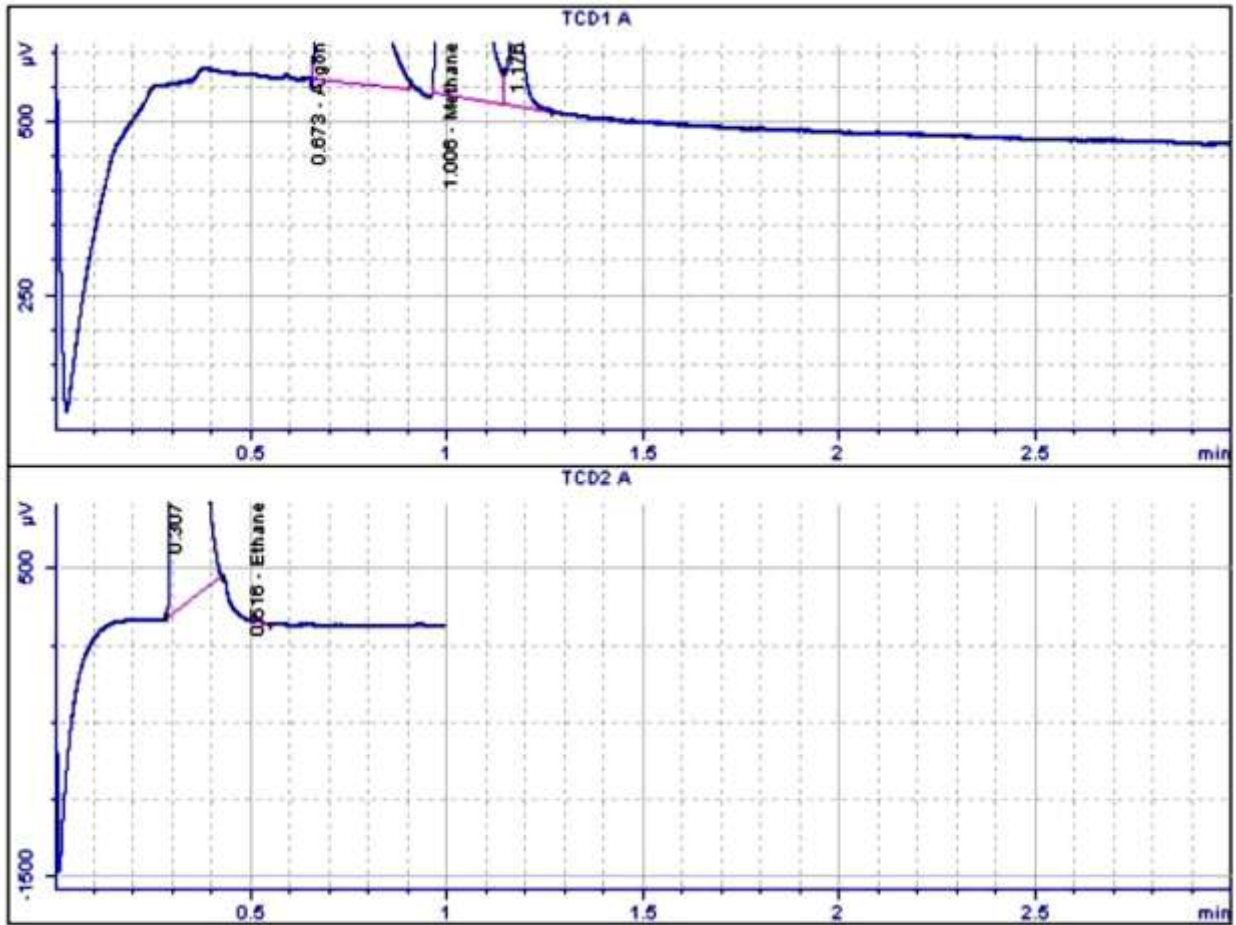
Twenty second run, after 105 minutes



Signal	Retention Time [min]	Type	Area [$\mu\text{V}\cdot\text{s}$]	Amt/Area	Norm %	Name
1	0.574		-	-	-	Neon
1	0.673	PB	9.6202e+005	7.61245e-005	91.194668	Argon
1	0.717		-	-	-	Oxygen
1	0.866		-	-	-	Nitrogen
1	1.007	BV	5.4424e+004	1.29910e-004	8.804298	Methane
1	1.176	VB	328.42622	0.00000e+000	0.000000	
1	1.465		-	-	-	Carbon Monoxide
2	0.307	BBOS	6.0000e+039	0.00000e+000	0.000000	
2	0.424		-	-	-	Carbon Dioxide
2	0.469		-	-	-	Ethylene
2	0.516	PBA	14.02785	5.91779e-005	0.001034	Ethane
2	0.671		-	-	-	Acetylene

Total norm percent = 100.00000

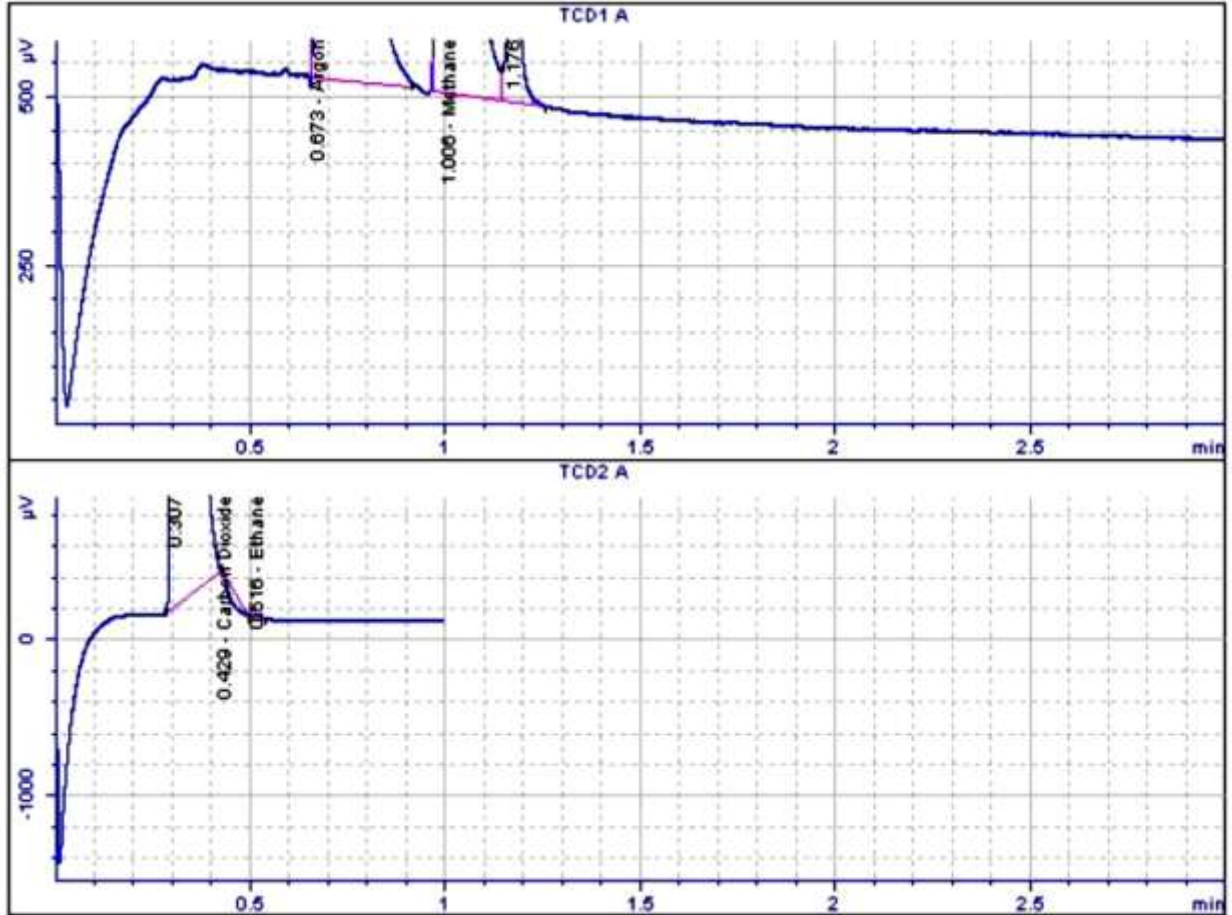
Twenty third run, after 110 minutes



Signal	Retention Time [min]	Type	Area [µV*s]	Amt/Area	Norm %	Name
1	0.574		-	-	-	Neon
1	0.673	BB	9.6238e+005	7.61245e-005	91.254418	Argon
1	0.717		-	-	-	Oxygen
1	0.866		-	-	-	Nitrogen
1	1.006	BV	5.4041e+004	1.29910e-004	8.744750	Methane
1	1.176	VB	429.25244	0.00000e+000	0.000000	
1	1.465		-	-	-	Carbon Monoxide
2	0.307	PBOS	6.0000e+039	0.00000e+000	0.000000	
2	0.424		-	-	-	Carbon Dioxide
2	0.469		-	-	-	Ethylene
2	0.516	PBA	11.29520	5.91779e-005	0.000833	Ethane
2	0.671		-	-	-	Acetylene

Total norm percent = 100.00000

Twenty fourth run, after 115 minutes

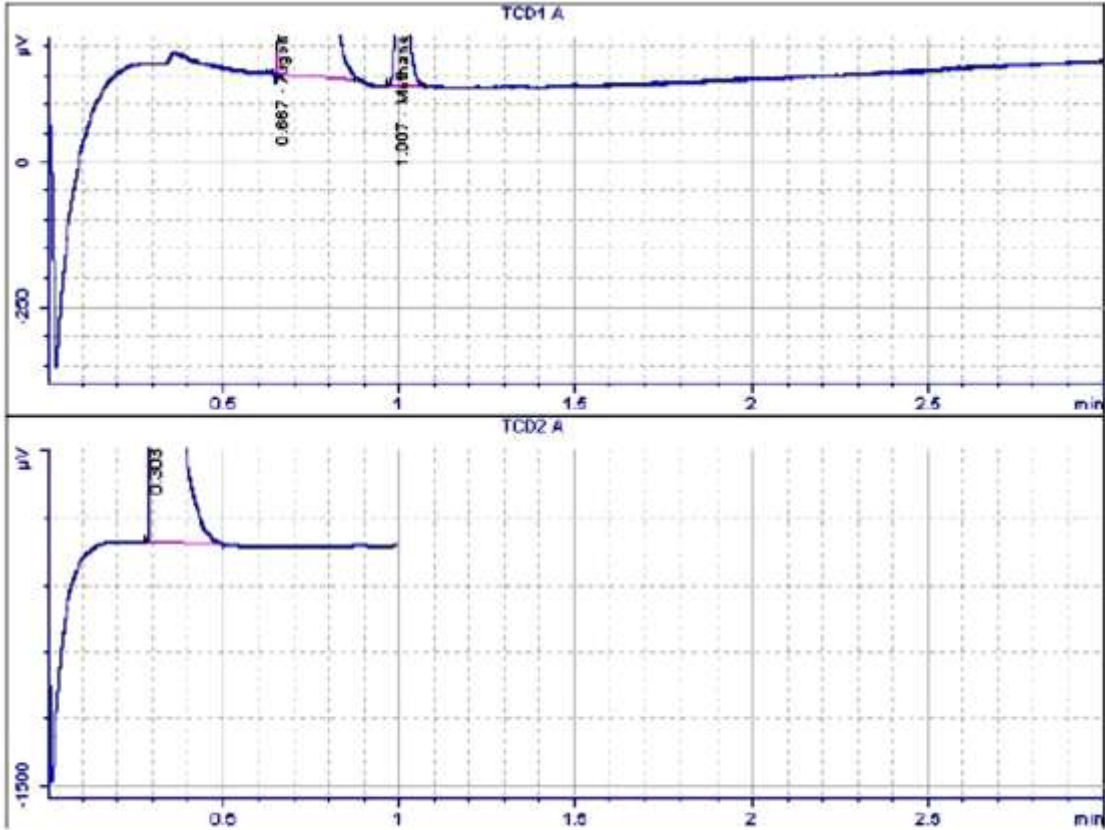


Signal	Retention Time [min]	Type	Area [µV*s]	Amt/Area	Norm %	Name
1	0.574		-	-	-	Neon
1	0.673	BB	9.6186e+005	7.61245e-005	91.269544	Argon
1	0.717		-	-	-	Oxygen
1	0.866		-	-	-	Nitrogen
1	1.006	BV	5.3908e+004	1.29910e-004	8.729397	Methane
1	1.176	VB	552.58851	0.00000e+000	0.000000	
1	1.465		-	-	-	Carbon Monoxide
2	0.307	PBOS	6.0000e+039	0.00000e+000	0.000000	
2	0.429	BBA	-222.70600	0.00000e+000	0.000000	Carbon Dioxide
2	0.469		-	-	-	Ethylene
2	0.516	BBA	14.34364	5.91779e-005	0.001058	Ethane
2	0.671		-	-	-	Acetylene

Total norm percent = 100.00000

APPENDIX B2: GAS CHROMATOGRAPH FILES OF TPR (B=10)

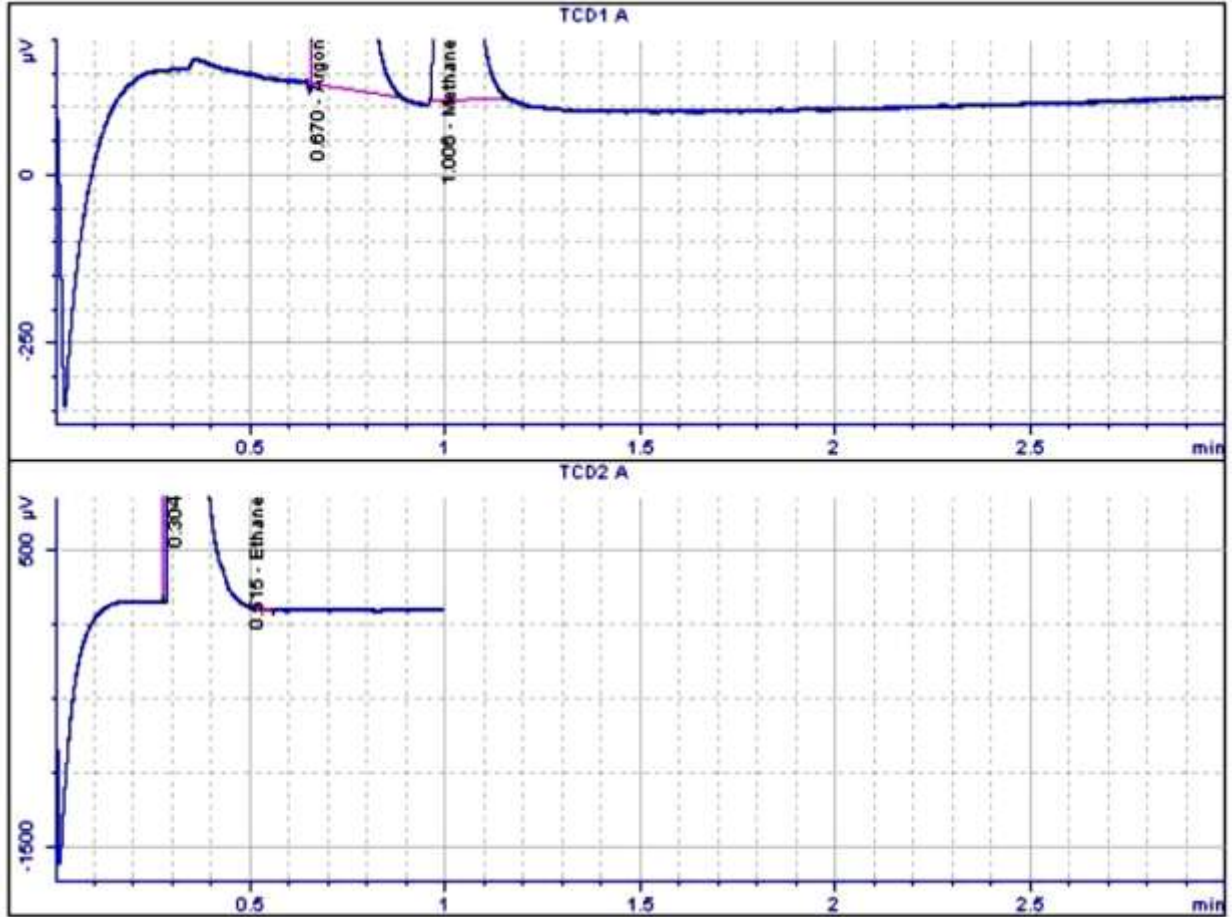
First run



Signal	Retention Time [min]	Type	Area [$\mu\text{V}\cdot\text{s}$]	Amt/Area	Norm %	Name
1	0.574		-	-	-	Neon
1	0.667	BB	1.0599e+006	7.61245e-005	99.910587	Argon
1	0.717		-	-	-	Oxygen
1	0.866		-	-	-	Nitrogen
1	1.007	PB	555.81263	1.29910e-004	0.089413	Methane
1	1.465		-	-	-	Carbon Monoxide
2	0.303	BBOS	6.6000e+039	0.00000e+000	0.000000	
2	0.424		-	-	-	Carbon Dioxide
2	0.469		-	-	-	Ethylene
2	0.514		-	-	-	Ethane
2	0.671		-	-	-	Acetylene

Total norm percent = 100.00000

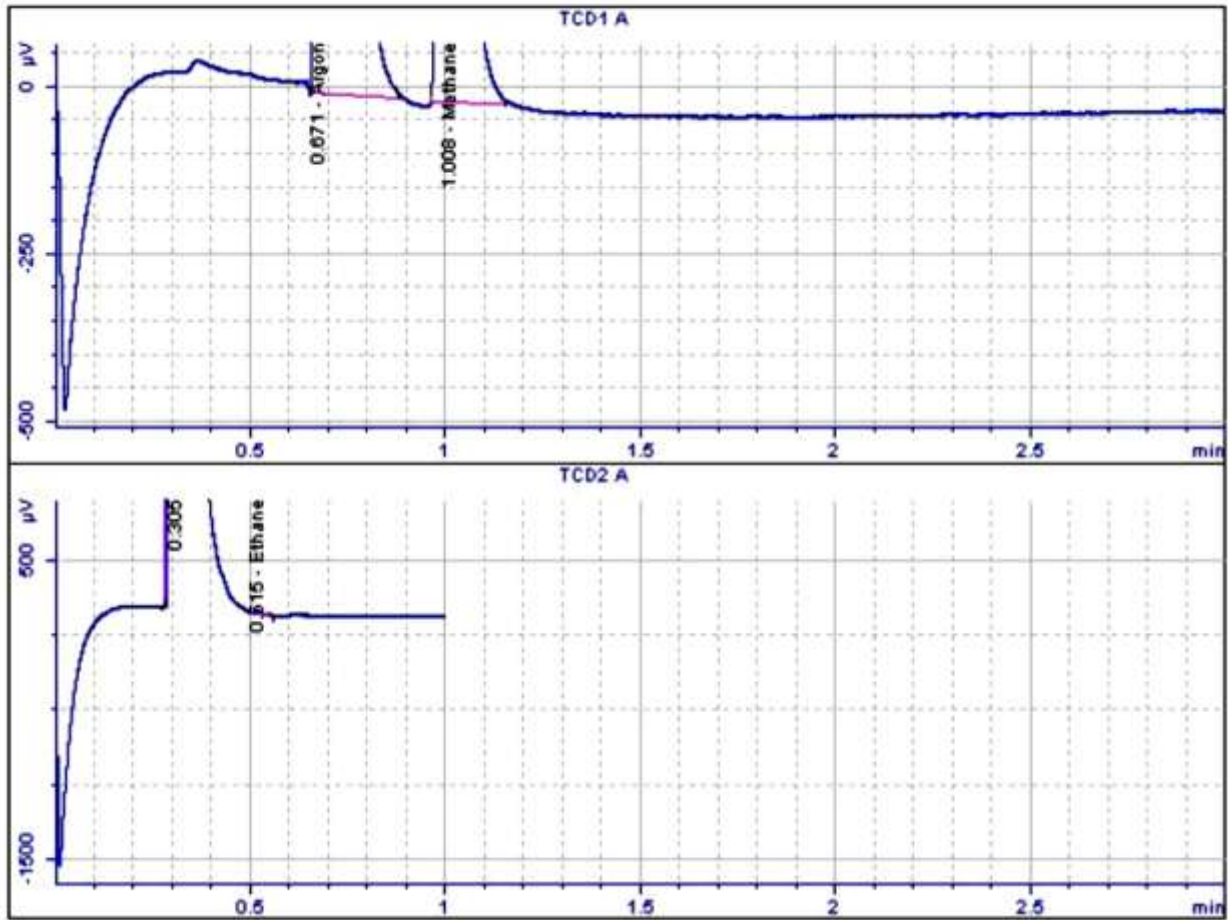
Second run, after 5 minutes



Signal	Retention Time [min]	Type	Area [$\mu\text{V}\cdot\text{s}$]	Amt/Area	Norm %	Name
1	0.574		-	-	-	Neon
1	0.670	BB	9.7883e+005	7.61245e-005	90.675588	Argon
1	0.717		-	-	-	Oxygen
1	0.866		-	-	-	Nitrogen
1	1.006	BB	5.8978e+004	1.29910e-004	9.323690	Methane
1	1.465		-	-	-	Carbon Monoxide
2	0.304	PBOS	6.0000e+039	0.00000e+000	0.000000	
2	0.424		-	-	-	Carbon Dioxide
2	0.469		-	-	-	Ethylene
2	0.515	PBA	10.02495	5.91779e-005	0.000722	Ethane
2	0.671		-	-	-	Acetylene

Total norm percent = 100.00000

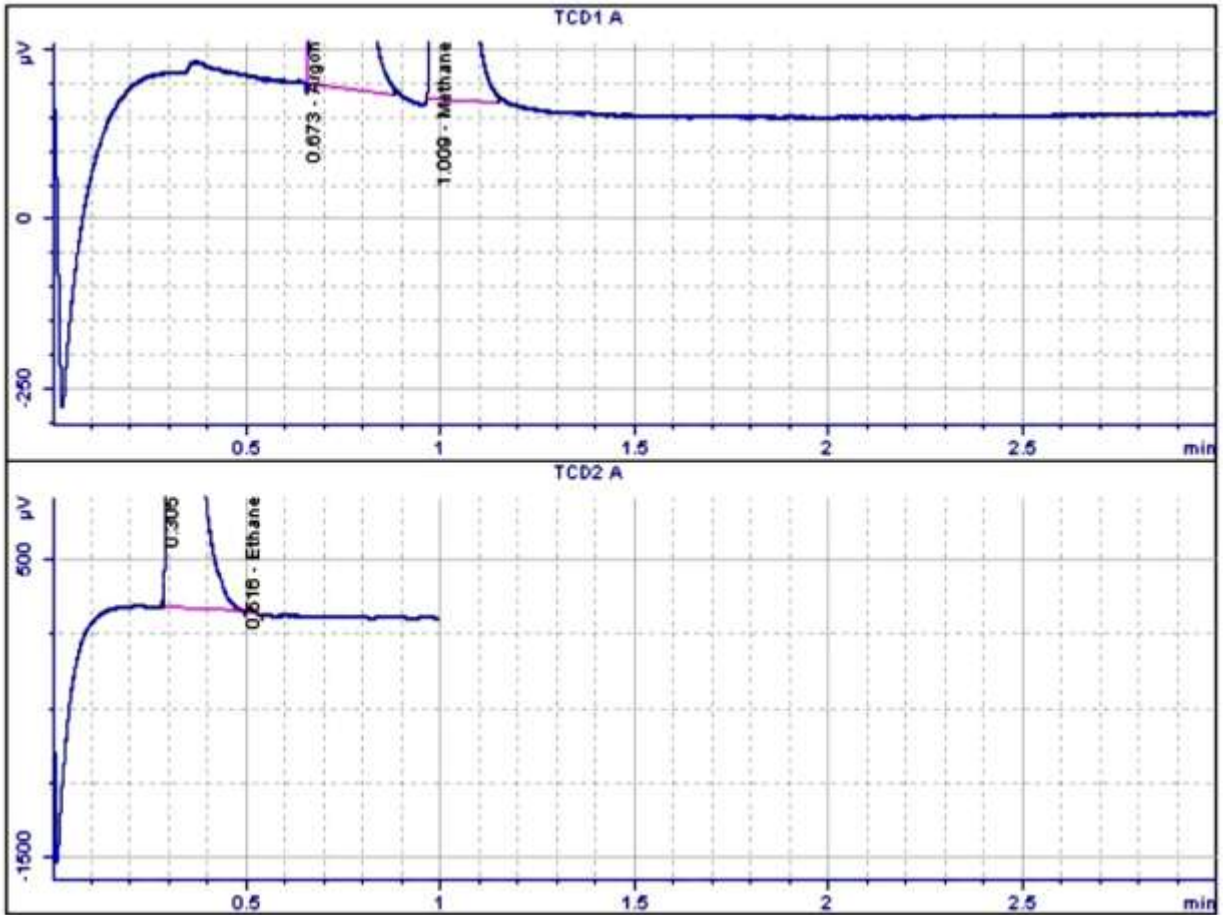
Third run, after 10 minutes



Signal	Retention Time [min]	Type	Area [$\mu\text{V}\cdot\text{s}$]	Amt/Area	Norm %	Name
1	0.574		-	-	-	Neon
1	0.671	PB	9.7353e+005	7.61245e-005	90.567661	Argon
1	0.717		-	-	-	Oxygen
1	0.866		-	-	-	Nitrogen
1	1.008	BB	5.9407e+004	1.29910e-004	9.431482	Methane
1	1.465		-	-	-	Carbon Monoxide
2	0.305	PBOS	6.0000e+039	0.00000e+000	0.000000	
2	0.424		-	-	-	Carbon Dioxide
2	0.469		-	-	-	Ethylene
2	0.515	PBA	11.85126	5.91779e-005	0.000857	Ethane
2	0.671		-	-	-	Acetylene

Total norm percent = 100.00000

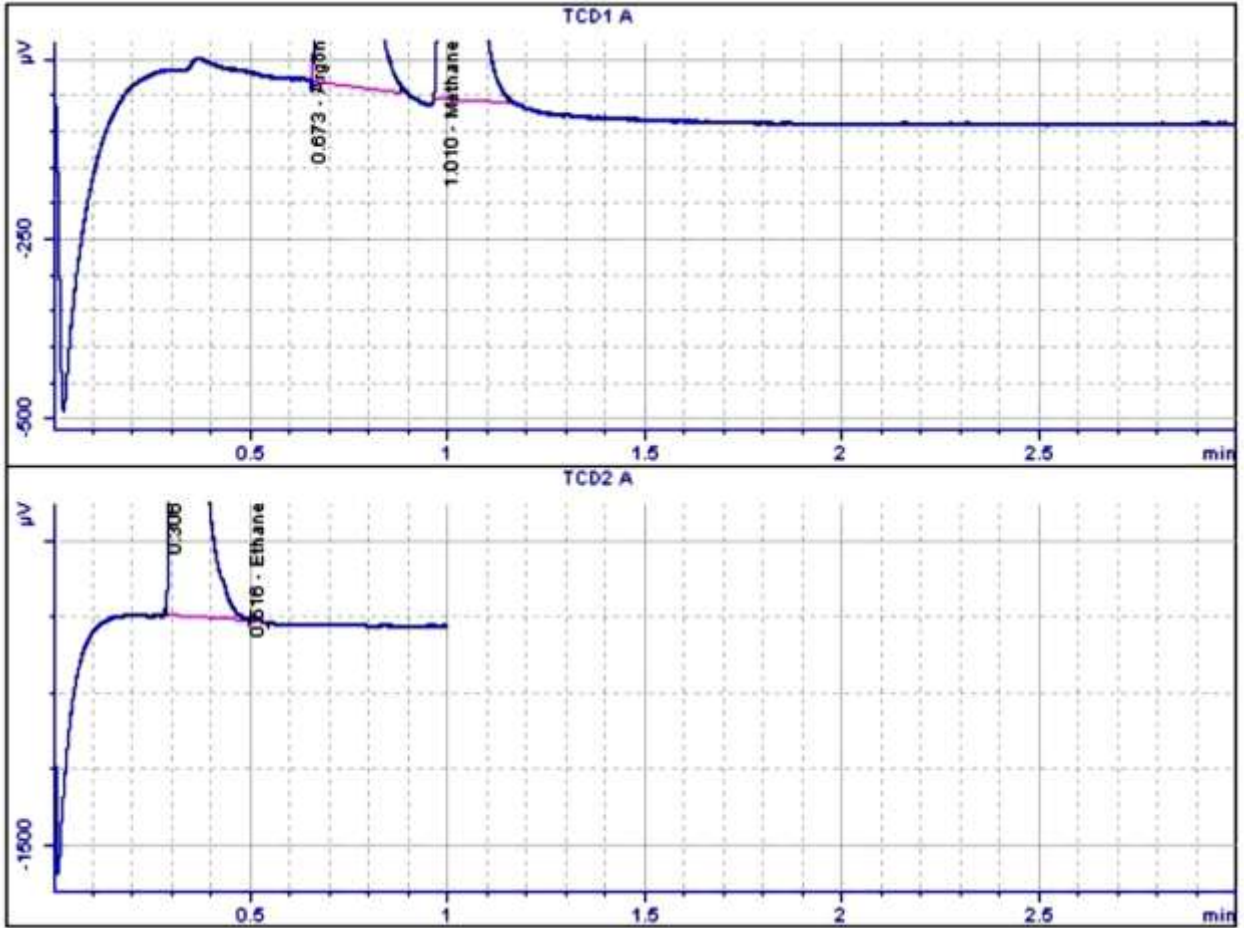
Forth run, after 15 minutes



Signal	Retention Time [min]	Type	Area [μV*s]	Amt/Area	Norm %	Name
1	0.574		-	-	-	Neon
1	0.673	BB	9.6813e+005	7.61245e-005	90.592185	Argon
1	0.717		-	-	-	Oxygen
1	0.866		-	-	-	Nitrogen
1	1.009	BB	5.8905e+004	1.29910e-004	9.406537	Methane
1	1.465		-	-	-	Carbon Monoxide
2	0.305	BBOS	6.0000e+039	0.00000e+000	0.000000	
2	0.424		-	-	-	Carbon Dioxide
2	0.469		-	-	-	Ethylene
2	0.516	PBA	17.56316	5.91779e-005	0.001278	Ethane
2	0.671		-	-	-	Acetylene

Total norm percent = 100.00000

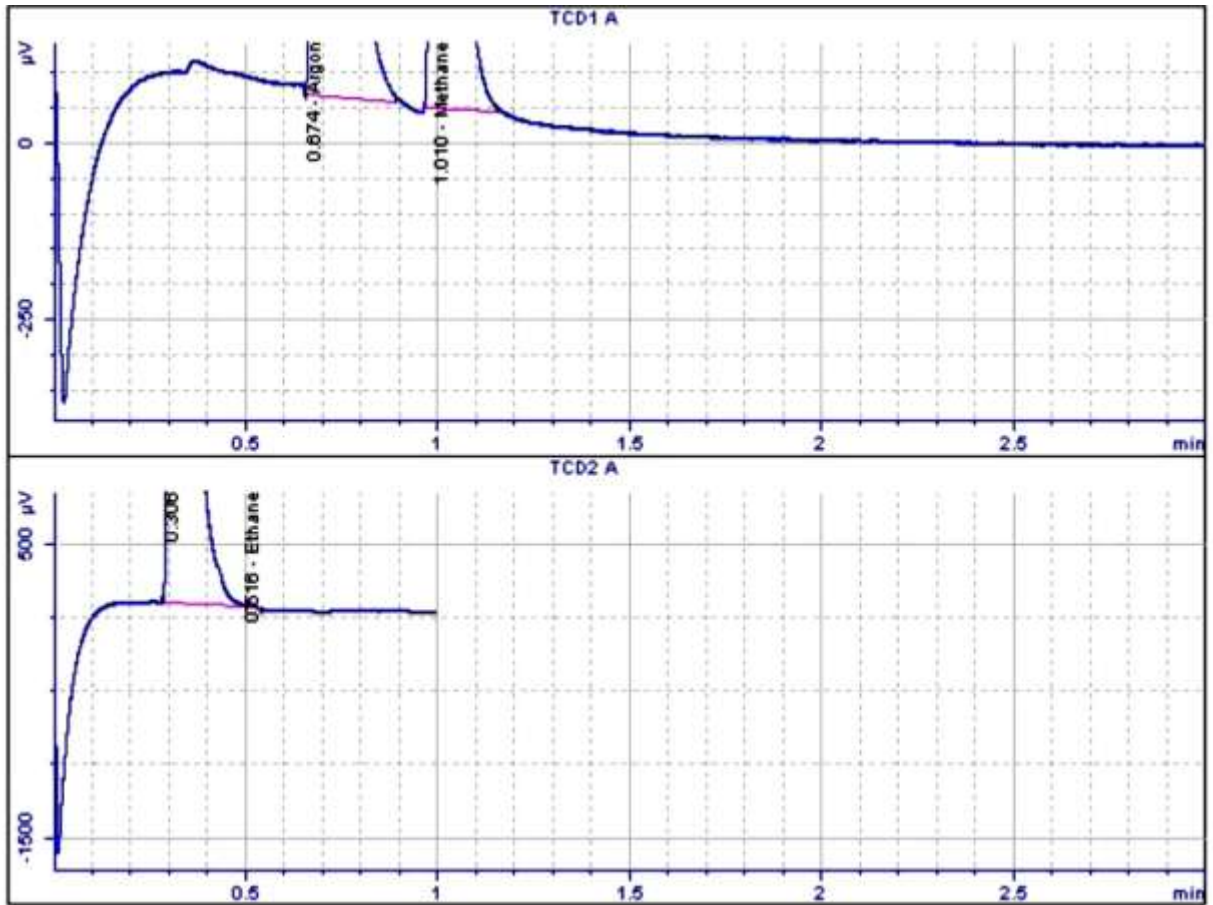
Fifth run, after 20 minutes



Signal	Retention Time [min]	Type	Area [$\mu\text{V}\cdot\text{s}$]	Amt/Area	Norm %	Name
1	0.574		-	-	-	Neon
1	0.673	BB	9.6594e+005	7.61245e-005	90.596127	Argon
1	0.717		-	-	-	Oxygen
1	0.866		-	-	-	Nitrogen
1	1.010	BB	5.8745e+004	1.29910e-004	9.402556	Methane
1	1.465		-	-	-	Carbon Monoxide
2	0.306	BBOS	6.0000e+039	0.00000e+000	0.000000	
2	0.424		-	-	-	Carbon Dioxide
2	0.469		-	-	-	Ethylene
2	0.516	PBA	18.06860	5.91779e-005	0.001317	Ethane
2	0.671		-	-	-	Acetylene

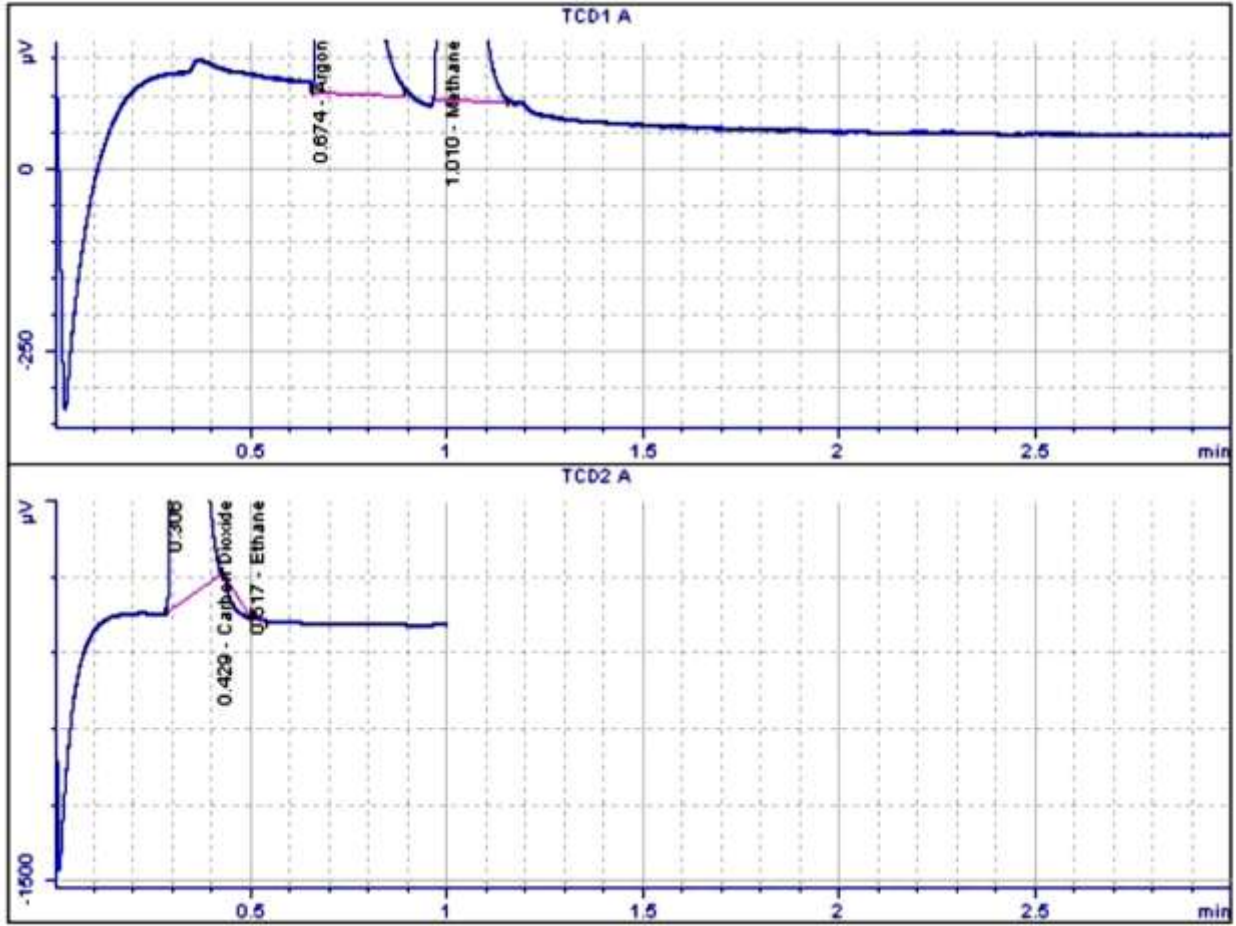
Total norm percent = 100.00000

Sixth run, after 25 minutes



Signal	Retention Time [min]	Type	Area [$\mu\text{V}\cdot\text{s}$]	Amt/Area	Norm %	Name
1	0.574		-	-	-	Neon
1	0.674	PB	9.6449e+005	7.61245e-005	90.669463	Argon
1	0.717		-	-	-	Oxygen
1	0.866		-	-	-	Nitrogen
1	1.010	BB	5.8154e+004	1.29910e-004	9.329496	Methane
1	1.465		-	-	-	Carbon Monoxide
2	0.306	BBOS	6.2000e+039	0.00000e+000	0.000000	
2	0.424		-	-	-	Carbon Dioxide
2	0.469		-	-	-	Ethylene
2	0.516	BBA	14.24130	5.91779e-005	0.001041	Ethane
2	0.671		-	-	-	Acetylene

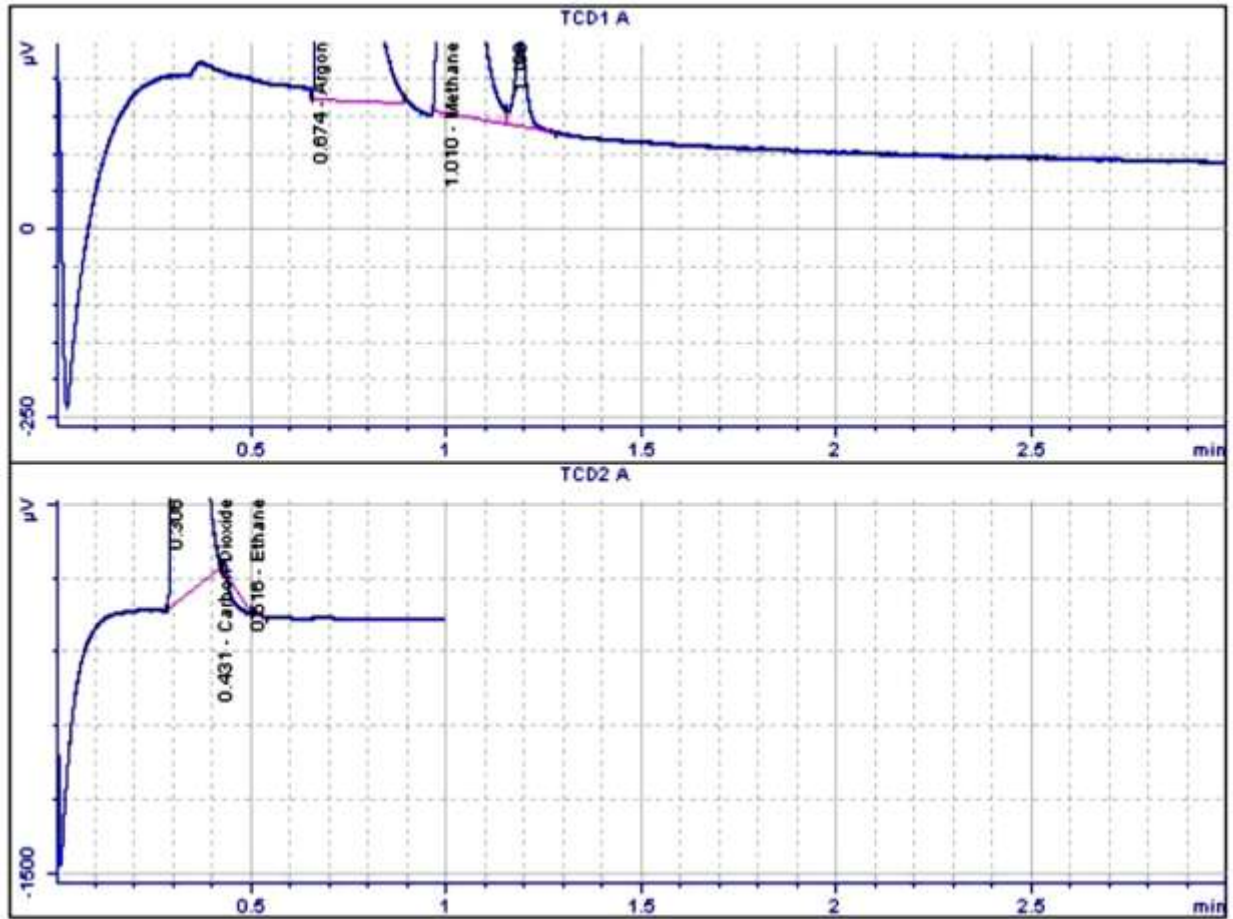
Seventh run, after 30 minutes



Signal	Retention Time [min]	Type	Area [µV*s]	Amt/Area	Norm %	Name
1	0.574		-	-	-	Neon
1	0.674	PB	9.6366e+005	7.61245e-005	90.840318	Argon
1	0.717		-	-	-	Oxygen
1	0.866		-	-	-	Nitrogen
1	1.010	BB	5.6932e+004	1.29910e-004	9.158590	Methane
1	1.465		-	-	-	Carbon Monoxide
2	0.306	PBOS	6.0000e+039	0.00000e+000	0.000000	
2	0.429	BBA	-219.88875	0.00000e+000	0.000000	Carbon Dioxide
2	0.469		-	-	-	Ethylene
2	0.517	BBA	14.90843	5.91779e-005	0.001092	Ethane
2	0.671		-	-	-	Acetylene

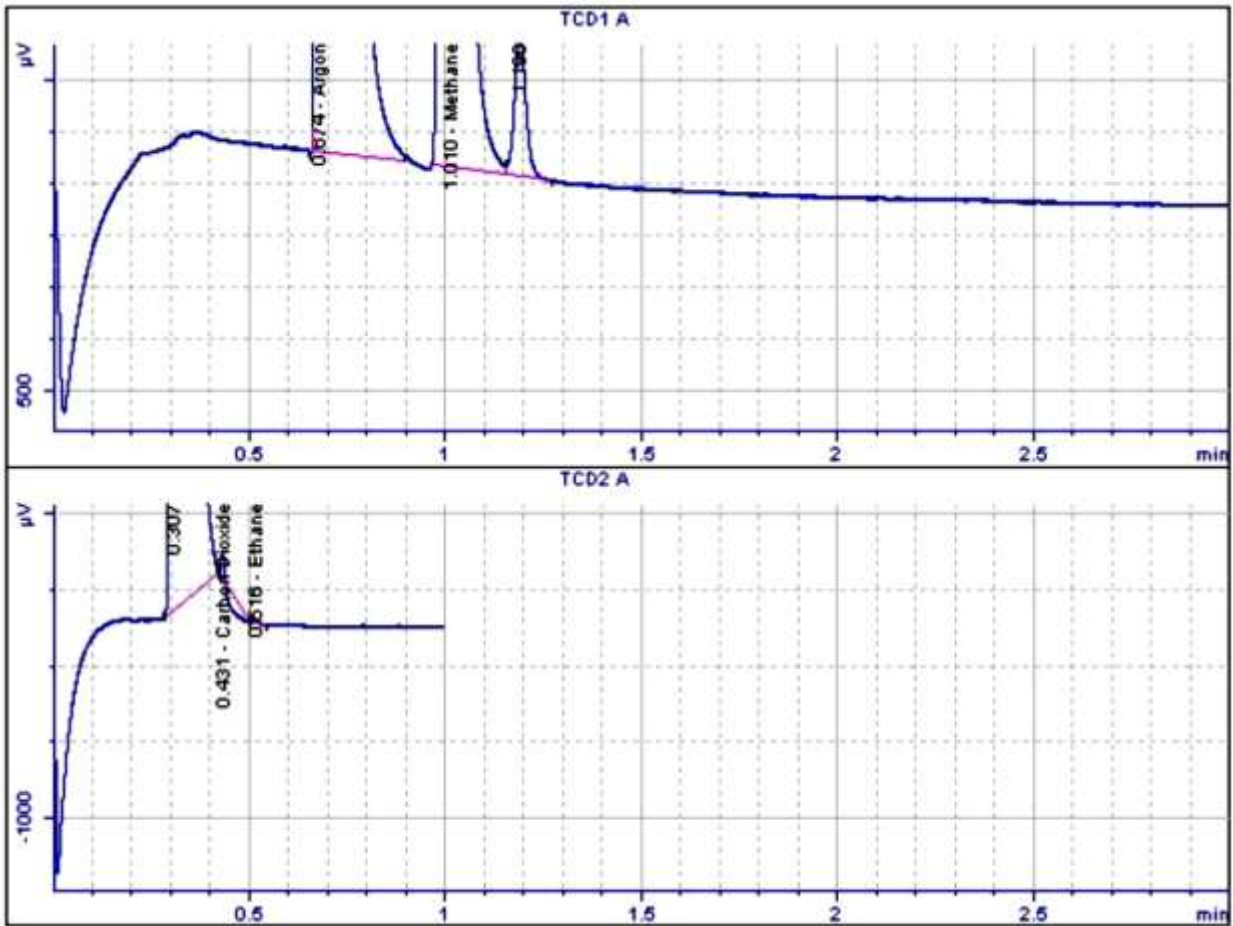
Total norm percent = 100.00000

Eighth run, after 35 minutes



Signal	Retention Time [min]	Type	Area [µV*s]	Amt/Area	Norm %	Name
1	0.574		-	-	-	Neon
1	0.674	PB	9.6249e+005	7.61245e-005	90.785751	Argon
1	0.717		-	-	-	Oxygen
1	0.866		-	-	-	Nitrogen
1	1.010	BB	5.7236e+004	1.29910e-004	9.213184	Methane
1	1.190	BB	233.61829	0.00000e+000	0.000000	
1	1.465		-	-	-	Carbon Monoxide
2	0.306	PBOS	6.0000e+039	0.00000e+000	0.000000	
2	0.431	BBA	-199.77285	0.00000e+000	0.000000	Carbon Dioxide
2	0.469		-	-	-	Ethylene
2	0.516	PBA	14.51803	5.91779e-005	0.001065	Ethane
2	0.671		-	-	-	Acetylene

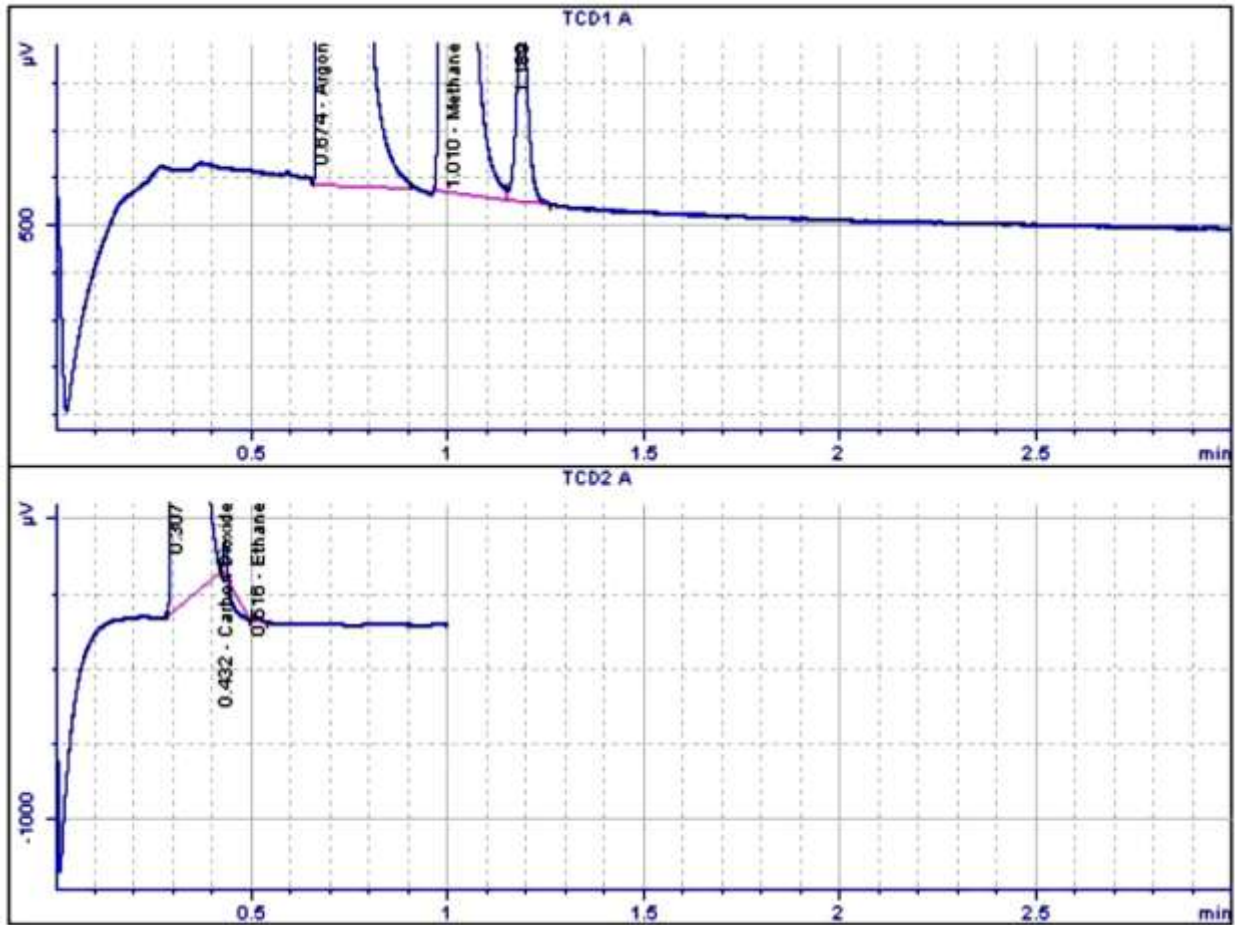
Ninth run, after 40 minutes



Signal	Retention Time [min]	Type	Area [$\mu\text{V}\cdot\text{s}$]	Amt/Area	Norm %	Name
1	0.574		-	-	-	Neon
1	0.674	BB	9.6147e+005	7.61245e-005	90.864732	Argon
1	0.717		-	-	-	Oxygen
1	0.866		-	-	-	Nitrogen
1	1.010	BV	5.6636e+004	1.29910e-004	9.134265	Methane
1	1.190	VB	568.83473	0.00000e+000	0.000000	
1	1.465		-	-	-	Carbon Monoxide
2	0.307	PBOS	6.0000e+039	0.00000e+000	0.000000	
2	0.431	BBA	-119.25200	0.00000e+000	0.000000	Carbon Dioxide
2	0.469		-	-	-	Ethylene
2	0.516	BBA	13.65545	5.91779e-005	0.001003	Ethane
2	0.671		-	-	-	Acetylene

Total norm percent = 100.00000

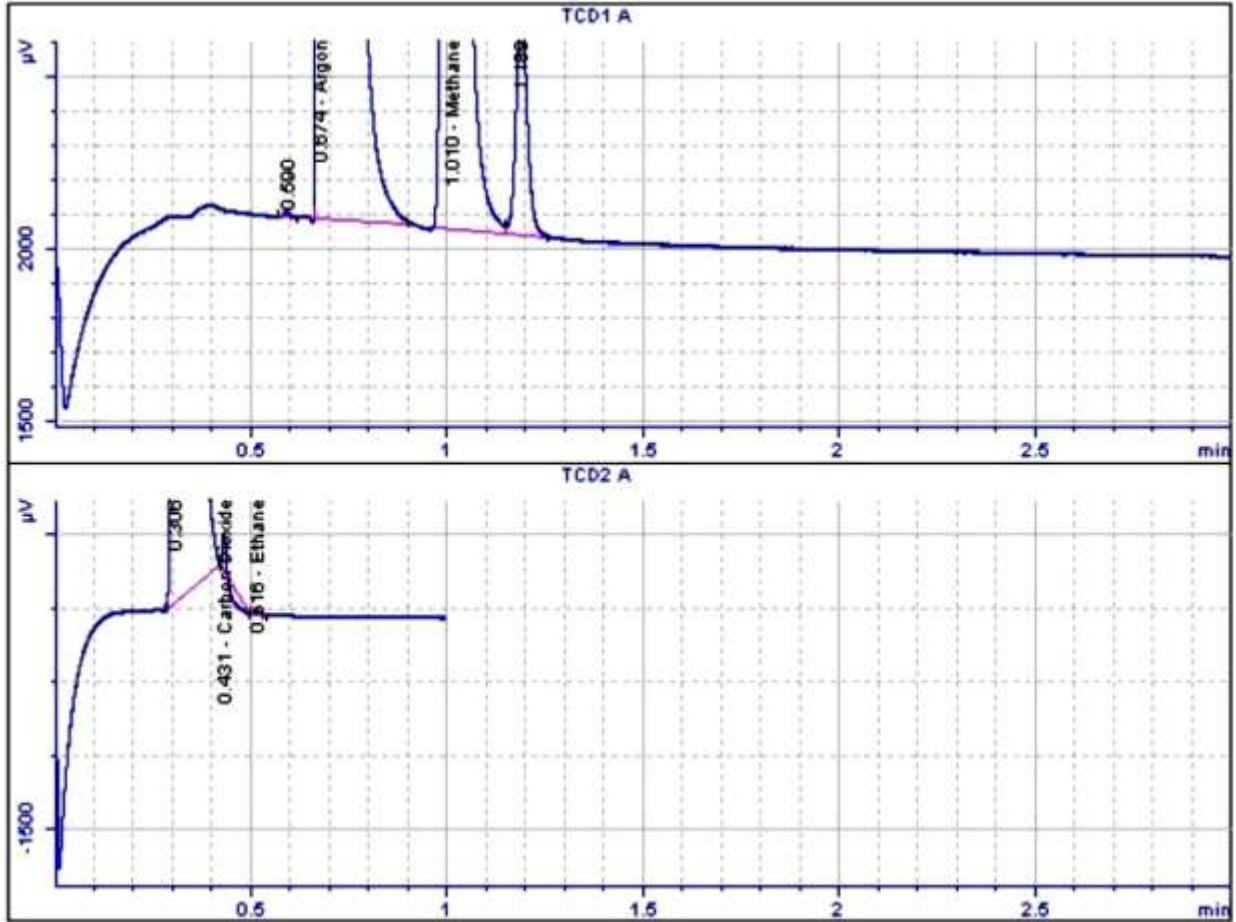
Tenth run, after 45 minutes



Signal	Retention Time [min]	Type	Area [μV*s]	Amt/Area	Norm %	Name
1	0.574		-	-	-	Neon
1	0.674	PB	9.6063e+005	7.61245e-005	90.926112	Argon
1	0.717		-	-	-	Oxygen
1	0.866		-	-	-	Nitrogen
1	1.010	BV	5.6167e+004	1.29910e-004	9.072614	Methane
1	1.189	VB	818.80934	0.00000e+000	0.000000	
1	1.465		-	-	-	Carbon Monoxide
2	0.307	PBOS	6.0000e+039	0.00000e+000	0.000000	
2	0.432	BBA	-53.80640	0.00000e+000	0.000000	Carbon Dioxide
2	0.469		-	-	-	Ethylene
2	0.516	PBA	17.31900	5.91779e-005	0.001274	Ethane
2	0.671		-	-	-	Acetylene

Total norm percent = 100.00000

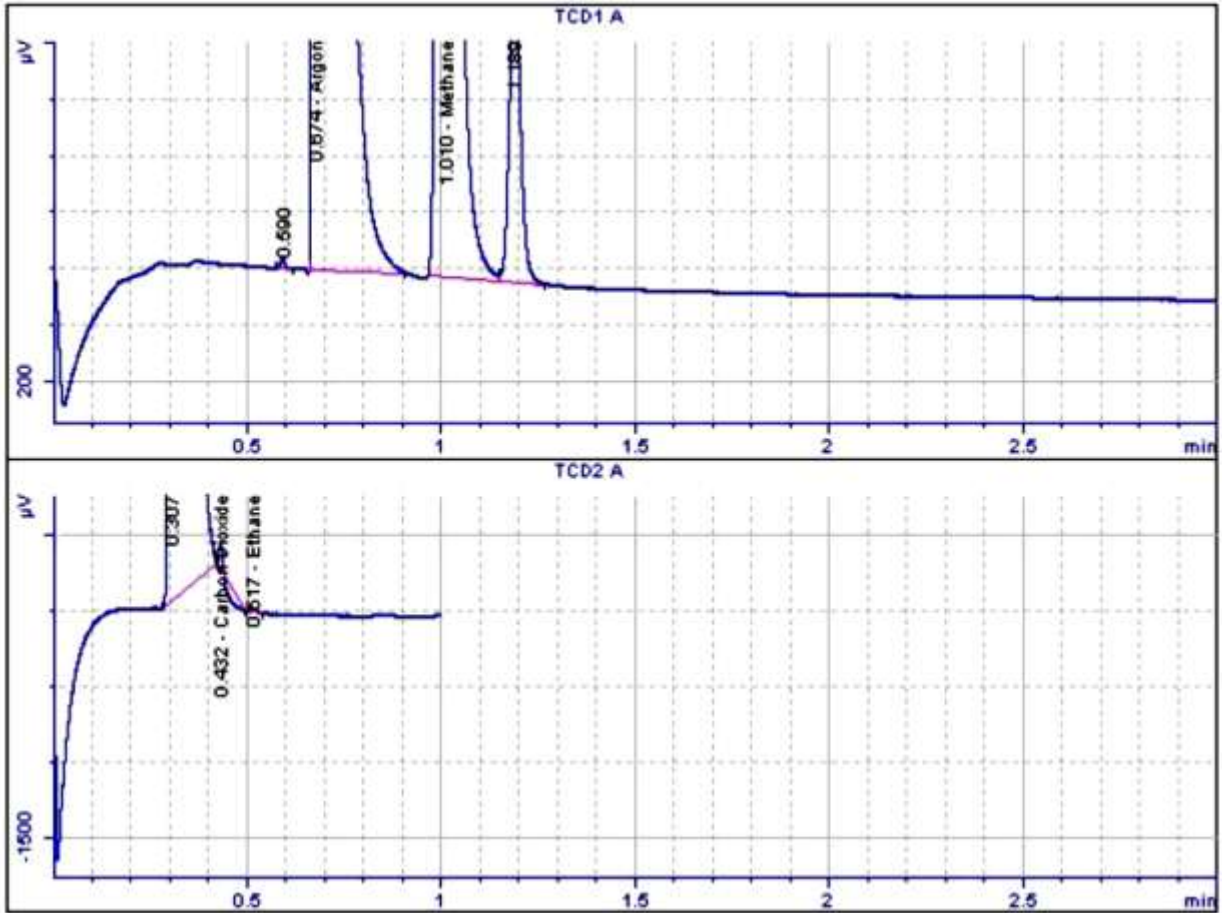
Eleventh run, after 50 minutes



Signal	Retention Time [min]	Type	Area [µV*s]	Amt/Area	Norm %	Name
1	0.574		-	-	-	Neon
1	0.590	PB	15.85863	0.00000e+000	0.000000	
1	0.674	BB	9.5953e+005	7.61245e-005	91.051021	Argon
1	0.717		-	-	-	Oxygen
1	0.866		-	-	-	Nitrogen
1	1.010	BV	5.5256e+004	1.29910e-004	8.947934	Methane
1	1.189	VB	1321.52054	0.00000e+000	0.000000	
1	1.465		-	-	-	Carbon Monoxide
2	0.306	PBOS	6.0000e+039	0.00000e+000	0.000000	
2	0.431	BBA	-51.06100	0.00000e+000	0.000000	Carbon Dioxide
2	0.469		-	-	-	Ethylene
2	0.516	BBA	14.15512	5.91779e-005	0.001044	Ethane
2	0.671		-	-	-	Acetylene

Total norm percent = 100.00000

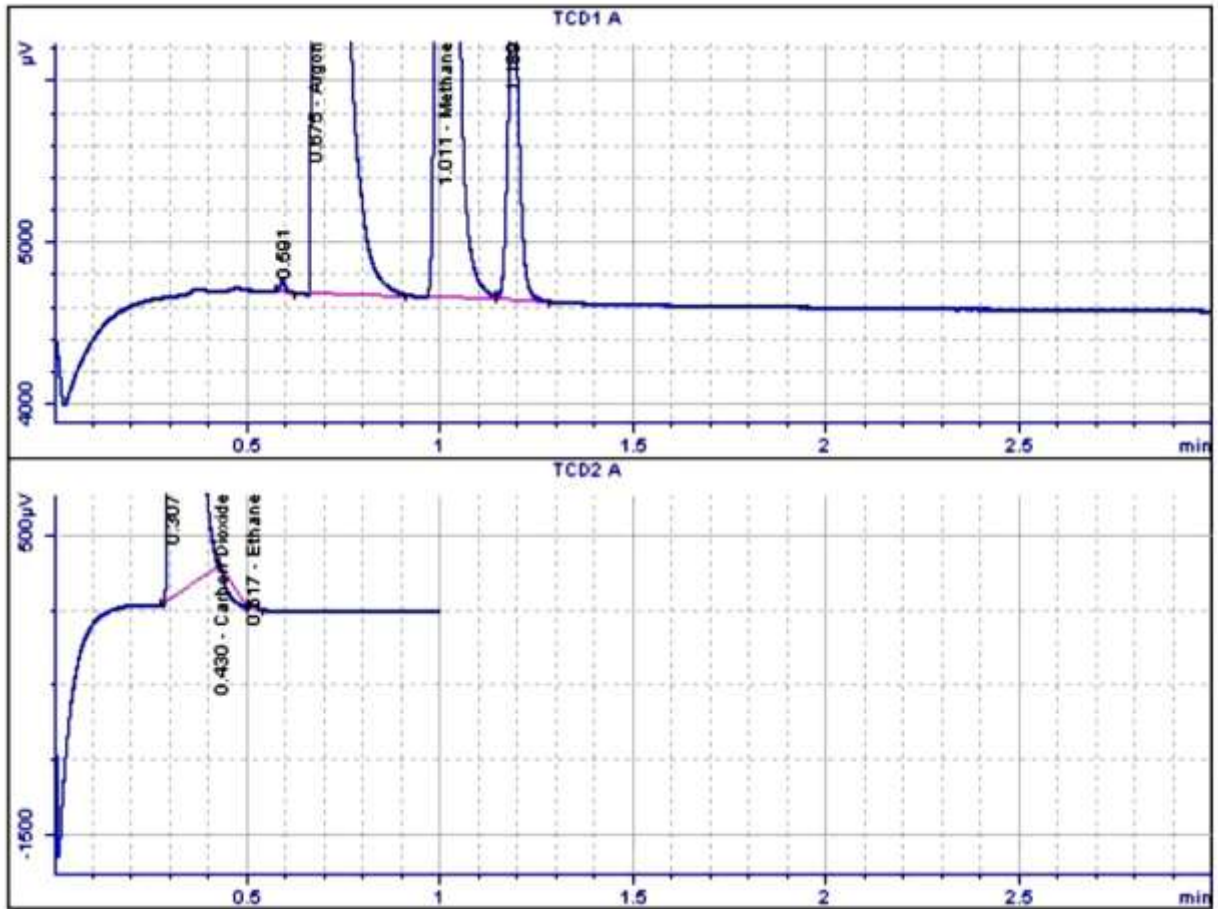
Twelvth run, after 55 minutes



Signal	Retention Time [min]	Type	Area [$\mu\text{V}\cdot\text{s}$]	Amt/Area	Norm %	Name
1	0.574		-	-	-	Neon
1	0.590	PB	30.59789	0.00000e+000	0.000000	
1	0.674	BB	9.5765e+005	7.61245e-005	91.182206	Argon
1	0.717		-	-	-	Oxygen
1	0.866		-	-	-	Nitrogen
1	1.010	BV	5.4258e+004	1.29910e-004	8.816207	Methane
1	1.189	VB	2256.02386	0.00000e+000	0.000000	
1	1.465		-	-	-	Carbon Monoxide
2	0.307	PBOS	6.0000e+039	0.00000e+000	0.000000	
2	0.432	BBA	-117.08250	0.00000e+000	0.000000	Carbon Dioxide
2	0.469		-	-	-	Ethylene
2	0.517	PBA	21.45154	5.91779e-005	0.001588	Ethane
2	0.671		-	-	-	Acetylene

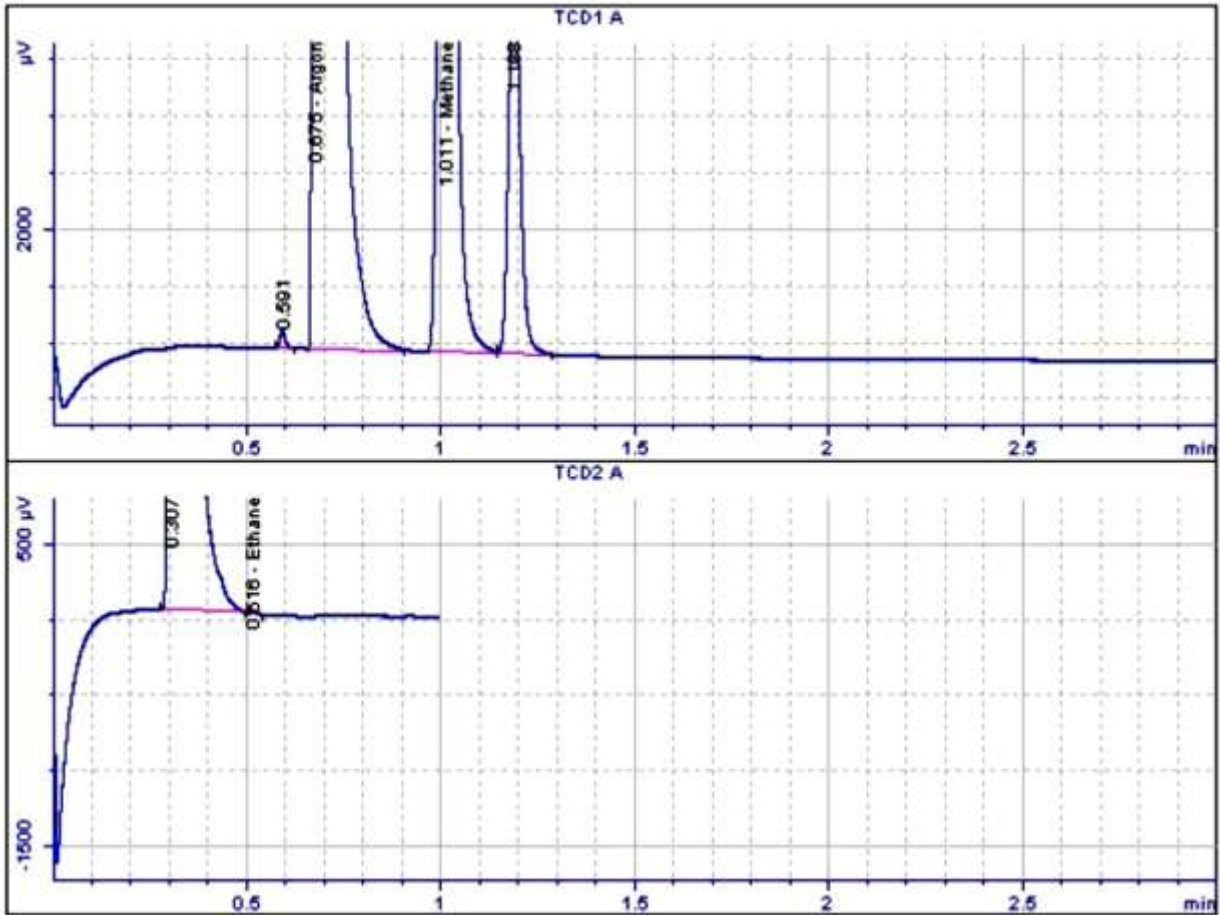
Total norm percent = 100.00000

Thirteenth run, after 60 minutes



Signal	Retention Time [min]	Type	Area [µV*s]	Amt/Area	Norm %	Name
1	0.574		-	-	-	Neon
1	0.591	PB	68.60849	0.00000e+000	0.000000	
1	0.675	BB	9.5175e+005	7.61245e-005	91.584727	Argon
1	0.717		-	-	-	Oxygen
1	0.866		-	-	-	Nitrogen
1	1.011	BV	5.1235e+004	1.29910e-004	8.413684	Methane
1	1.189	VB	3975.48797	0.00000e+000	0.000000	
1	1.465		-	-	-	Carbon Monoxide
2	0.307	PBOS	6.0000e+039	0.00000e+000	0.000000	
2	0.430	BBA	-234.58838	0.00000e+000	0.000000	Carbon Dioxide
2	0.469		-	-	-	Ethylene
2	0.517	BBA	21.24277	5.91779e-005	0.001589	Ethane
2	0.671		-	-	-	Acetylene

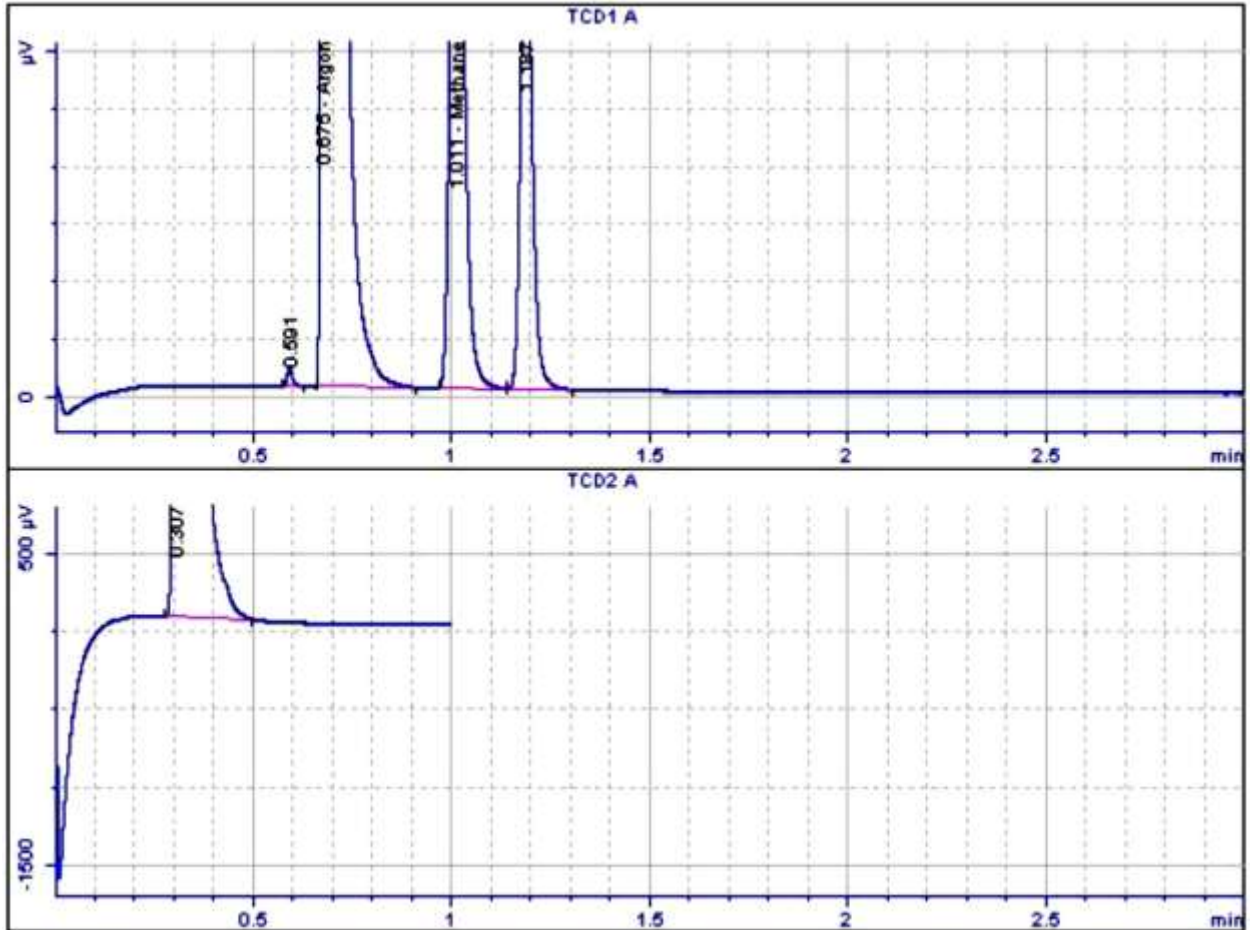
Forteenth run, after 65 minutes



Signal	Retention Time [min]	Type	Area [$\mu\text{V}\cdot\text{s}$]	Amt/Area	Norm %	Name
1	0.574		-	-	-	Neon
1	0.591	BB	150.34202	0.00000e+000	0.000000	
1	0.675	BB	9.4391e+005	7.61245e-005	92.372385	Argon
1	0.717		-	-	-	Oxygen
1	0.866		-	-	-	Nitrogen
1	1.011	BV	4.5667e+004	1.29910e-004	7.626566	Methane
1	1.188	VB	7736.00153	0.00000e+000	0.000000	
1	1.465		-	-	-	Carbon Monoxide
2	0.307	PBOS	5.8000e+039	0.00000e+000	0.000000	
2	0.424		-	-	-	Carbon Dioxide
2	0.469		-	-	-	Ethylene
2	0.516	PBA	13.78930	5.91779e-005	0.001049	Ethane
2	0.671		-	-	-	Acetylene

Total norm percent = 100.00000

Fifteenth run, after 70 minutes



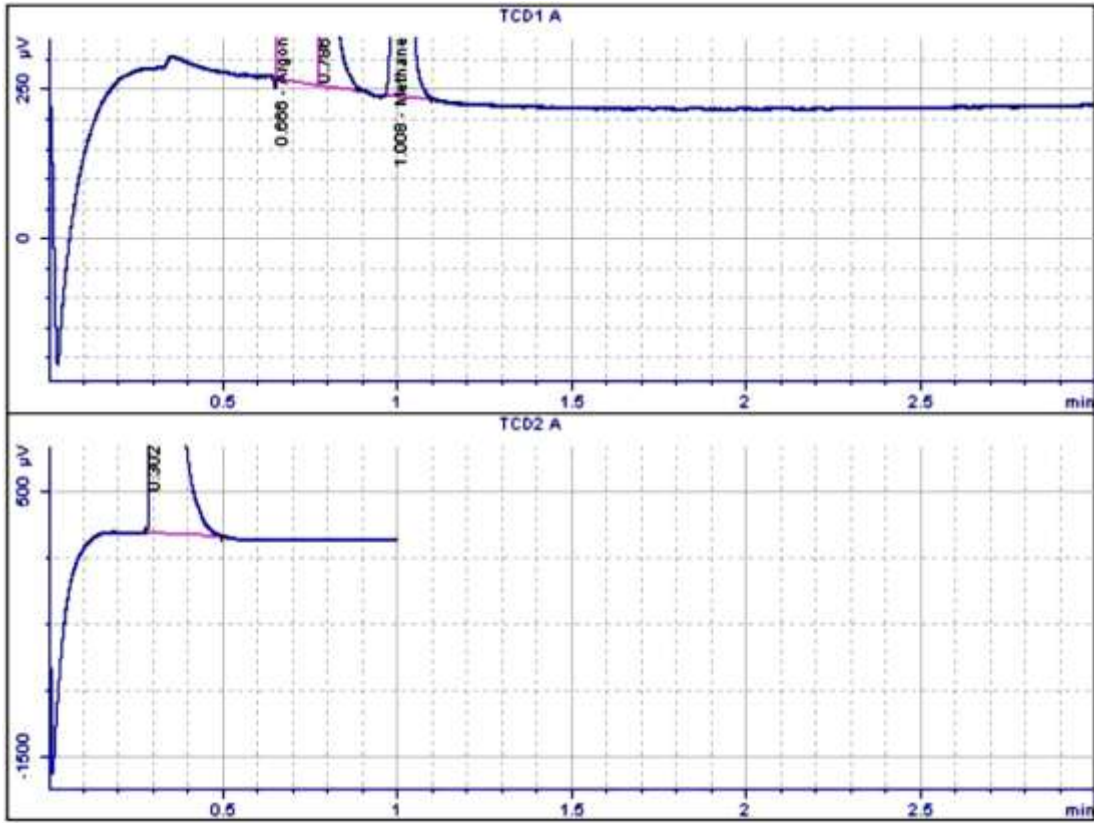
Signal	Retention Time [min]	Type	Area [$\mu\text{V}\cdot\text{s}$]	Amt/Area	Norm %	Name
1	0.574		-	-	-	Neon
1	0.591	BB	308.76715	0.00000e+000	0.000000	
1	0.675	BB	9.1997e+005	7.61245e-005	94.205151	Argon
1	0.717		-	-	-	Oxygen
1	0.866		-	-	-	Nitrogen
1	1.011	BV	3.3161e+004	1.29910e-004	5.794849	Methane
1	1.187	VB	1.8045e+004	0.00000e+000	0.000000	
1	1.465		-	-	-	Carbon Monoxide
2	0.307	PBOS	5.8000e+039	0.00000e+000	0.000000	
2	0.424		-	-	-	Carbon Dioxide
2	0.469		-	-	-	Ethylene
2	0.514		-	-	-	Ethane
2	0.671		-	-	-	Acetylene

Total norm percent = 100.00000

APPENDIX B3: GAS CHROMATOGRAPH FILES OF TPR

(B=15)

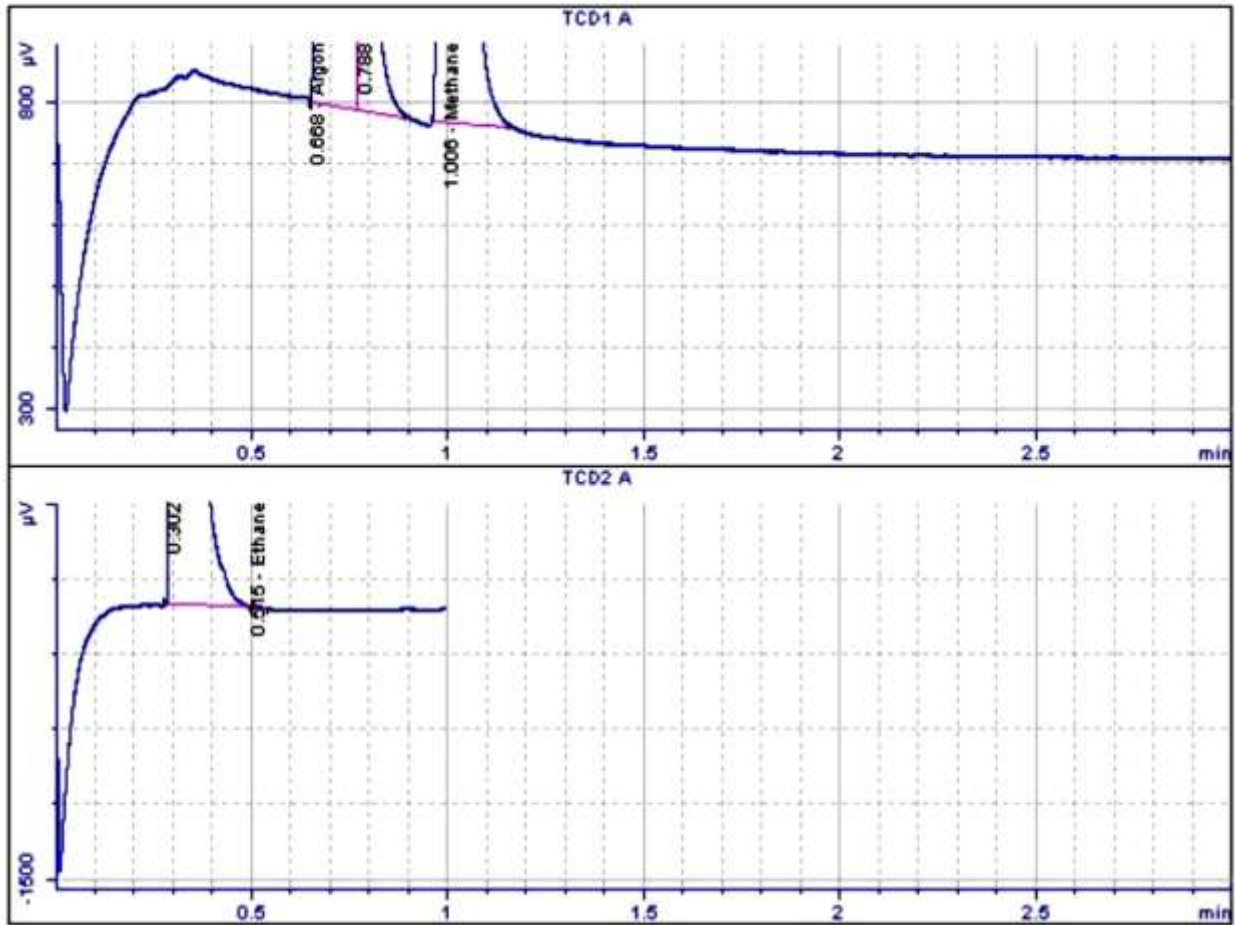
First run



Signal	Retention Time [min]	Type	Area [$\mu\text{V}\cdot\text{s}$]	Amt/Area	Norm %	Name
1	0.574		-	-	-	Neon
1	0.666	BV	1.0448e+006	7.61245e-005	99.427932	Argon
1	0.717		-	-	-	Oxygen
1	0.786	VB	2989.19250	0.00000e+000	0.000000	
1	0.866		-	-	-	Nitrogen
1	1.008	BB	3522.65497	1.29910e-004	0.572068	Methane
1	1.465		-	-	-	Carbon Monoxide
2	0.302	BBOS	6.4000e+039	0.00000e+000	0.000000	
2	0.424		-	-	-	Carbon Dioxide
2	0.469		-	-	-	Ethylene
2	0.514		-	-	-	Ethane
2	0.671		-	-	-	Acetylene

Total norm percent = 100.00000

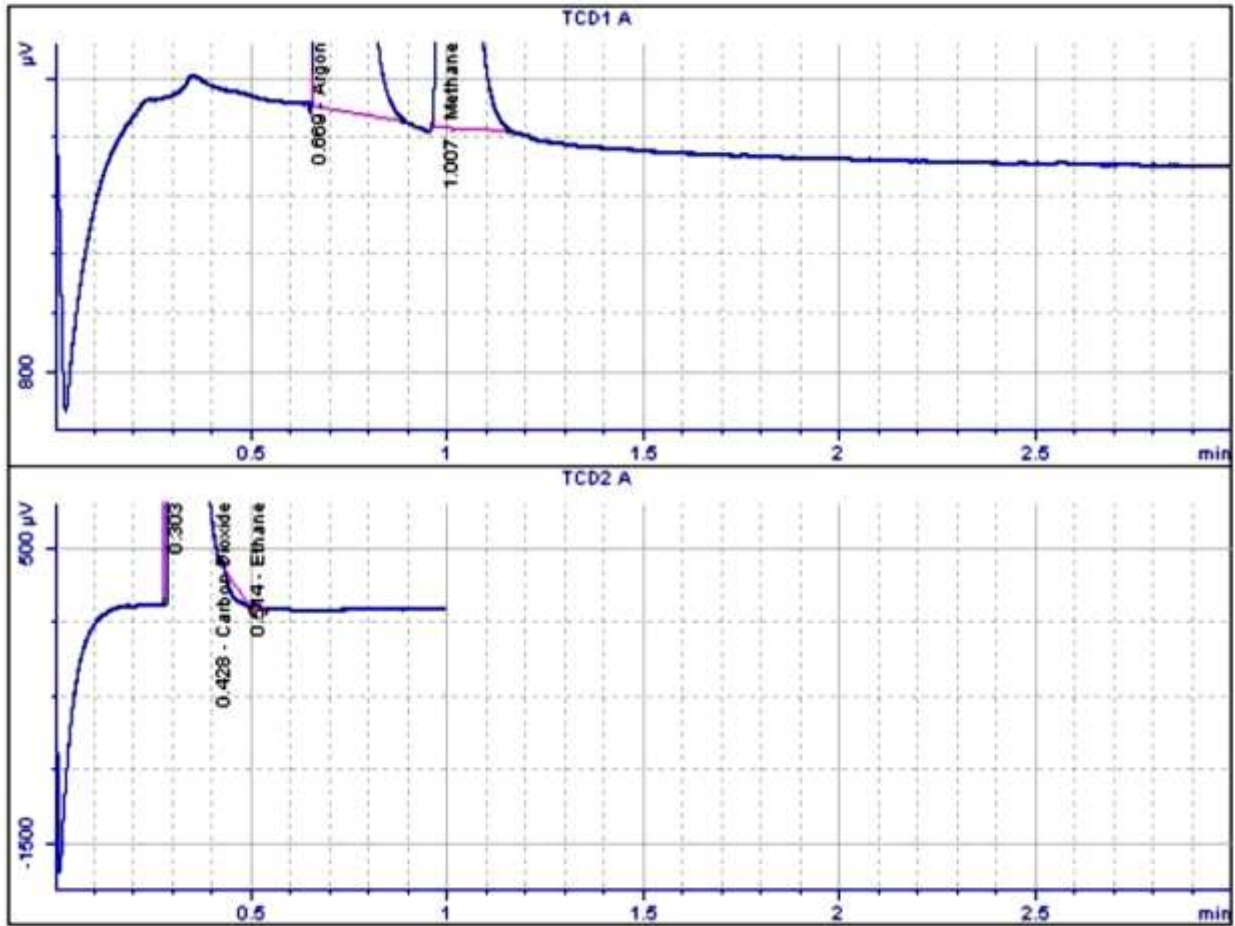
Second run, after 5 minutes



Signal	Retention Time [min]	Type	Area [μV*s]	Amt/Area	Norm %	Name
1	0.574		-	-	-	Neon
1	0.668	PV	9.7789e+005	7.61245e-005	91.387402	Argon
1	0.717		-	-	-	Oxygen
1	0.788	VB	4714.73606	0.00000e+000	0.000000	
1	0.866		-	-	-	Nitrogen
1	1.006	BB	5.3997e+004	1.29910e-004	8.611597	Methane
1	1.465		-	-	-	Carbon Monoxide
2	0.302	BBOS	6.0000e+039	0.00000e+000	0.000000	
2	0.424		-	-	-	Carbon Dioxide
2	0.469		-	-	-	Ethylene
2	0.515	BBA	13.78899	5.91779e-005	0.001002	Ethane
2	0.671		-	-	-	Acetylene

Total norm percent = 100.00000

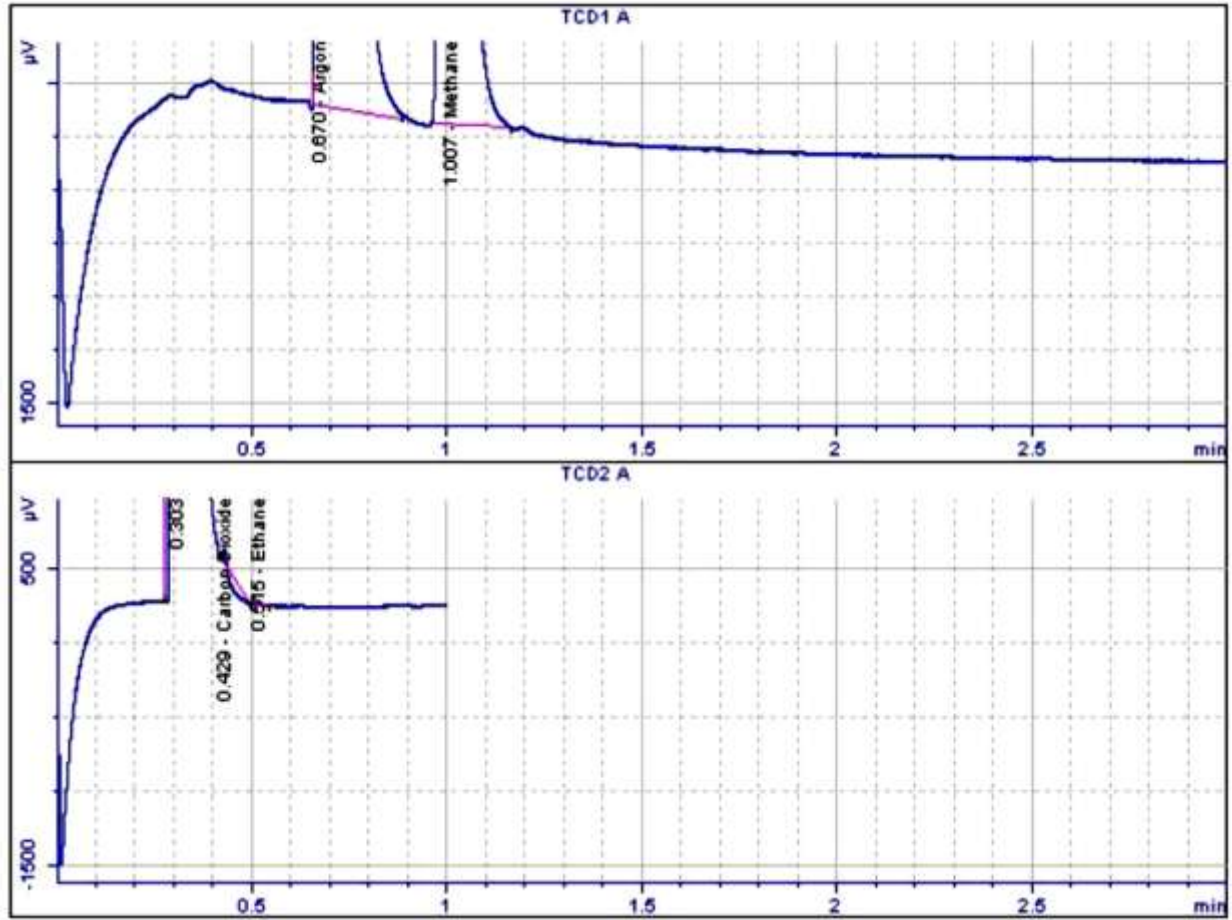
Third run after 10 minutes



Signal	Retention Time [min]	Type	Area [μV*s]	Amt/Area	Norm %	Name
1	0.574		-	-	-	Neon
1	0.669	BB	9.6947e+005	7.61245e-005	90.098667	Argon
1	0.717		-	-	-	Oxygen
1	0.866		-	-	-	Nitrogen
1	1.007	BB	6.2422e+004	1.29910e-004	9.900013	Methane
1	1.465		-	-	-	Carbon Monoxide
2	0.303	PBOS	6.2000e+039	0.00000e+000	0.000000	
2	0.428	BBA	-205.39700	0.00000e+000	0.000000	Carbon Dioxide
2	0.469		-	-	-	Ethylene
2	0.514	BBA	18.27433	5.91779e-005	0.001320	Ethane
2	0.671		-	-	-	Acetylene

Total norm percent = 100.00000

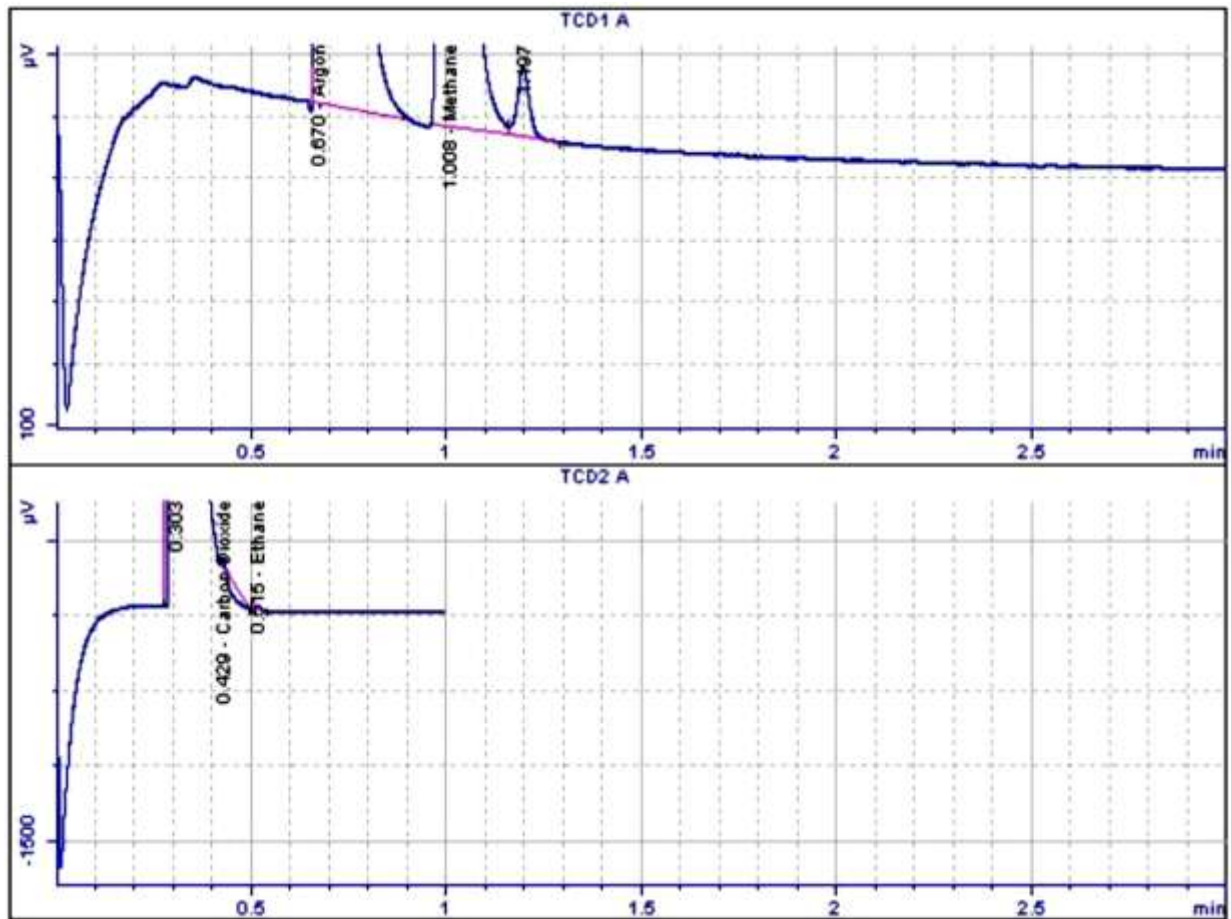
Forth run, after 15 minutes



Signal	Retention Time [min]	Type	Area [$\mu\text{V}\cdot\text{s}$]	Amt/Area	Norm %	Name
1	0.574		-	-	-	Neon
1	0.670	BB	9.6632e+005	7.61245e-005	89.945424	Argon
1	0.717		-	-	-	Oxygen
1	0.866		-	-	-	Nitrogen
1	1.007	BB	6.3289e+004	1.29910e-004	10.053171	Methane
1	1.465		-	-	-	Carbon Monoxide
2	0.303	PBOS	6.2000e+039	0.00000e+000	0.000000	
2	0.429	BBA	-151.23990	0.00000e+000	0.000000	Carbon Dioxide
2	0.469		-	-	-	Ethylene
2	0.515	BBA	19.41355	5.91779e-005	0.001405	Ethane
2	0.671		-	-	-	Acetylene

Total norm percent = 100.00000

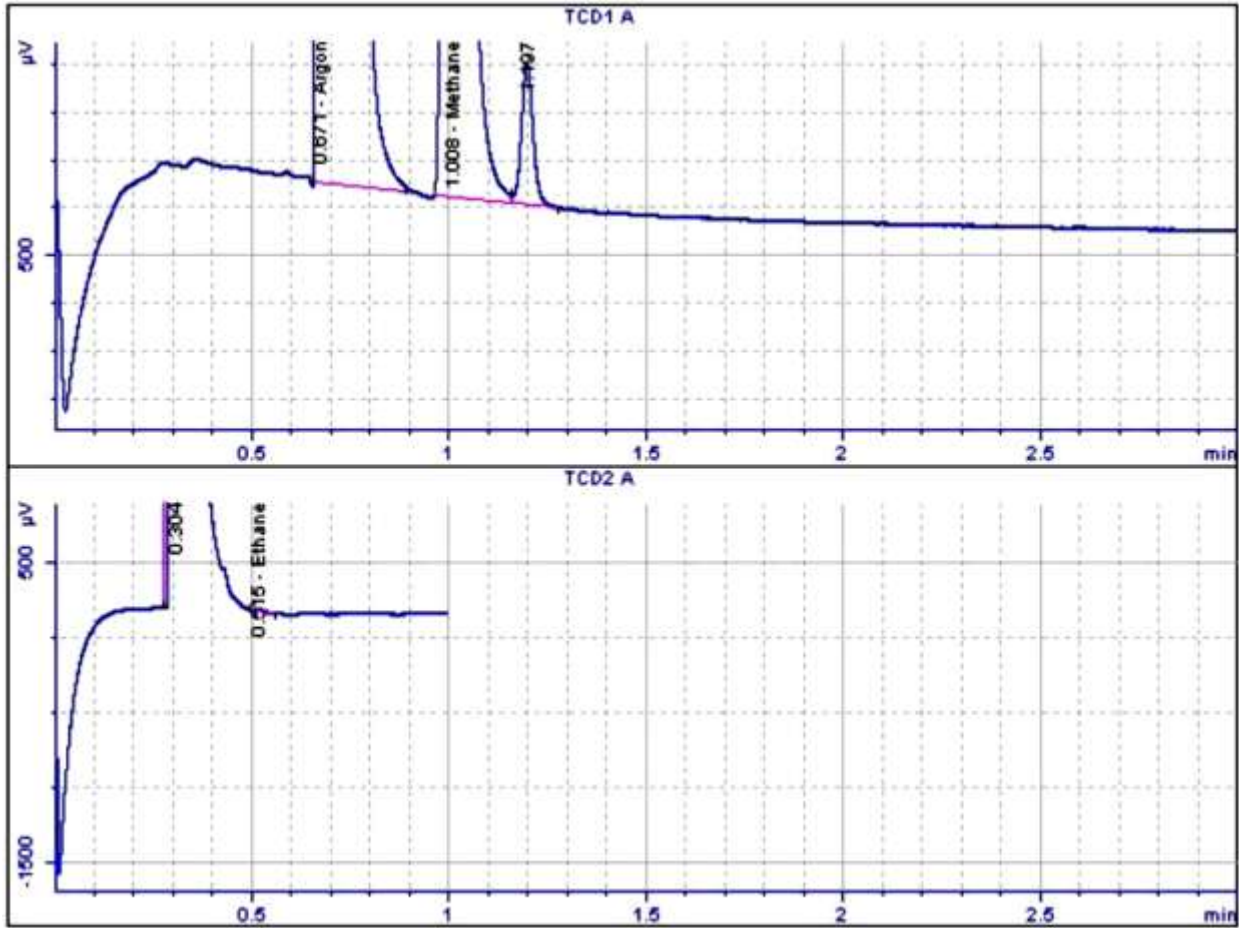
Fifth run, after 20 minutes



Signal	Retention Time [min]	Type	Area [$\mu\text{V}\cdot\text{s}$]	Amt/Area	Norm %	Name
1	0.574		-	-	-	Neon
1	0.670	BB	9.6324e+005	7.61245e-005	89.780037	Argon
1	0.717		-	-	-	Oxygen
1	0.866		-	-	-	Nitrogen
1	1.008	BB	6.4243e+004	1.29910e-004	10.218598	Methane
1	1.197	BP	242.08018	0.00000e+000	0.000000	
1	1.465		-	-	-	Carbon Monoxide
2	0.303	PBOS	6.0000e+039	0.00000e+000	0.000000	
2	0.429	BBA	-165.38700	0.00000e+000	0.000000	Carbon Dioxide
2	0.469		-	-	-	Ethylene
2	0.515	PBA	18.84672	5.91779e-005	0.001366	Ethane
2	0.671		-	-	-	Acetylene

Total norm percent = 100.00000

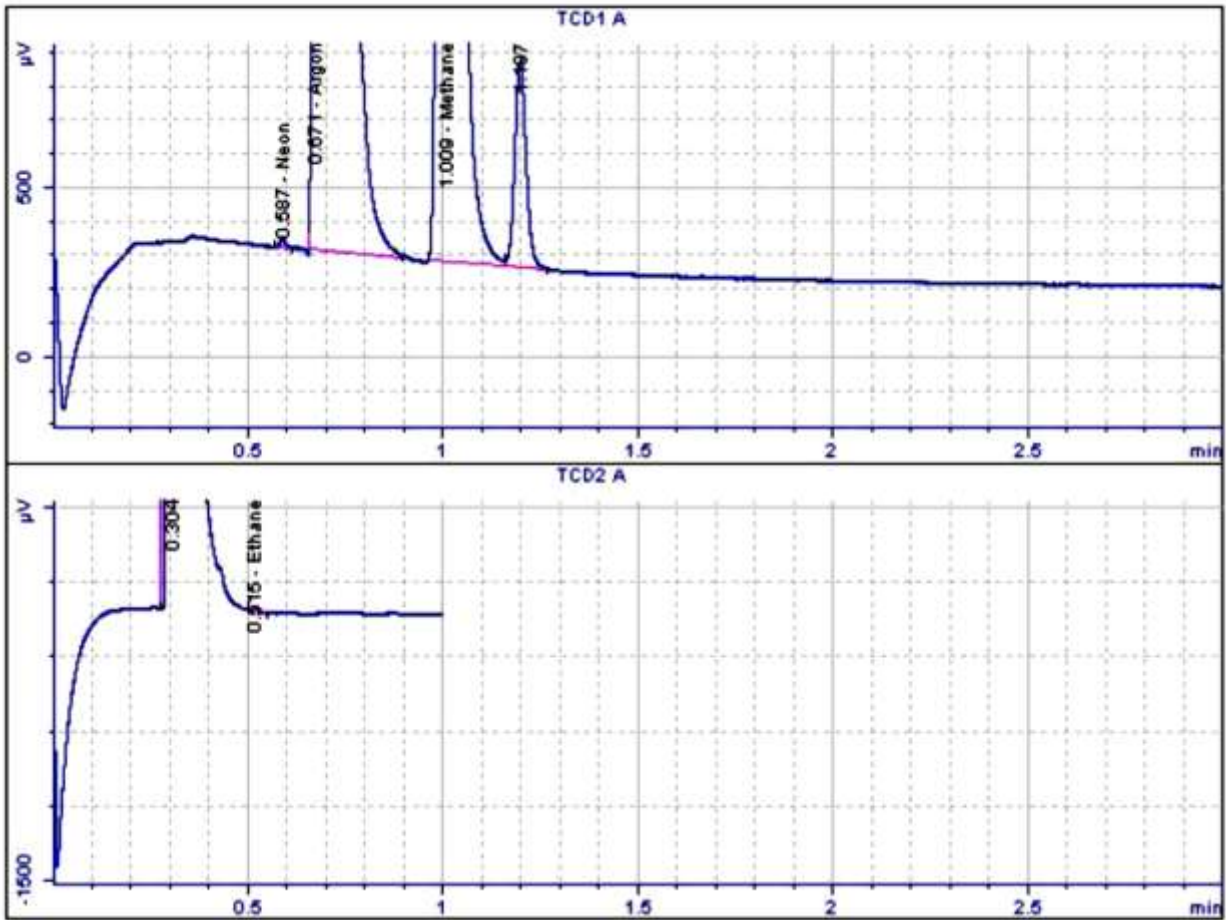
Sixth run, after 25 minutes



Signal	Retention Time [min]	Type	Area [$\mu\text{V}\cdot\text{s}$]	Amt/Area	Norm %	Name
1	0.574		-	-	-	Neon
1	0.671	PB	9.6215e+005	7.61245e-005	89.840115	Argon
1	0.717		-	-	-	Oxygen
1	0.866		-	-	-	Nitrogen
1	1.008	BB	6.3752e+004	1.29910e-004	10.158789	Methane
1	1.197	BB	610.95634	0.00000e+000	0.000000	
1	1.465		-	-	-	Carbon Monoxide
2	0.304	PBOS	6.0000e+039	0.00000e+000	0.000000	
2	0.424		-	-	-	Carbon Dioxide
2	0.469		-	-	-	Ethylene
2	0.515	PBA	15.10490	5.91779e-005	0.001096	Ethane
2	0.671		-	-	-	Acetylene

Total norm percent = 100.00000

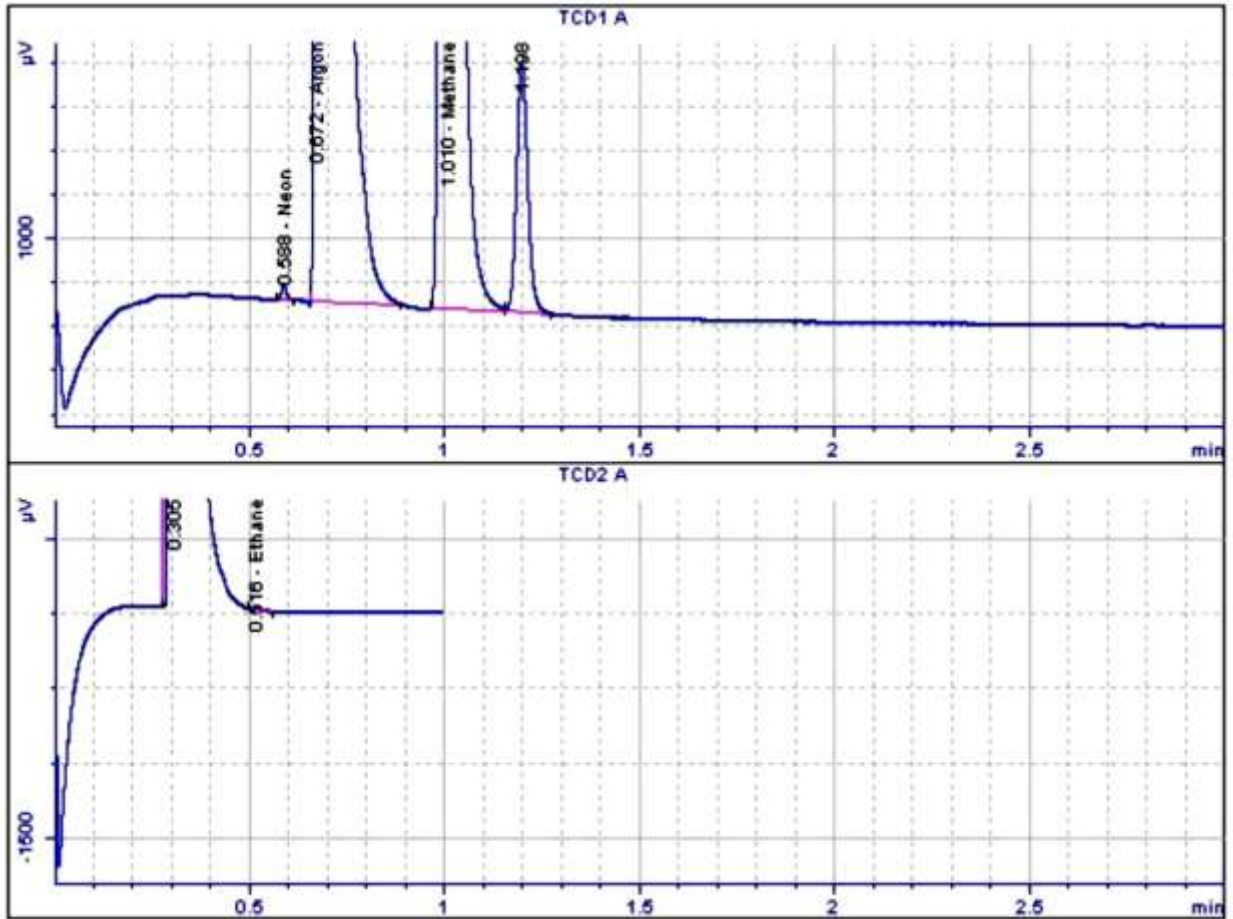
Seventh run, after 30 minutes



Signal	Retention Time [min]	Type	Area [µV*s]	Amt/Area	Norm %	Name
1	0.587	BB	24.35994	2.68238e-004	0.008050	Neon
1	0.671	BB	9.5955e+005	7.61245e-005	89.994607	Argon
1	0.717		-	-	-	Oxygen
1	0.866		-	-	-	Nitrogen
1	1.009	BB	6.2455e+004	1.29910e-004	9.996067	Methane
1	1.197	BB	1233.95786	0.00000e+000	0.000000	
1	1.465		-	-	-	Carbon Monoxide
2	0.304	PBOS	6.0000e+039	0.00000e+000	0.000000	
2	0.424		-	-	-	Carbon Dioxide
2	0.469		-	-	-	Ethylene
2	0.515	PBA	17.50215	5.91779e-005	0.001276	Ethane
2	0.671		-	-	-	Acetylene

Total norm percent = 100.00000

Eighth run, after 35 minutes

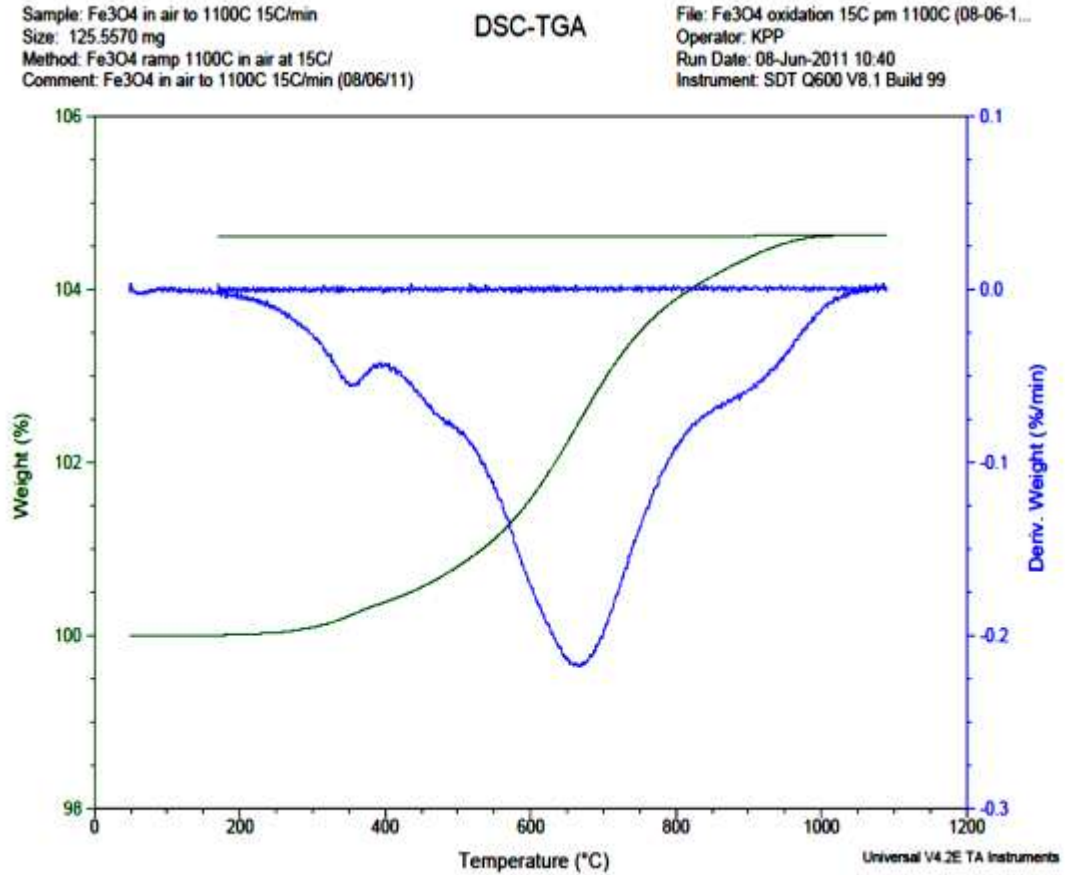


Signal	Retention Time [min]	Type	Area [$\mu\text{V}\cdot\text{s}$]	Amt/Area	Norm %	Name
1	0.588	BB	61.76578	2.68238e-004	0.020598	Neon
1	0.672	BB	9.5404e+005	7.61245e-005	90.290948	Argon
1	0.717		-	-	-	Oxygen
1	0.866		-	-	-	Nitrogen
1	1.010	BV	5.9978e+004	1.29910e-004	9.687042	Methane
1	1.198	VB	2305.27114	0.00000e+000	0.000000	
1	1.465		-	-	-	Carbon Monoxide
2	0.305	PBOS	6.0000e+039	0.00000e+000	0.000000	
2	0.424		-	-	-	Carbon Dioxide
2	0.469		-	-	-	Ethylene
2	0.516	PBA	19.20300	5.91779e-005	0.001413	Ethane
2	0.671		-	-	-	Acetylene

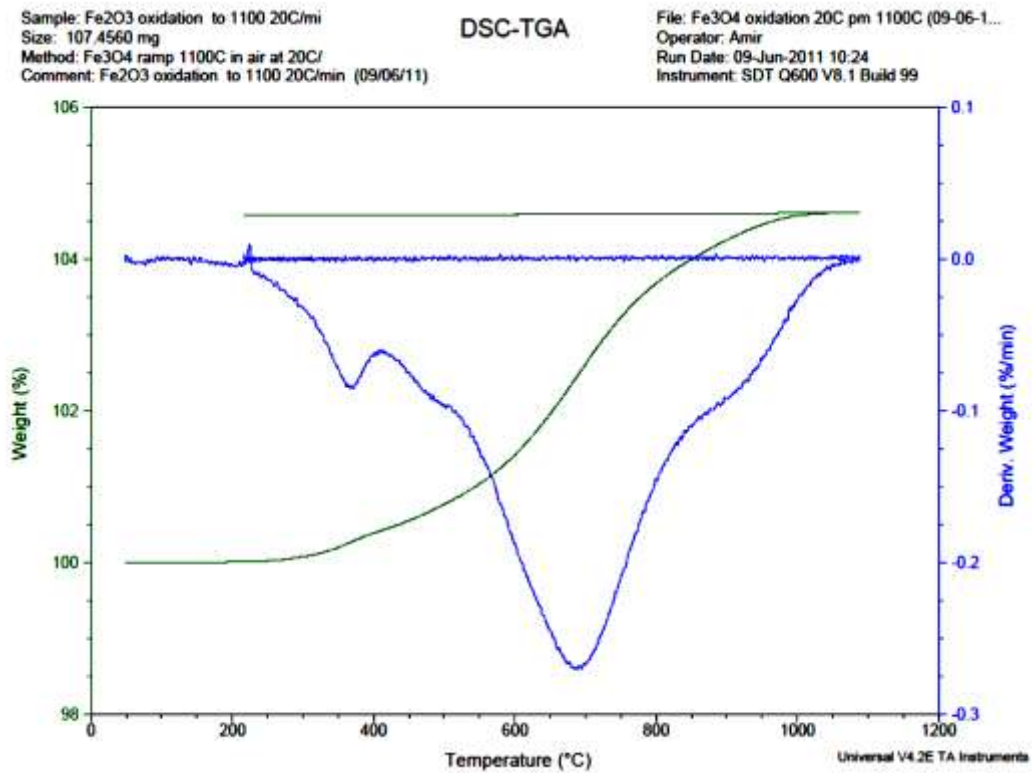
Total norm percent = 100.00000

APPENDIX B4: TGA GRAPHS

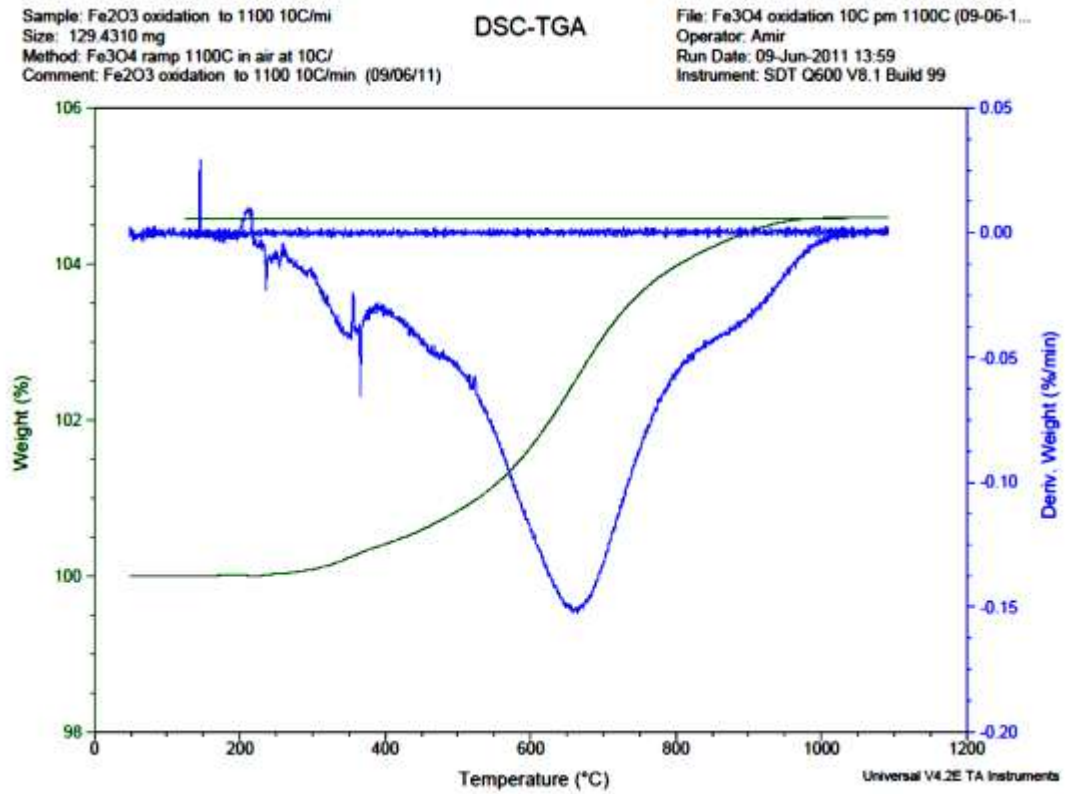
APPENDIX B4.1: TGA GRAPH OF OXIDATION OF IRON OXIDE OBTAINED FROM TPR TEST 2 WITH AIR, B=15



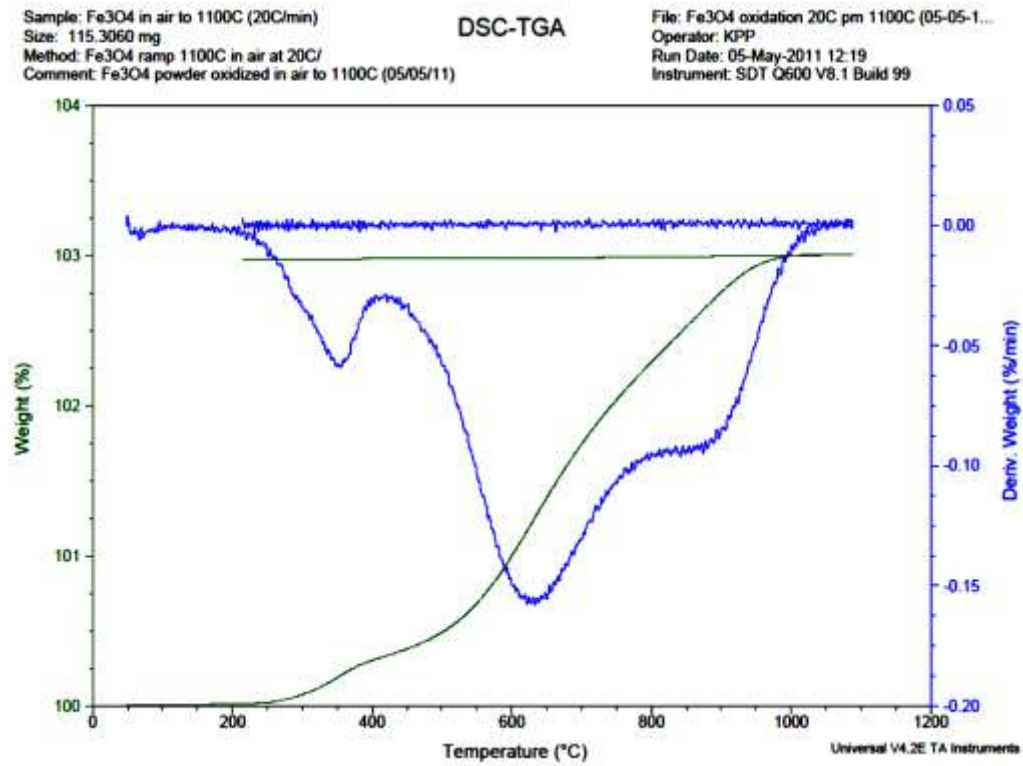
APPENDIX B4.2: TGA GRAPH OF OXIDATION OF IRON OXIDE OBTAINED FROM TPR TEST 2 WITH AIR, B=20



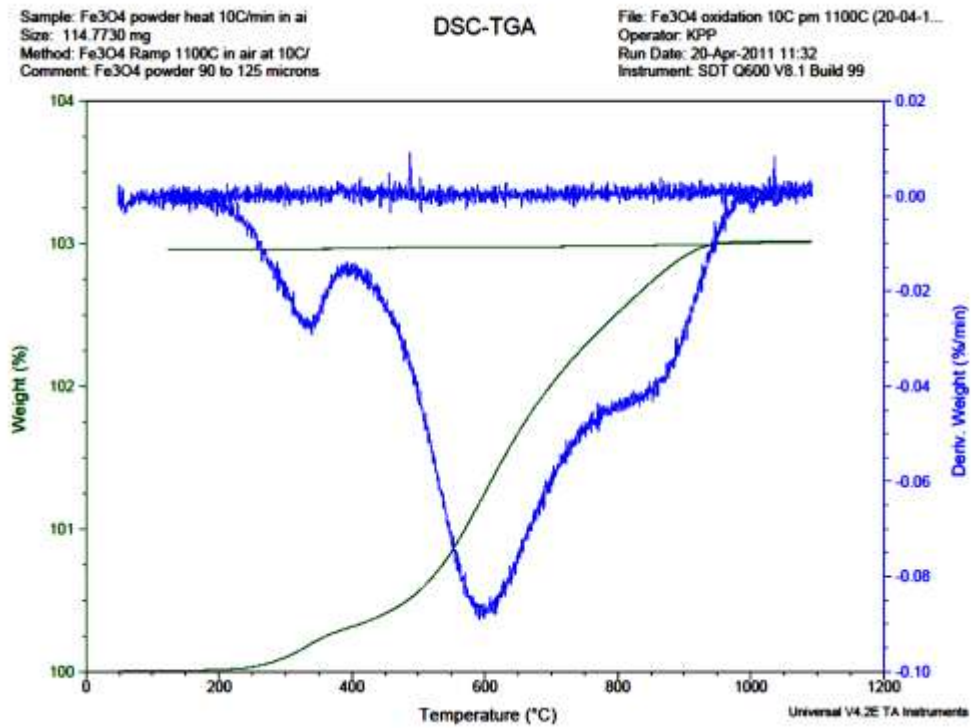
APPENDIX B4.3: TGA GRAPH OF OXIDATION OF IRON OXIDE OBTAINED FROM TPR TEST 2 WITH AIR, B=10



APPENDIX B4.4: TGA GRAPH OF OXIDATION OF IRON OXIDE OBTAINED FROM TPR TEST 1 WITH AIR, B=20



APPENDIX B4.5: TGA GRAPH OF OXIDATION OF IRON OXIDE OBTAINED FROM TPR TEST 1 WITH AIR, B=10



APPENDIX C: MICROSOFT EXCEL SPREAD SHEET

Table C.1 and Fig. C.1 shows the calculation of the two-dimensional diffusion mechanism. The variables of the table are defined as following extracted from Maple:

$$x = (E/RT)$$

$$P(x) = (\text{EXP}(-x)/x) \left((674.56 + (57.42x) - (6.55(x^2))(x^3)) / (1699 + (841x) + (49(x^2))(8(x^3)) - (x^4)) \right)$$

$$Q = \text{EXP}((P(x)^2)/(-2))$$

$$f(\alpha) = Q(-2\text{LN}(Q))^{(1/2)}$$

$$d(\alpha)/dT = (\text{EXP}(-x))f(\alpha)$$

Table C.1 Microsoft excel spread sheet for two-dimensional diffusion mechanism

x	T	P(x)	Q	f(α)	d(α)/dT
10.72047	1	2.13045E-07	1	2.12831E-07	4.70104E-12
0.974588	11	0.1095408	0.994018	0.108885567	0.041087715
0.510499	21	0.385699436	0.928317	0.358051337	0.214901059
0.345822	31	0.711286242	0.776496	0.552310772	0.390836463
0.261475	41	1.055659015	0.572806	0.604687945	0.465558433
0.210205	51	1.409072015	0.370559	0.522144646	0.423155332
0.175745	61	1.767513264	0.209705	0.370657084	0.310918836
0.150993	71	2.129035657	0.103685	0.220749373	0.189812253
0.132351	81	2.492581494	0.044758	0.111563389	0.097733212
0.117807	91	2.857527124	0.016861	0.048181795	0.04282722
0.106143	101	3.223481155	0.005542	0.017864255	0.016065249
0.096581	111	3.590185598	0.001589	0.005704429	0.005179259
0.088599	121	3.957463521	0.000397	0.001572395	0.001439075
0.081836	131	4.325189541	8.67E-05	0.000374778	0.000345329
0.076032	141	4.693272331	1.65E-05	7.73421E-05	7.16796E-05
0.070996	151	5.061643799	2.73E-06	1.38334E-05	1.28853E-05
0.066587	161	5.43025214	3.95E-07	2.14615E-06	2.0079E-06
0.062693	171	5.799057242	4.98E-08	2.89001E-07	2.71439E-07
0.059229	181	6.168027564	5.48E-09	3.37967E-08	3.18531E-08
0.056128	191	6.537137964	5.25E-10	3.43384E-09	3.24641E-09
0.053336	201	6.906368155	4.39E-11	3.03234E-10	2.87484E-10
0.050808	211	7.275701584	3.2E-12	2.32812E-11	2.21278E-11
0.048509	221	7.645124616	2.03E-13	1.55445E-12	1.48085E-12

0.046409	231	8.014625914	1.13E-14	9.02813E-14	8.61872E-14
0.044483	241	8.384195977	5.44E-16	4.56197E-15	4.36348E-15
0.042711	251	8.75382678	2.29E-17	2.00594E-16	1.92206E-16
0.041075	261	9.123511502	8.41E-19	7.67644E-18	7.36752E-18
0.039559	271	9.493244305	2.69E-20	2.55705E-19	2.45787E-19
0.038151	281	9.863020165	7.52E-22	7.41493E-21	7.13737E-21
0.03684	291	10.23283473	1.83E-23	1.87202E-22	1.80431E-22
0.035616	301	10.60268423	3.88E-25	4.11522E-24	3.97123E-24
0.034471	311	10.97256535	7.18E-27	7.87754E-26	7.61062E-26
0.033397	321	11.34247519	1.16E-28	1.31322E-27	1.27008E-27
0.032388	331	11.7124112	1.63E-30	1.90661E-29	1.84585E-29
0.031438	341	12.08237112	2E-32	2.41099E-31	2.33638E-31
0.030543	351	12.45235292	2.13E-34	2.6556E-33	2.57572E-33
0.029697	361	12.82235484	1.99E-36	2.54792E-35	2.47337E-35
0.028896	371	13.19237526	1.61E-38	2.12954E-37	2.06888E-37
0.028138	381	13.56241276	1.14E-40	1.55054E-39	1.50752E-39
0.027418	391	13.93246604	7.06E-43	9.83543E-42	9.56942E-42
0.026734	401	14.30253394	3.8E-45	5.43545E-44	5.29206E-44
0.026084	411	14.6726154	1.78E-47	2.61712E-46	2.54974E-46
0.025464	421	15.04270949	7.3E-50	1.09793E-48	1.07032E-48
0.024873	431	15.41281532	2.6E-52	4.01325E-51	3.91466E-51
0.024309	441	15.78293211	8.1E-55	1.27822E-53	1.24752E-53
0.02377	451	16.15305914	2.2E-57	3.5474E-56	3.46407E-56
0.023255	461	16.52319576	5.19E-60	8.57874E-59	8.38154E-59
0.022761	471	16.89334135	1.07E-62	1.80782E-61	1.76713E-61
0.022288	481	17.26349538	1.92E-65	3.3198E-64	3.24662E-64
0.021834	491	17.63365732	3.01E-68	5.31257E-67	5.19783E-67
0.021398	501	18.00382671	4.12E-71	7.40868E-70	7.25183E-70
0.020979	511	18.37400312	4.9E-74	9.00386E-73	8.81693E-73
0.020577	521	18.74418616	5.09E-77	9.53618E-76	9.34197E-76
0.020189	531	19.11437543	4.6E-80	8.80209E-79	8.62616E-79
0.019816	541	19.48457062	3.63E-83	7.08057E-82	6.94164E-82
0.019456	551	19.85477139	2.5E-86	4.96396E-85	4.86831E-85
0.01911	561	20.22497746	1.5E-89	3.03299E-88	2.97558E-88
0.018775	571	20.59518854	7.84E-93	1.61511E-91	1.58507E-91
0.018452	581	20.96540439	3.58E-96	7.49598E-95	7.35893E-95
0.01814	591	21.33562475	1.4E-99	3.03216E-98	2.97765E-98
0.017838	601	21.70584942	4.9E-103	1.069E-101	1.0501E-101
0.017546	611	22.07607817	1.5E-106	3.2848E-105	3.2277E-105
0.017263	621	22.44631082	3.9E-110	8.7975E-109	8.6469E-109
0.01699	631	22.81654718	9E-114	2.0536E-112	2.019E-112

0.016725	641	23.18678707	1.8E-117	4.1783E-116	4.109E-116
0.016468	651	23.55703035	3.1E-121	7.4097E-120	7.2887E-120
0.016219	661	23.92727684	4.8E-125	1.1453E-123	1.1269E-123
0.015977	671	24.29752642	6.4E-129	1.5431E-127	1.5186E-127
0.015742	681	24.66777895	7.3E-133	1.8121E-131	1.7838E-131
0.015514	691	25.0380343	7.4E-137	1.8548E-135	1.8263E-135
0.015293	701	25.40829235	6.5E-141	1.6549E-139	1.6298E-139
0.015078	711	25.77855298	5E-145	1.287E-143	1.2677E-143
0.014869	721	26.1488161	3.3E-149	8.7242E-148	8.5955E-148
0.014665	731	26.5190816	1.9E-153	5.1549E-152	5.0799E-152
0.014468	741	26.88934938	9.9E-158	2.655E-156	2.6169E-156
0.014275	751	27.25961936	4.4E-162	1.192E-160	1.1751E-160
0.014087	761	27.62989144	1.7E-166	4.6645E-165	4.5993E-165
0.013905	771	28.00016555	5.7E-171	1.5911E-169	1.5692E-169
0.013727	781	28.37044161	1.7E-175	4.7312E-174	4.6667E-174
0.013553	791	28.74071955	4.3E-180	1.2263E-178	1.2098E-178
0.013384	801	29.11099929	9.5E-185	2.7706E-183	2.7337E-183
0.013219	811	29.48128077	1.9E-189	5.4564E-188	5.3848E-188
0.013058	821	29.85156393	3.1E-194	9.3673E-193	9.2458E-193
0.012901	831	30.22184871	4.6E-199	1.4018E-197	1.3838E-197
0.012747	841	30.59213505	6E-204	1.8286E-202	1.8055E-202
0.012597	851	30.96242289	6.7E-209	2.0794E-207	2.0534E-207
0.012451	861	31.33271218	6.6E-214	2.0612E-212	2.0357E-212
0.012308	871	31.70300288	5.6E-219	1.781E-217	1.7592E-217
0.012169	881	32.07329493	4.2E-224	1.3415E-222	1.3253E-222
0.012032	891	32.4435883	2.7E-229	8.8083E-228	8.7029E-228
0.011898	901	32.81388293	1.5E-234	5.0416E-233	4.982E-233
0.011768	911	33.18417879	7.6E-240	2.5155E-238	2.4861E-238
0.01164	921	33.55447583	3.3E-245	1.0941E-243	1.0814E-243
0.011515	931	33.92477402	1.2E-250	4.1483E-249	4.1008E-249
0.011393	941	34.29507332	4E-256	1.3711E-254	1.3555E-254
0.011273	951	34.6653737	1.1E-261	3.9503E-260	3.906E-260
0.011156	961	35.03567512	2.8E-267	9.9218E-266	9.8117E-266
0.011041	971	35.40597756	6.1E-273	2.1724E-271	2.1485E-271
0.010928	981	35.77628097	1.2E-278	4.1463E-277	4.1012E-277
0.010818	991	36.14658534	1.9E-284	6.8988E-283	6.8246E-283
0.01071	1001	36.51689062	2.7E-290	1.0006E-288	9.8997E-289

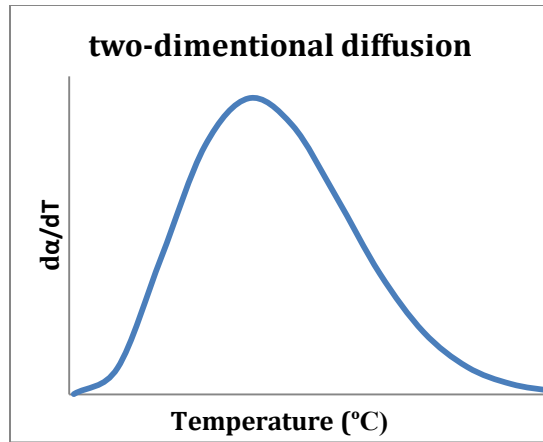


Figure C.1 Simulated graph of two-dimensional diffusion mechanism made by Microsoft Excel.